

cl

17176

DEVELOPMENT OF *LLTV* TECHNIQUES FOR DETECTION/ANALYSIS  
OF SPECTRA WITH APPLICATION TO  $\beta$  CEPHEI STARS AND OTHER OBJECTS

by

BRUCE ARTHUR GOLDBERG

B.S. Engr. (Hons), Case Institute of Technology, 1967  
M.S., Case Western Reserve University, 1969

A THESIS SUBMITTED IN PARTIAL FULFILMENT OF  
THE REQUIREMENTS FOR THE DEGREE OF  
DOCTOR OF PHILOSOPHY

in the Department  
of  
Geophysics and Astronomy

We accept this thesis as conforming to the  
required standard

THE UNIVERSITY OF BRITISH COLUMBIA

July 1973

In presenting this thesis in partial fulfilment of the requirements for an advanced degree at the University of British Columbia, I agree that the Library shall make it freely available for reference and study. I further agree that permission for extensive copying of this thesis for scholarly purposes may be granted by the Head of my Department or by his representatives. It is understood that copying or publication of this thesis for financial gain shall not be allowed without my written permission.

Department of Geophysics and Astronomy

The University of British Columbia  
Vancouver 8, Canada

Date 13 July 1973

*ABSTRACT*

New techniques for the detection and analysis of astronomical spectra have been developed and applied successfully in a study of the spectral variations of  $\beta$  Cephei stars and other objects of astrophysical interest.

The method involves the replacement of the photographic plate as the detection and recording medium by a television camera and an associated data acquisition system, with resulting improvements in sensitivity, precision, and facility of data reduction. The system limitations have been set primarily by the particular television camera selected, with important deficiencies being degraded resolution and a limited integration capability.

This paper follows, from one viewpoint, development of the system hardware, assessment of the system potential and its subsequent application to astrophysical problems, development of the software package for optimal data retrieval, and interpretation of the results within the framework of current theory. The results and contributions are discussed under two headings: (i) Engineering Development and (ii) System Applications.

*(i) Engineering Development*

The operation of many detectors used in astronomy benefits from an environment of reduced and stabilized temperature. Such is the case for the television detectors used in this program. As a consequence, a cooling system was developed for an Image Isocon tube, the prime detector employed. This system circulates cold air through the yoke of the television camera in a closed circuit and cools the tube uniformly by forced convection. It

satisfies the requirements for successful operation of the Isocon and has general value in demonstrating (a) the feasibility of an air-cooling approach in situations of awkward geometry or unusual heat dissipation and (b) that the hardware associated directly with a detector can be simple, compact, and inexpensive.

*(ii) System Applications*

The capability of the detection system for improved time resolution spectroscopy was of particular benefit in examining the short-term spectral changes in the  $\beta$  Cephei stars, a group distinguished by their regular variation in light and radial velocity. The stars  $\alpha$  Virginis (Spica),  $\beta$  Cephei, and BW Vulpeculae, representing some of the extremes in variability within the group, were observed in 1971 and 1972. The observations of Spica, the first of the program, served to demonstrate the value of the new instrumentation for this application.

Marked gains were made in the case of BW Vul where, for the first time, sufficient time and spectral resolution were attained to resolve the very rapid spectral variations occurring at certain phases of its pulsation cycle. The observations made possible a more accurate determination of the dynamic properties of its atmosphere and critical tests of 'models' attempting to explain its variation. A refined picture is presented of this variation, taking as its basis the shock wave 'model' of Odgers (1956).

The long-term variation in BW Vul's period and in the amplitudes of its light and velocity curves were also considered. The present data, viewed in context with that obtained over the past fifty years, demonstrate the existence of a pseudo-sinusoidal variation in the pulsation period, super-

imposed on a mean rate of increase of +3.7 sec/century, plus a secularly increasing velocity amplitude. Thus the *pulsation* amplitude is also increasing and the star may be in a rapid phase of evolution.

For  $\beta$  Cep, the first definitive record of a variation in line profile correlated with its variation in light and radial velocity was obtained. The result is critical to an understanding of its pulsation.

In summary, the main astronomical program has provided information important in understanding the physical processes occurring in the  $\beta$  Cephei stars and has demonstrated the value of a new type of instrumentation for studies of rapid spectrum variables.

## TABLE OF CONTENTS

ABSTRACT	i
TABLE OF CONTENTS	iv
LIST OF TABLES	viii
LIST OF FIGURES	ix
ACKNOWLEDGMENTS	xii
CHAPTER 1. <u>INTRODUCTION</u>	
1.1 INTRODUCTORY REMARKS	1
1.2 DEVELOPMENT OF THE DETECTION SYSTEM	2
1.3 COOLING THE DETECTOR	3
1.4 APPLICATION OF THE DETECTION SYSTEM	3
CHAPTER 2. <u>INSTRUMENTATION</u>	
2.1 THE DETECTION SYSTEM: A GENERAL DESCRIPTION	4
2.2 THE COOLING SYSTEM	5
<i>Design Constraints</i>	5
<i>The Feasibility Study</i>	8
<i>The Camera Hardware</i>	9
<i>The Cold Air 'System'</i>	10
<i>Operation of the System</i>	11
<i>System Control</i>	13
<i>System Performance</i>	14
CHAPTER 3. <u>THE ASTRONOMICAL PROGRAMS</u>	
3.1 SELECTING THE PROGRAM	15

3.2	THE PROGRAM	16
3.3	OBSERVATIONAL GOALS	20
CHAPTER 4. <u>OBSERVATION AND ANALYSIS</u>		
4.1	INTRODUCTION	21
4.2	THE $\beta$ CEPHEI OBSERVATIONS	24
	<i>A General Description</i>	24
	<i>The Preliminary Observations</i>	24
	<i>The Primary Observations</i>	26
4.3	DATA REDUCTION AND ANALYSIS	27
	<i>Introduction</i>	27
	<i>The Preliminary Data Check</i>	27
	<i>The Preliminary Data Analysis</i>	27
	<i>The Refinement Process</i>	28
	<i>The Quantitative Analysis</i>	28
	<i>Techniques for Resolution Enhancement and</i>	
	<i>Improved Signal Extraction</i>	32
	<i>Summary</i>	32
CHAPTER 5. <u>RESULTS AND DISCUSSION: THE INDIVIDUAL STARS</u>		
BW VULPECULAE		
5.1	INTRODUCTION	34
5.2	THE OBSERVATIONS	35
5.3	THE RADIAL VELOCITY VARIATION	35
	<i>The Velocity Curve</i>	35
	<i>The Accuracy of the Velocities</i>	38
	<i>The 'Van Hoof Effect'</i>	38
	<i>The Repeatability of Successive Cycles</i>	39
	<i>The 1971 Data</i>	39

5.4	THE LINE PROFILE VARIATION	42
5.5	THE LIGHT VARIATION	51
5.6	THE VARIATIONS IN RADIUS AND ACCELERATION	54
5.7	DISCUSSION	59
	<i>Introduction</i>	59
	<i>Previous Interpretations</i>	60
	<i>The Role of Shock Waves</i>	61
	<i>A Refined Interpretation</i>	67
	<i>The Line Doubling Phase Preceding Stillstand</i>	71
5.8	THE LONG-TERM VARIATIONS	72
	<i>Introduction</i>	72
	<i>Variation in the Period</i>	72
	<i>Amplitude Variations in the Light and</i>	
	<i>Radial Velocity Curves</i>	73
	<i>Summary</i>	76
5.9	FUTURE WORK	77
$\beta$ CEPHEI		
5.10	INTRODUCTION	78
5.11	THE NEW DATA	80
5.12	THE LONG-TERM VARIATION	81
5.13	FUTURE WORK	85
CHAPTER 6.	<u>SUMMARY AND CONCLUSIONS</u>	86
	BIBLIOGRAPHY	92

## APPENDIX

A.	EXPERIMENTAL ANALYSIS OF THE COOLING SYSTEM	97
B.	DESCRIPTION OF THE COOLING SYSTEM HARDWARE	98
C.	THE RECTIFICATION PROGRAM	101
D.	THE VARIATION IN EFFECTIVE DISPERSION ACROSS THE SCANNING RASTER	105
E.	SHOCK WAVE COMPUTATIONS FOR BW VUL	106

*LIST OF TABLES*

Table 4.I	Observed physical properties of the program stars $\alpha$ Virginis, BW Vulpeculae, and $\beta$ Cephei	22
Table 4.II	General features of the $\beta$ Cephei observations	25
Table 5.I	Observations of BW Vul	36
Table 5.II	Observations of $\beta$ Cep	82

## LIST OF FIGURES

- Fig. 2.1 Geometry of the Isocon and camera yoke plus the method of read-out. The target is scanned sequentially perpendicular to the direction of dispersion. Two spectra may be accommodated. For the present program, a target background level is obtained at the position of the second spectrum. 6
- Fig. 2.2 Schematic of the cooling system. 12
- Fig. 4.1 A sample application of the data processing techniques. All spectra shown are centered on the same epoch. They are: (A) a single frame normalized; (B) the mean of 8 frames normalized (a one-minute effective exposure); (C) the mean of 24 frames normalized; (D) the mean of 24 frames rectified and low-pass filtered; (E) the mean of 24 frames rectified, low-pass filtered, and deconvolved. The horizontal scale has also been expanded in the case of (D) and (E). 33
- Fig. 5.1 Radial velocities for BW Vul on 9 August 1972 UT: 1.1 cycle of the pulsation. A hollow circle indicates the velocity of the weaker component of a spectral line where two components are present. A bar over the circle indicates that the result is uncertain. 37
- Fig. 5.2 Radial velocities for BW Vul on 9 August 1972 UT: the phases of rapid variation preceding stillstand. Successive cycles are shown. 40
- Fig. 5.3 Radial velocities for BW Vul on 8 August 1971 UT: the phases of rapid variation preceding stillstand. 41
- Fig. 5.4 Radial velocities for BW Vul on 9 August 1971 UT: the phases of rapid variation preceding stillstand. 41
- Fig. 5.5 Line profiles for BW Vul on 9 August 1972 UT: the variation over approximately one cycle. 43
- Fig. 5.6 Line profiles for BW Vul on 9 August 1972 UT: a demonstration of the extremes in variability over one cycle. 44
- Fig. 5.7 The variation in line depth over 1.1 cycle for BW Vul on 9 August 1972 UT. 45

- Fig. 5.8 Line profiles for BW Vul on 9 August 1972 UT: the phases of rapid variation preceding stillstand for the first cycle. 47
- Fig. 5.9 Line profiles for BW Vul on 9 August 1972 UT: the phases of rapid variation preceding stillstand for the second cycle. 48
- Fig. 5.10 Deconvolved line profiles for BW Vul on 9 August 1972 UT: the phases of rapid variation preceding stillstand for the first cycle. 49
- Fig. 5.11 Line profiles for BW Vul on 9 August 1971 UT: the phases of rapid variation preceding stillstand. 50
- Fig. 5.12 Intensity ratios of the line components for the phases of rapid variation preceding stillstand for BW Vul on 9 August 1972 UT. 52
- Fig. 5.13 Equivalent widths for the phases of rapid variation preceding stillstand for BW Vul on 9 August 1972 UT. 53
- Fig. 5.14 Individual observations of the brightness  $v$ ; and of the Stromgren indices  $(u-v)$ ,  $(v-b)$ , and  $(b-y)$  for BW Vul. Taken from Kubiak (1972, p. 23). 55
- Fig. 5.15 Individual observations of the Stromgren  $[C_1]$  index. The broken curve is the adopted mean. Taken from Kubiak (1972, p. 27). 55
- Fig. 5.16 The displacement curve for BW Vul on 9 August 1972 UT: 1.1 cycle of the pulsation. A hollow circle indicates the displacement obtained from the weaker component of a spectral line when two components are present. A bar over the circle indicates that the result is uncertain. 56
- Fig. 5.17 The acceleration curve for BW Vul on 9 August 1972 UT: 1.1 cycle of the pulsation. A hollow circle indicates the acceleration obtained from the weaker component of a spectral line when two components are present. 57
- Fig. 5.18 Theoretical profiles for a star undergoing non-radial oscillations in Ledoux's (1951)  $P_2^2$  mode. The abscissa is  $\Delta\lambda/\Delta\lambda_R$  (or  $V/V_e \sin i$ ), where  $\Delta\lambda_R$  is the rotational width defined as  $\Delta\lambda_R = \lambda(V_e \sin i/c)$ ;  $V_e$  denotes the equatorial rotational velocity,  $i$  the inclination of its equator to the celestial plane ( $90^\circ$  for this case), and  $c$  the velocity of light. The ordinate uses an arbitrary scale and  $\phi$  is the phase. A 'typical' result from Osaki (1971, p. 488). 62

- Fig. 5.19 The radial velocity curve corresponding to the line profiles given in Fig. 5.18. Taken from Osaki (1971, p. 489). 62
- Fig. 5.20 Theoretical radial velocity curves; A and B respectively represent the cases for  $\alpha = 0$  and  $\alpha = 0.2$ , where  $\alpha$  is the ratio of radiation pressure to the gas pressure. The observations of Odgers (1956) during the cycle beginning J.D. 2435009,760 are represented by solid dots. Taken from Bhatnagar et al. (1971, p. 136). 66
- Fig. 5.21 The same as Fig. 5.20 but with the effects of a 2.1 Gauss magnetic field included. Taken from Bhatnagar et al. (1971, p. 136). 66
- Fig. 5.22 A summary of the observed features of the variation of BW Vul. 69
- Fig. 5.23 The variation in the period of BW Vul as indicated by the phase of  $V_{\circ}$ -crossing, plotted against the square of the time elapsed since J.D. 2428000. The line represents the relation found by Petrie (1954) to fit the observations of 1924-1952; the data are based on observations made since 1952 (the hollow circles are from the present program). The Figure is taken from Percy (1971). 74
- Fig. 5.24 The variation in the radial velocity amplitude (2K) for BW Vul. The vertical bars indicate the range in the observed amplitude in a single year if there were more than one observation; the dots are the mean. Observations through 1952 are from Petrie (1954); from 1953 to 1954 from Odgers (1956), from 1966 from Kubiak (1972), and from 1971 to 1972 from the present program. 75
- Fig. 5.25 Line profiles for  $\beta$  Cep on 16 October 1972 UT. Only a portion of the observations are shown. 83
- Fig. 5.26 Measures of the radial velocity, line asymmetry, and line depth for  $\beta$  Cephei. The asymmetries of the lines are indicated by the difference between the angle of a straight line fitted through the red side of the profile and one through the blue. 84

## ACKNOWLEDGMENTS

I am grateful to my supervisor (and the project director) Dr. G.A.H. Walker, for the opportunity to work with the instrumentation and for providing me with financial support (through a National Research Council of Canada grant) throughout the program. His many helpful and stimulating discussions were greatly appreciated.

Particular thanks go to Dr. Z. Rotem of the Department of Mechanical Engineering for his help and guidance at virtually every stage of the program, and to Drs. G.J. Odgers and K.O. Wright of the Dominion Astrophysical Observatory for their encouragement and interest during the astronomical phases. I would also like to thank Dr. Wright for his generous contribution of observing time on the D.A.O. telescopes.

During the instrumental design stages, Dr. Rotem and Dr. A.C. Pinchak of Case Western Reserve University provided many helpful suggestions. During the construction phases, K.D. Schreiber, B.C. Isherwood, and V. Buchholz of the Department of Geophysics and Astronomy gave willing and valuable assistance.

I am pleased to thank Dr. G. Hill of the D.A.O. for his valuable advice concerning the astronomical program (particularly during its early stages), to Drs. M.W. Ovenden and J.R. Auman, Jr., for their many helpful suggestions, to Dr. J. Glaspey for his participation in obtaining the observations, and to Drs. T.J. Ulrych and H. Fast for their assistance in the data processing.

Mrs. R. Rumley and Miss J. Bercov deserve credit for their efforts in typing this paper, as does Mr. S. Mochnacki for his help with the preparation of the tables and figures.

A program of this type is in several respects a team effort. I am indebted to many others for their contributions to its success.

1.1 *INTRODUCTORY REMARKS*

One of the goals of astronomy has been to obtain a detector that could respond in a completely predictable fashion to *all* electromagnetic radiation incident upon it in a desired spectral region and provide an output suitable for analysis and interpretation.

In the visible region of the spectrum, the photographic plate is the mainstay of astronomical detectors; representing a tremendous improvement in most applications over its predecessor, the human eye. Its strength lies in its integration capability and its huge storage capacity; its weakness in its poor quantum efficiency (about one percent), its limited dynamic range, and its somewhat unpredictable and difficult to calibrate response. In addition, considerable effort is frequently required to recover its store of information.

Advances in detectors and detection systems have followed three avenues: (i) attempts at improving the photographic plate; (ii) attempts at developing instrumentation to complement it; and (iii) attempts at replacing it entirely. Better emulsions and processing techniques fall into the first category, image intensifiers into the second, and photomultipliers into the last; while television and electronographic techniques may come under more than one.

These efforts have generally resulted in moderate gains with few restrictions (as with improved emulsions), or large gains with substantial restrictions (as with image intensifiers). If the ideal is to be approached, the photographic plate as we know it must be supplanted. No single detector

or system yet devised has the necessary flexibility to do so. The most promising candidates are the recently developed low-light-level television detectors and the electronographic techniques, with current trends in technology favoring the television approach (Livingston, 1973; Carruthers, 1971). Indeed, some of the television detectors now being developed (particularly those employing photoemissive devices) may come close to achieving this goal.

It is clear that the development of television detectors and their associated systems represents an important phase in the development of astronomical instrumentation. This paper follows one such system from the initial design stages through its successful application to astrophysical problems. The discussion ranges from the initial engineering contributions through the interpretation of the astronomical data obtained from the working system. Emphasis is placed on the development of one major portion of the instrumentation, on the basic problems encountered in applying the system and the methods of their solution, on the astronomical results, and on the avenues for future work in using the instrumentation and interpreting the results.

## *1.2 DEVELOPMENT OF THE DETECTION SYSTEM*

The present system is comprised of a low-light-level television camera and its associated instrumentation: the camera control unit, the camera cooling system, and the data acquisition system. The prime detector has been an English Electric P850 Image Isocon tube in a modified Marconi TF1709 camera.

Major hardware development has followed the divisions just indicated. The camera control unit has been discussed by Buchholz (1972), the data acquisition system by Isherwood (1971), and the camera cooling system

Goldberg et al. (1973b). The system is discussed further in Chapter 2, with the cooling system as a separate topic.

### *1.3 COOLING THE DETECTOR*

Cooling of the Isocon was necessary for its intended application to problems of stellar spectroscopy. The design restrictions, coupled with the awkward geometries of the Isocon and its associated television camera, made development of a suitable cooling system difficult. The adopted system represents a novel approach to cooling detectors of this type.

### *1.4 APPLICATION OF THE DETECTION SYSTEM*

The observational program was selected on the basis of astrophysical merit and the perceived advantages and limitations of the instrumentation. The system showed promise of offering substantial gains in the area of high-dispersion, high-time-resolution spectroscopy; and thus appeared well suited for studies of rapid spectrum variables. On this basis, a study of the spectral variations of the  $\beta$  Cephei stars (and additional objects as circumstance would permit) was initiated, with the intention of filling the gaps left by traditional observational techniques. A general discussion of the program is given in Chapter 3, the observational results and their interpretation are presented in Chapters 4 and 5.

## 2.1 THE DETECTION SYSTEM: A GENERAL DESCRIPTION

The detection system has been discussed in detail by Walker et al. (1971, 1972), the operation of the Image Isocon by Nelson (1969), and the Modulation Transfer Function (MTF) of the system by Buchholz (1972).

The Isocon has an S-20 photocathode with a peak quantum efficiency of about 10 percent, a typical resolution of 0.2 mm (about  $0.5 \text{ \AA}$  at a dispersion of  $2.4 \text{ \AA/mm}$ ) over a usable target length (i.e., its diameter) of  $\sim 70$  mm, and a linear dynamic range of  $\sim 100:1$ .\* With cooling to  $0^\circ\text{C}$  in order to reduce noise levels and maintain resolution, integration for periods of up to four minutes is possible.

Spectra are imaged on the photocathode, from which photoelectrons are emitted to form a related charge pattern on a thin glass target. After an exposure time sufficient for adequate charge accumulation (the integration period), the target is scanned sequentially normal to the direction of spectral dispersion by an electron beam. The portion of the beam that is 'scattered' from the target\*\* is amplified in a dynode chain and constitutes the tube output, which is sampled and digitized at each passage of the reading beam across the [charge] spectrum. For purposes of calibration, a measure of the target 'background' is also obtained in this fashion.

*Effective* exposure times are determined on the basis of the number of individual read-outs (or frames) that must be averaged point by point to achieve

---

\*The *effective* dynamic range is based on a lower bound set by the onset of non-linearities at low light levels and an upper bound fixed by target saturation. The *working* range is roughly half the effective range.

\*\*The remainder of the beam is either neutralized by the positive charge on the target or specularly reflected and subsequently screened out.

an acceptable signal-to-noise ratio. The geometry of the Isocon and the camera yoke plus the method of read-out are indicated in Figure 2.1.

The output of the system is a uni-dimensional digital representation of the light intensity distribution on the photocathode of the Isocon which is stored on 9-track, IBM 360 compatible magnetic tape via an Interdata Model Four mini computer. The number of data points (or channels) representing a spectrum and the *effective dispersion* in points per angstrom are dependent on both the configuration of the scanning raster and the spectrograph dispersion. For the observations discussed here, the number of channels was between 680 and 900, and the spectrograph dispersion between 0.5 Å/mm\* and 2.4 Å/mm. Further information concerning the system output is given in Section 4.3.

A silicon-target (S-T) vidicon (RCA No. 4532A) was also used for some of the observations. The vidicon has excellent red sensitivity (the peak in responsivity being at  $\sim 7000$  Å), much higher resolution than the Isocon ( $\sim 30\mu$ ), but a smaller 'collecting' area ( $\sim .62$ -inch diameter). Neither the tube nor the observational results obtained with it (which were of a preliminary nature) will be discussed in any detail. The method of read-out is similar to that of the Isocon.

## 2.2 THE COOLING SYSTEM

### *Design Constraints*

The principal reasons for cooling the Isocon were twofold: (i) to increase the target resistivity in order to prevent charge diffusion

---

\*Obtained with a 5X transfer lens developed by E.H. Richardson of the D.A.O.

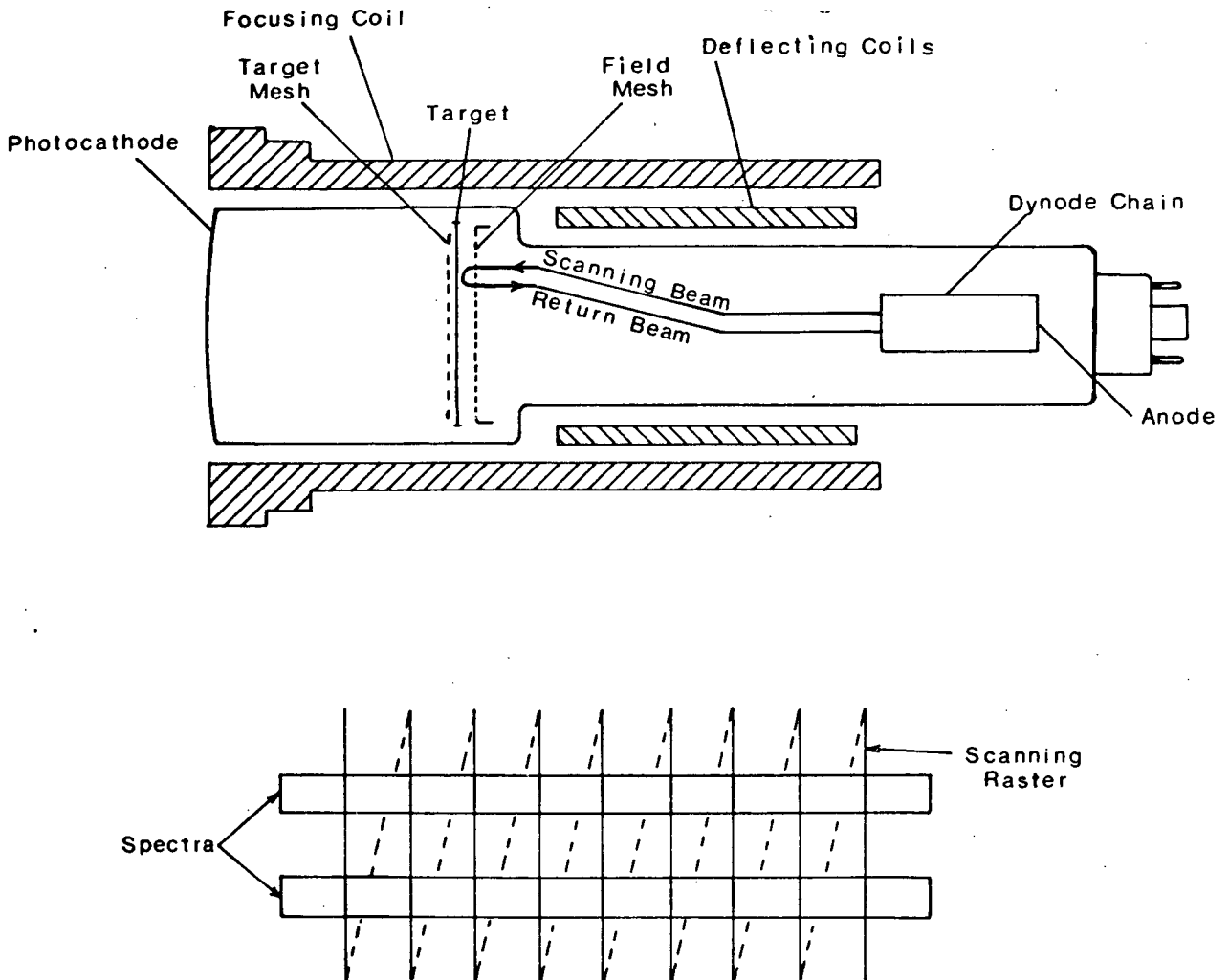


Fig. 2.1 Geometry of the Isocon and camera yoke plus the method of read-out. The target is scanned sequentially perpendicular to the direction of dispersion. Two spectra may be accommodated. For the present program, a target background level is obtained at the position of the second spectrum.

during extended integration times (which results in a serious deterioration of the MTF) and (ii) to reduce thermal background noise which is due to random electron emission at the photocathode, the scanning beam gun, and the dynode chain. A discussion of the effects of cooling on a thin glass target such as that found in the Isocon has been given by Livingston (1963). An operating temperature of  $+10^{\circ}\text{C}$  is suggested for achieving optimum resolution under 'normal' conditions, with a lower operating limit of about  $-50^{\circ}\text{C}$ . If the target is operated at too low a temperature, the problem of *remnant images* ('sticking') occurs. Its severity increases with the total charge involved. However, it can be reduced by exposing the tube to a source of relatively high illumination for *brief* time intervals. The optimum operating temperature is clearly dependent on the application.

For the case in point, the basic cooling requirements were to achieve an optimum target temperature for the periods of astronomical observation, and to keep the remainder of the tube at a sufficiently low temperature to reduce the thermal background noise to negligible levels. Initially it was thought to be about  $0^{\circ}\text{C}$  but later found to be somewhat lower.

Additional considerations were the cool-down time, the temperature stability, and the constraints on the size and weight of the camera, dictated by its potential use at the Cassegrain focus of a telescope. A maximum cool-down time of approximately one hour was set by considerations of convenience and a minimum cool-down time by considerations of stress (namely that the maximum temperature differential between any two points on the tube surface not exceed  $11^{\circ}\text{C}$ ). Temperature stability to better than  $3^{\circ}\text{C}$  at the operating temperature was required. Some of the improve-

ments realized in cooling the Isocon have been considered in the analysis of the system MTF mentioned previously.

It was further required that the entire system be portable, economical, operable under normal observatory conditions, and that the coolant be readily obtainable.

### *The Feasibility Study*

A feasibility study was undertaken initially to determine the most reasonable cooling approach.\* The design constraints eliminated the possibility of using 'conventional' methods such as a cold box. In addition, the close tolerance between camera yoke and tube plus the substantial heat generation in the yoke made liquid cooling impractical without *major* modifications to the camera. A forced-convection system using air or a similar gas as coolant circulated between yoke and tube appeared to offer the best alternative. Three coolants were considered: (i) liquid nitrogen vapor; (ii) freon which had undergone expansion cooling; (iii) air which had passed through a heat exchanger containing a cooling fluid. The first two were eliminated because of expense and/or their limited availability.

A model tube was constructed by J. Lees of the U.B.C. Physics Department (later to be replaced by a real, substandard tube), instrumented with copper-constantan thermocouples and inserted into the camera. The camera was sealed and liquid nitrogen vapor pumped through it. Flow rates were measured using a DISA hot-wire anemometer<sup>\*\*</sup> (calibrated in the large

---

\*The original camera had no special provision for cooling other than a small thermostatically-controlled fan to prevent over-heating (the standard operating temperature was  $\sim 75^{\circ}\text{F}$ ).

\*\*Type 55D50.

subsonic wind tunnel of the U.B.C. Mechanical Engineering Department), temperatures and temperature differentials were determined from thermocouple outputs, and flow patterns charted by smoke tracers observed through a window over the photocathode. Temperatures were measured as a function of time for a variety of flow rates and hardware configurations. In particular, close attention was given to the variation in temperature over the photocathode as a function of the separation between it and the adjacent imaging optics. A schematic of the test instrumentation and results of the initial measures are given in Appendix A. The experimental work during this stage was supplemented by a theoretical analysis of heat transfer rates, flow rates, and flow patterns, aimed at providing the quantitative information necessary for selecting the system components and optimizing the hardware configurations. Emphasis was placed on understanding the heat loading within the system, the pressure losses in the airstream, and the flow patterns needed for uniform cooling of the Isocon.

The feasibility study indicated that the air-cooling approach could satisfy the operational requirements within the framework of the design constraints. The next stage was to finalize the hardware configurations associated with the camera and to develop the equipment necessary for the requisite production of cold air. The system components and this part of the development are described in the following sections.

#### *The Camera Hardware*

The cooling system components associated directly with the camera were designed to fit within its original housing. These consisted of inlet and outlet flow manifolds, flow chambers, control valves and sealing devices,

mounts for the imaging optics (integrated with one of the outlet flow chambers) and temperature and pressure sensors. Material selection was based on requirements for low thermal conductivity, a low coefficient of thermal expansion, dimensional stability, machinability, and compatibility with other system hardware. A cotton cloth-phenolic laminate (Taylorite, Grade CE) was found to satisfy these requirements, as well as the requirement of availability. Most camera sealing was based on the use of rubber O-rings, sometimes applied in a non-standard fashion. Working drawings of some of the components are given in Appendix B.

### *The Cold-Air 'System'*

In principle, this portion of the system need only include a pump for circulating air and a heat exchanger for cooling it. The practical demand for a smooth, dry, clean flow of air at sufficient head to overcome the pressure losses through the entire system dictated the use of several additional components. The specific flow requirement at the pump was 8 CFM @ 5 PSIG.

Selecting an air pump represented the major difficulty. A survey was made of the available units, and experimental tests of a vortex (Ranque-Hilsch) tube, centrifugal blower, and an assortment of fans were carried out. A rotary, graphite-vane compressor (Gast Model 1550) was finally chosen, being an off-the-shelf item and meeting the general project requirements. The compressor had the unpleasant side effects of injecting graphite particles into the airstream, introducing substantial flow pulsations, and raising the air temperature significantly (an unavoidable consequence of air compression).\* To counteract these problems it was necessary to intro-

---

\*The adiabatic temperature rise for air is  $\sim 9^{\circ}\text{F}$  per PSI during compression.

duce a vibration-damper, an aftercooler (a water-cooled heat exchanger at the compressor outlet), and filters into the system.

For primary cooling of the airstream, a heat exchanger using a copper coil (made of 1-inch diameter copper tubing) submersed in a bath of methanol cooled by solid  $\text{CO}_2$  was constructed. When the ambient temperature was below about  $75^\circ\text{F}$ , the exit temperature of the air was sufficiently low to accommodate the temperature rise through the system between heat exchanger and camera. Water condensing or freezing out of the airstream due to cooling either remained in the coil of the primary heat exchanger (as ice) or was removed by two vortex traps, one following each of the two heat exchangers.

This portion of the system was constructed as a single unit; all components mounted on a *Dexion* frame with the compressor and motor isolated by vibration dampers.

### *Operation of the System*

A schematic of the cooling system is shown in Figure 2.2. An outline of the operation of the system following that given by Goldberg et al (1973b) is now given.

The system circulates cold, filtered air in an essentially closed circuit. From the portion of the system described in the previous section, the air is ducted to the camera by heavily insulated, low-temperature *Tygon* tubing (length  $\sim 50$  feet) and is injected into the toroidal air-space between camera yoke and tube near the target. The flow is drawn off tangentially from both front and rear ends of the camera through toroidal exit chambers and returns to the compressor. The aerodynamic properties of the television camera are utilized to reduce temperature differentials across the

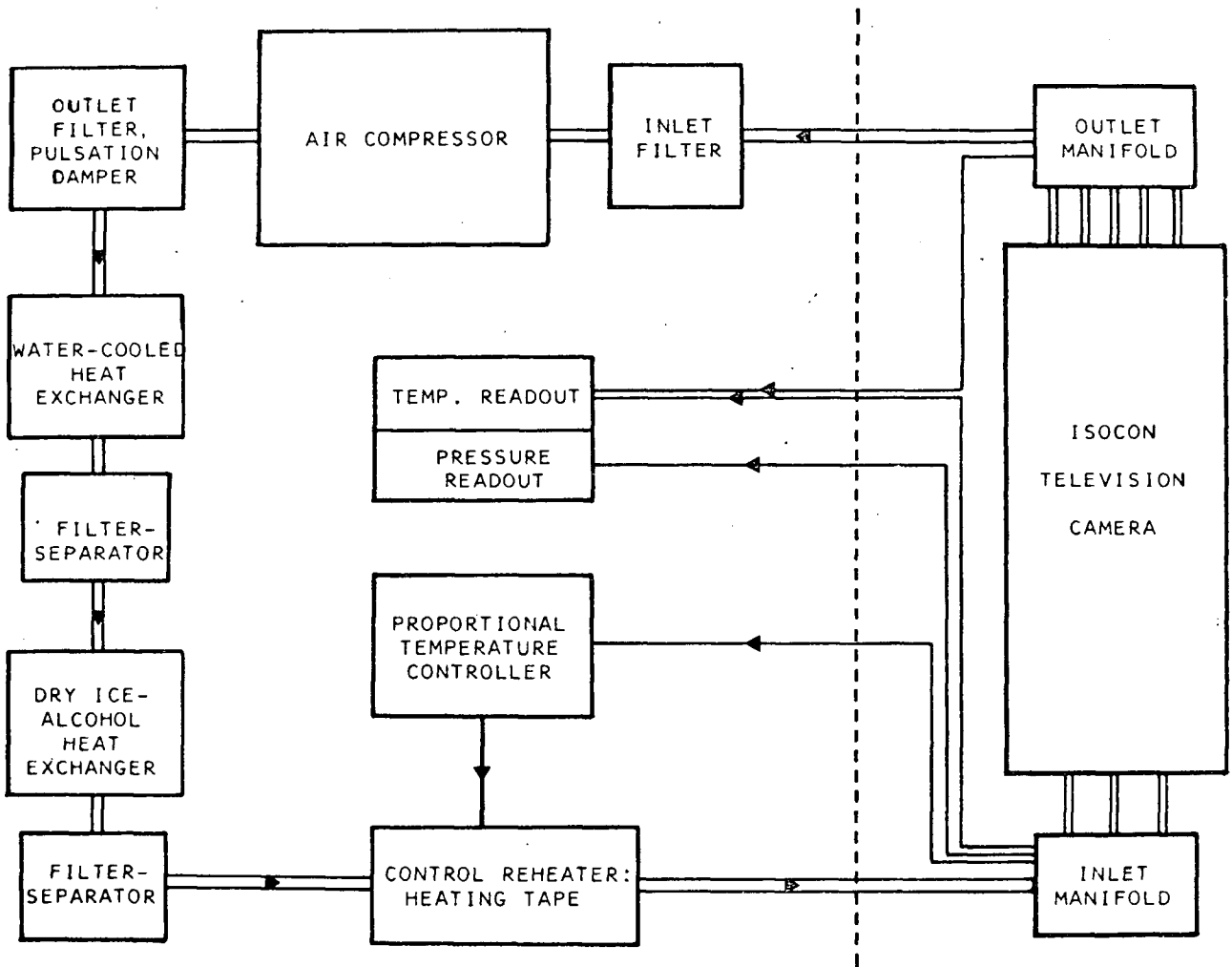


Fig. 2.2 Cooling system schematic.

tube and to counteract the effects of heat generation in the camera yoke. Uniform longitudinal cooling is ensured by the axial symmetry of the flow pattern and the relatively high flow rate through the camera body. Cooling of the photocathode is accomplished by a secondary convective flow induced by the exiting vortex flow at the photocathode edge. The investigation of the flow pattern and heat transfer rate there showed the effectiveness of this convective flow to be dependent upon the separation between photocathode and imaging optics, with the optimum about 5 mm. A safe cooling rate allows equilibrium to be reached in less than one hour, with temperature differentials across the tube not exceeding 5°C. Thermocouples set in the camera inlet and outlet and a pressure transducer at the inlet (Edcliffe Model 4-105-5D) allow checks of system performance.

#### *System Control*

Close temperature stability can be maintained by a control reheater consisting of a heating tape switched by a proportional-type temperature controller (Howe et al., 1969). The controller is activated from a platinum resistance sensor in the inlet manifold.

An indication of the thermal transfer function (see, e.g., Kutz, 1968) of the system was obtained experimentally by testing its stability against various temperature changes. The system as a whole, as well as the tube itself, has a substantial thermal inertia. This is a situation of inherent stability but one where precise temperature control can be difficult if there is a sudden change of temperature. In this case, the ambient temperature generally changes by only a small amount over relatively long periods of time and the heat exchanger can be operated at nearly constant temperature; making the system so stable under most circumstances

that *active* temperature control is unnecessary. When it is required, the arrangement described proves satisfactory. The response of the control system is rapid and there is little overshoot. The temperature probe monitors the airstream as it enters the camera and temperature adjustment is made by heating the air at an upstream point not so far removed that there is significant thermal lag. Temperature control of the airstream entering the camera ensures a stable tube temperature. *The control system is not the limiting factor in the system stability.*

### *System Performance*

Essentially all the design requirements were met and the system has performed in a generally satisfactory fashion for more than two years. It has at present a few important flaws due to unforeseen problems: on occasion the ambient temperature has exceeded 75°F preventing cooling to desired levels; and under conditions of extreme humidity icing-up within the primary heat exchanger has occurred due to incomplete system sealing, with consequent losses in pressure. The present system must, however, be considered a prototype, and it would be relatively simple to alleviate the problems. The required improvements would be a larger coil in the primary heat exchanger, more complete system sealing, and more efficient vapor traps.

Besides serving its function in cooling the Isocon, the cooling system has demonstrated that the air-cooling approach can offer an attractive solution in situations of awkward geometry or unusual heat dissipation. It differs from most other cooling apparatus used for astronomical detectors by separating most of the usually bulky cooling system hardware from the detector itself - a more flexible and convenient arrangement.

3.1 *SELECTING THE PROGRAM*

At the time the astronomical program was chosen, the general operating characteristics of the detection system and the sensitivity and resolution of the Isocon were 'known' from printed specifications and initial test runs (some at the D.A.O. 48-inch, the telescope to be used for the prospective program). It was clear that a certain degree of photometric precision could be achieved, the precise degree dependent on certain elusive quantities such as the instrumental stability and scattering effects within the Isocon. It was not at all clear what the ultimate integration capabilities would be.

This information - or lack of it - made applications requiring long integrations or precise quantitative spectroscopy uncertain. It did indicate that use of the detection system could bring about a considerable reduction in exposure time relative to the photographic plate or spectrum scanner.

In light of the burgeoning in the study of rapid light variations of many kinds of objects and the knowledge that many of these objects display (or should display) spectrum variations as well, it appeared that the new system could make a real contribution in the field of high-time-resolution spectroscopy. In addition, this application would lend itself to differential measurement techniques, exploiting the data handling capabilities of the system while subjugating its possible (and probable) shortcomings.

### 3.2 THE PROGRAM

It was felt that the new instrumentation could be used to advantage in a study of the  $\beta$  Cephei (or  $\beta$  Canis Majoris) stars; a small group of early B stars thought to be pulsationally unstable and characterized by short-period variations in light and velocity. In the H-R diagram, they are located in a strip parallel to and about one magnitude above the main sequence, extending from  $M_V = -3$  to above  $M_V = -5.5$ . The group can be broken into two major divisions: those having a known velocity variation (the 'classical  $\beta$  Cephei stars') and those having a known light variation. The former are slow rotators which follow a fairly well-defined period-luminosity relation; the latter, for the most part discovered by Hill (1966, 1967), are rapid rotators which apparently do not. The identification of several members of this latter group as  $\beta$  Cephei stars is somewhat uncertain. The  $\beta$  Cephei stars are bright, many being 'naked-eye' stars. Their general characteristics have been reviewed by Struve (1955a), Underhill (1966), Percy (1967), and van Hoof (1970), among others.

Within the class *as presently defined*, there exist many large differences. Projected rotational velocities vary from near 0 to more than 250 km/sec, pulsational velocity amplitudes from near 0 to more than 200 km/sec, light variations from a few hundredths to several tenths of a magnitude, and 'pulsation' period from less than  $4^h$  to more than  $7^h$ . The range in luminosity class is Ib to V; in temperature class it is from O9.5 to B3. Some of these stars are singly periodic, some multi-periodic, and some display a beat phenomenon. The actual limits of these characteristics within the group are not known, and the correct interpretation of some of

them uncertain.\* The differences may be the result of a number of factors - variations in mass and composition, evolutionary state, mode of pulsation, aspect effects, etc. Lists of the  $\beta$  Cephei stars and their individual features have been given by Hill (1967), Watson (1972), and Lesh (1973).

A fundamental difficulty is the lack of understanding of the instability mechanism affecting these stars. One key to solving this problem is knowledge of their state of evolution. Watson (1972) and Lesh (1973) have shown that the  $\beta$  Cephei 'instability strip' corresponds roughly with the S-bend region of evolutionary tracks in the H-R diagram, encompassing phases of core hydrogen-burning, secondary contraction following depletion of hydrogen in the core, and shell hydrogen-burning. It is presently impossible to determine which of these phases describes the  $\beta$  Cephei stars. Lesh suggests that normal B stars found in this same region of the H-R diagram are near the end of the core hydrogen-burning phase, while the  $\beta$  Cephei stars are in the secondary contraction or shell hydrogen-burning phase. This idea is based on the assumption that the instability is triggered in some fashion by structural changes within the stars, associated with transitions between the evolutionary phases. Watson cites statistical evidence which contradicts this view, indicating that the *majority* of  $\beta$  Cephei stars are in the core hydrogen-burning phase. An understanding of the physical processes associated with transitions between these phases should offer clues to the pulsation-triggering mechanism.

Stothers and Simon (1969) have proposed the ' $\mu$ -Mechanism Theory' to explain the instability:

---

\*For example, line broadening interpreted as Doppler broadening due to rotation may in fact be due to other types of velocity fields (Le Contel, 1970).

In a close binary system, the original primary star, being more massive than the secondary, will evolve first, expanding its radius during hydrogen burning until it reaches its Roche lobe. Thereupon it will quickly lose mass to the secondary, which accretes first the outer zero-age envelope of the primary star and then, on top of that, the helium enriched outer portions of the primary's core. If sufficient helium is accreted and the total mass exceeds  $6 M_{\odot}$ , the compression of the secondary's envelope by the weight of the helium ( $\mu$  mechanism) has been found to raise the effective temperature and to permit the development of radial pulsations which are strongly energized by the hydrogen-burning reactions in the core.

Criteria for the discovery of  $\beta$  Cephei stars on this basis have also been set forth (Stothers and Simon, 1971). At least two major aspects of the theory are contradicted by the observations: the requirement that all  $\beta$  Cephei stars be binaries and the suggestion of anomalous abundances (Watson, 1971).

Pulsation models have been proposed by several people (e.g., Ledoux, 1951; Chandrasekhar and Lebovitz, 1962; Clement, 1965, 1966, 1967; Osaki, 1971). Some of the observational features - spectrum variations, velocity variations, and multiple periodicities, for example - can be accounted for by these models. Some can be explained in terms of simple radial pulsations, others seem to require non-radial pulsations or interactions between more than one pulsation mode. There is evidence to suggest that a star's pulsation mode may be unstable and change in the course of a few years (Shobbrook et al., 1972). The pulsation mode(s) may be a critical factor in the basic instability.

Analyses have been made of the pulsational stability of evolutionary models to various types of oscillation. Davey (1973) considered the pulsational stability toward radial oscillation of models passing through those portions of the H-R diagram occupied by the  $\beta$  Cephei stars at several

stages of evolution. All were found to be stable in several modes of oscillation, making it impossible to determine the evolutionary state of the  $\beta$  Cephei stars on this basis.

The longer-term variations in these stars; particularly important from an evolutionary standpoint, have also been studied. Included are the changes in period, velocity amplitude, light amplitude, and pulsation mode as noted above. In several cases, the observations extend over intervals of more than fifty years, but with results that are far from conclusive. The long-term variations of BW Vulpeculae and  $\beta$  Cephei are discussed in Sections 5.8 and 5.12 respectively.

It is obvious that the basic problems of understanding the instability mechanism in these stars and of reconciling the great variety of observational characteristics within the framework of the group can be approached in a number of ways. One is to improve the observational data. An important gap in this area has resulted from an inability to resolve certain aspects of the spectral variations due to limitations set by exposure times and spectrographic resolution.

It appeared that the new instrumentation could help fill this observational gap. The brightness of these stars would put them well within reach of the detection system at coude dispersions, their short periods would make possible the acquisition of a meaningful quantity of data within a limited time of observation, and the cyclical nature of their variation would be an asset in distinguishing real from instrumentally-induced changes. It was hoped that the new data would serve as a basis for testing more critically the current models and provide the information needed for the solution of some of the major problems just discussed.

### 3.3 OBSERVATIONAL GOALS

The primary goal for this phase of the program was to obtain data for stars representing the widest possible range of characteristics of the  $\beta$  Cephei group and were, at the same time, individually interesting. The search for new  $\beta$  Cephei stars was not a part of the present program.

The secondary goal was to observe additional stars of interest for which observations of a similar nature could be of benefit.

## 4.1 INTRODUCTION

The  $\beta$  Cephei stars  $\alpha$  Virginis (Spica, HD 116658),  $\beta$  Cephei (HD 205021), and BW Vulpeculae (HD 199140) were observed in the course of this program. Two of these,  $\beta$  Cep and BW Vul, are classical  $\beta$  Cephei stars, while  $\alpha$  Vir was classified as a  $\beta$  Cephei star only recently (Shobbrook et al., 1969). All have an extensive observational history. Spica is a known binary and  $\beta$  Cep is a suspected one. The extremes in pulsational velocity amplitude, projected rotational velocity, and light variation for the group are represented by these stars. Their characteristics are summarized in Table 4.I.

The  $\beta$  Cephei star 12 Lacertae was also monitored with the present instrumentation by G. Hill of the D.A.O. These observations cover approximately two cycles of the pulsation. They will not be considered here in detail.

Additional programs using the instrumentation were carried out in association with K.O. Wright and G.C.L. Aikman of the D.A.O. With Dr. Wright, observation of 32 Cygni (HD 192909/10, K5I + B3V) were made near eclipse in an attempt to detect short-term changes (on the order of minutes) in the H and K lines of CaII. Changes in the profiles of these lines might be expected as a result of chromospheric effects (Wright, 1952; Wellmann, 1957). The emission features usually found in their centers might also change as a result of causes not associated with the eclipse (Liller, 1968). From observations covering the eclipses of 1949 and 1952-53, Wellmann found that the chromospheric effects in the K line were visible up to 70 days

Table 4.I. Observed physical properties of program stars  $\alpha$  Virginis, BW Vulpeculae, and  $\beta$  Cephei.

	Symbol	BW Vul	Ref.	$\alpha$ Vir	Ref.	$\beta$ Cep	Ref.
MK Spectral Type	-	B 2 III	1,2,3	B 1 IV B 1 V	2 3	B 2 III B 1 III	1,3 2
Visual Magnitude	V	6.44 6.29	1 6	0.97	5	3.32	1
Color Index	B-V	-0.130	1	-0.23	1,5	-0.22	1
Ultra-Violet Color Index	U-B	-0.870	1	-0.94 -0.93	1 5	-0.94	1
Ultra-Violet Reddening Excess	E(U-B)	0.11	1	0.05	1	0.02	1
Absolute Magnitude	$M_v$	-4.42 -3.57 -4.10	1 2 3	-3.83 -4.05	2 3	-4.26 -3.83 -4.00	1 2 3
Effective Temperature Parameter = $\frac{5040}{T_e^{\circ}K}$	$\theta_{eff}$	0.207	2	0.214	2	0.207	2
Log of Gravity	log g	3.81	3	3.85	3	3.88	3
Log of Period (days)	log P	-0.697	1	-0.760(var.)	6	-0.719	1
Apparent Rotational Broadening	$v_e \sin i$	26 38(narrow) 60(broad)	1 3 3	155	3	43 25	1 4
Amplitude of Light Curve (passband given).	$\Delta m$	0.200(v) 0.260(v)	7 8	0.014-0.03(v)	6	0.034(blue)	7
Radial Velocity Range (Km./sec.)	2K	150 190	7 8	16(var.)	6	23	7

References:

- |                             |                                   |
|-----------------------------|-----------------------------------|
| 1. Hill (1967)              | 5. Shobbrook <u>et al.</u> (1969) |
| 2. Lesh & Aizenman (1973)   | 6. Shobbrook <u>et al.</u> (1972) |
| 3. Watson (1972).           | 7. Percy (1967)                   |
| 4. McNamara & Hansen (1961) | 8. Kubiak (1972)                  |

from the beginning or end of totality.

Mid-eclipse (which was not total) was estimated to be J.D. 2441256.96 (Saito et al, 1972). Saito and Sato (1972) concluded that at mid-eclipse about half the disc of the B-type component was eclipsed by the photosphere of the K star. The partial phases lasted for seventeen days.

Observations were made with the Isocon on J.D. 2441210, 11, 12, and 48 at a dispersion of  $2.4 \text{ \AA/mm}$  using the D.A.O. 48-inch telescope. The longest single period of observation was about one hour.

The resolution was not sufficient to show whether the central emissions were present. The results were consequently inconclusive.

With Mr. Aikman, an attempt was made to detect the secondary component of the spectroscopic binary  $\Theta^2$ Orionis (HD 37041, 09k) by utilizing the increased\* dynamic range of the television system. The observations were made with the Isocon in October 1971 at a dispersion of  $2.4 \text{ \AA/mm}$ . Three spectral regions (centered on  $\sim 3860$ ,  $4026$ , and  $4860 \text{ \AA}$ ) were covered. A preliminary data analysis produced no definite evidence of the secondary.

Interest was revived in the program when  $\Theta^2$ Ori was found to lie in the error box of the X-ray source 2U0525-06 (Barbon et al., 1972). It was the only binary to do so which had an unseen secondary component sufficiently massive to be a black hole. Since the existence of X-ray sources in binary systems with non-luminous massive companions is the most convincing evidence of black holes (Barbon et al.), the coincidence is significant. Furthermore, the co-existence of a highly evolved black hole in a binary system with a very young O-star would be extraordinary!

---

\*Relative to the photographic plate

Further processing of the television data has been carried out and Mr. Aikman is presently reducing plate material which he has obtained of the object.

#### 4.2 THE $\beta$ CEPHEI OBSERVATIONS

##### *A General Description*

Virtually all observations were made between May 1971 and October 1972 using either the Image Isocon or silicon vidicon television cameras as detectors at the coudé focus of the D.A.O. 48-inch telescope. Only the best of these are discussed in depth. The main features of the observations have been summarized by Goldberg et al. (1973a) and are repeated in Table 4.II. Further information is provided in Tables 5.I and 5.II.

##### *The Preliminary Observations*

The star  $\alpha$  Vir was the first of the program stars. Its variable velocity was found from observations begun in 1876, it has been known to be a spectroscopic binary since 1890 (Vogel, 1890), and its light variability was discovered by Stebbins (1914). It was classified as a  $\beta$  Cephei star on the basis of a 4.17-hour period in its light variation. A thorough analysis of the characteristics of this system has been made by Evans et al. (1971).

The observed light curve is the superposition of the 4.17-hour variation and a 4-day variation due to aspect changes in the tidally distorted primary (Shobbrook et al., 1969). The pulsational variation is essentially sinusoidal with an amplitude of  $\sim 0.016$  mag. in V, while the orbital variation has an amplitude of  $\sim 0.03$  mag.

The short period variation in velocity was first reported by

Table 4.II. General features of the  $\beta$  Cephei observations

Star	Detector	Spectral Region ( $\text{\AA}$ )	Dispersion ( $\text{\AA}/\text{mm}$ )	Spectral Resolution ( $\text{\AA}$ )	Maximum Time Resolution* (Min.)	Spectrograph**
$\alpha$ Vir	Isocon	4000 - 4160	2.4	0.5	0.3	9682M
BW Vul	Isocon	4460 - 4590	2.4	0.5	1	9682M
	Isocon	6540 - 6585	4.8	1.0	3	9681M
$\beta$ Cep	Isocon	4548 - 4572	0.5	0.1	2	9682M + T.L.
	Vidicon	6490 - 6630	10.1	0.3	9	32121
12 Lac	Isocon	4548 - 4572	0.5	0.1	-	9682M + T.L.

\*An estimate based on the minimum acceptable signal-to-noise ratio.

\*\*Code: focal length of camera in inches; hundreds of grooves per mm of grating; order of diffraction;  
M = mosaic grating; T.L. = transfer lens (Richardson, E.H., *J.R.A.S. Canada* 62, No. 6.)

Shobbrook et al. (1972). The amplitude is  $\sim 15$  km/sec. The earlier velocities indicated the presence of at least three more periodicities, including one of about 6 hours. It appeared that the mode of pulsation had changed a number of times since 1908.

Variability in the line profiles has been reported in a number of papers. Struve (1948) found that some of the lines were occasionally double (or alternatively had emission cores) and in a later paper (Struve et al., 1958) noted that the line structure sometimes varied on a time scale of hours. The variability is associated with the orbital motion, the times of change coincident with the conjunctions. Dukes (1973) found a possible variation of from 2 to 5 percent in scans of HeI  $\lambda 4471$ , with a very tentative frequency of 4.10 cycles per day (very close to the frequency he obtained from his radial velocity data).

An attempt was made in May 1971 to detect a pulsation-correlated variation in the line profiles by using the Isocon (see Table 4.II). Nearly two cycles were covered at orbital phases intermediate between the conjunctions and the times of maximum velocity separation. A preliminary analysis indicated no significant change in the profiles. However, the ease with which the instrumentation could be applied to programs of this type (as well as the advantages of obtaining the data in digital form) was demonstrated.

The analysis is presently being continued by using some of the techniques described in Section 4.3. Further observations of this type, but at a higher dispersion and probably in a different spectral region, may be required to define the pulsational line profile variation if one exists.

#### *The Primary Observations*

The observations of BW Vul and  $\beta$  Cep will be discussed in detail in Chapter 5.

### 4.3 DATA REDUCTION AND ANALYSIS

#### *Introduction*

Data reduction and analysis takes place in five stages: (i) a preliminary data check during the time of data acquisition; (ii) a preliminary analysis designed to provide a measure of the signal level during the course of observations and an indication of the nature and degree of processing required in the overall analysis; (iii) a refinement process designed to put the spectra in a form suitable for quantitative study; (iv) quantitative analysis; (v) application of techniques for resolution enhancement and improved signal extraction.

#### *The Preliminary Data Check*

A preliminary data check is accomplished *on line* with the use of an Interdata Model Four mini computer. Checks are made for the acceptability of the signal level, for errors associated with the digitization process, and for accuracy of the data transfer to magnetic tape (Walker et al., 1972).

#### *The Preliminary Data Analysis*

A preliminary data analysis, based on a program developed by A.C. Gower of the U.B.C. Department of Geophysics and Astronomy involves the computation of normalized means of specified numbers of single frames. Normalization is accomplished by equalizing the areas under each mean spectrum between specified wavelength limits. The signal level is indicated by the normalization factor. A background level recorded during each read-out of the tube and a dark level obtained at the end of each 'run' on a

source are generally subtracted from the signal before normalization.

### *The Refinement Process*

Included in the refinement process are noise reduction and rectification procedures; the former to enhance the signal-to-noise ratio, the latter to remove the instrumental response characteristics and restore the proper intensities. The spectra are rectified to a continuum defined by a least squares fit of third-order orthogonal polynomials to points selected from those spectral regions representing real continuum. This selection is carried out automatically once the continuum boundaries are defined (the process is described in Appendix C). The accuracy of the process is dependent on the quality of fit; and the stability, linearity, and response characteristics of the system. The assumption of a linear response is implicit in this approach. The work by Buchholz (1972) plus the general experience gained in using the instrumentation has shown this assumption to be correct to at least a first order. A new continuum fit is made for each mean spectrum to compensate for possible fluctuations in the system response. A background and a dark level are subtracted from the signal before rectification in a fashion similar to that used in the normalization process. At present, the computed means are based on equal time intervals. Noise reduction is accomplished by two methods: (i) averaging single frames to give an  $N^{\frac{1}{2}}$  improvement in the signal-to-noise ratio, where N is the number of frames; and (ii) by linear smoothing or use of a low-pass filter. Use of an optimum filter was found to be an unnecessary refinement.

### *The Quantitative Analysis*

The quantitative analysis involves the computation of radial

velocities, line depths, equivalent widths, and similar parameters from the rectified and filtered (or smoothed) spectra.

Radial velocities are determined numerically by two methods: (i) by the positions of line minima (*Method I*), and (ii) by the positions found from bisecting the area between continuum and line (*Method II*). Measurements of multiple component profiles are made manually when the position of other than the strongest component is required. Method II provides a weighted mean of the positions of all components within set wavelength limits and is quite sensitive to variations in the line profiles. It requires an accurate knowledge of the extent of the spectral lines\* and a precise continuum fit. Method I gives only the velocity of the deepest component of a line. A good signal-to-noise ratio is required if acceptable results are to be obtained. A technique proposed by Hutchison (1971) would probably be more effective than the present methods in situations where the line profiles do not change rapidly or have a complex structure. It involves a least-squares fit of a polynomial to the first derivative of a line profile, with the position of line minimum determined by the zero crossing of the polynomial.

The primary limitations on the accuracy of the radial velocities were set by the stability of the instrumentation (in association with the calibration procedures employed) and the techniques of data reduction (in association with the signal-to-noise ratios, which frequently had to be compromised for the sake of better time resolution).

In all numerical radial velocity computations, line positions

---

\*Determined on the basis of the line profiles given by Wilson (1956), Butler and Seddon (1958), and Wright et al. (1964).

were determined only to the nearest instrumental channel, resulting in quantized values limited in accuracy by the size of the quantum jump (which can be inferred from the effective dispersion). In addition, corrections for variations in the effective dispersion across the spectrum (due to non-linearities associated with the scanning raster and the imaging process) have not been applied because of insufficient calibration procedures. However, this correction should be relatively small (see Appendix D).

The instrumentation generally proved stable in the wavelength regime (i.e., the position of the scanning raster remained nearly fixed). This was demonstrated by the stability in the positions of two fiducial marks located on the photocathode during *some* of the observations, as well as by some of the longer sets of observations on a single source. One example of the stability realized during satisfactory operation of the system is given by the  $\sim 5^{\text{h}}$  observing run of 9 August 1972 UT on BW Vul; during which a fairly uniform drift of 1 channel ( $\sim 18$  km/sec) occurred. Occasionally, large non-linear shifts occurred over periods of minutes. These were readily identifiable as being instrumental in origin even in the absence of the fiducial marks. Hardware improvements over the past year have helped eradicate this problem.

Guiding errors also have an effect on the accuracy of the radial velocities. The maximum possible error corresponds to the projected slit width; typically  $\sim 25$  km/sec for the present observations. Errors of this type did not appear to manifest themselves.

Radial velocity standards were taken during most observing sessions, but have not yet been used in the present analysis. All velocity

computations have so far been differential; not a serious deficiency as the primary concern has been motion within the frame of the star.

A *general* error analysis is not particularly meaningful because of the wide variations encountered in the operation of the instrumentation. Quantitative assessments of the accuracy must be made on the basis of individual sets of observations. They are therefore relegated to the individual discussions of the stars observed.

The epochs given are based on an interpolation between the recorded starting and ending times for a single set of observations. The 'frame time' is used as the interpolation factor. The absolute accuracy is on the order of five minutes, the relative accuracy considerably higher.

Line depths are given by the differences between the continuum, and the intensity values at the positions of line minima. Their accuracy is most strongly influenced by the quality of the rectification, but application of a filter with a cut-off at too low a frequency can lead to erroneously shallow lines, especially when the lines are sharp. Poor resolution has a similar effect.

Equivalent widths *may* be computed on the basis of the areas determined during the radial velocity computations by Method II. This program option has not yet been exercised.

The program can be expanded without difficulty to accommodate computations of additional spectrum parameters (such as half-widths of lines, line asymmetries, etc.).

*Techniques for Resolution Enhancement and Improved Signal Extraction*

Additional information may be obtained from the data under certain circumstances by application of the techniques described below. The deconvolution techniques developed by Ulrych (1972) are used for resolution enhancement. In particular, they provide a relatively good indication of the true separations between blended lines or components. The basic procedure is to (i) examine the power spectrum of the data; (ii) construct an appropriate low-pass filter to reduce the high frequency noise content to very low levels; and (iii) deconvolve the filtered spectra. The optimum result is achieved by a trial and error process. The component separations derived in this fashion are not particularly dependent on the assumptions made in choosing the deconvolution parameters. The prime requirement for satisfactory application of the technique is a good signal-to-noise ratio.

Taking ratios or differences of spectra is particularly useful in isolating small changes in the continuum or in the structure of a line. The spectra of different stars may be compared in this fashion as well. Ratios or differences are taken of the *normalized* spectra.

*Summary*

Some of the processing techniques just discussed are demonstrated on spectra of the  $\beta$  Cephei star BW Vul in Figure 4.1.

Certain aspects of the data processing are discussed in more detail under the headings of the individual stars. Relevant discussions of data processing techniques have been given by Bonsack (1971), Brault and White (1971), Biraud (1969), and Lorre (1973).

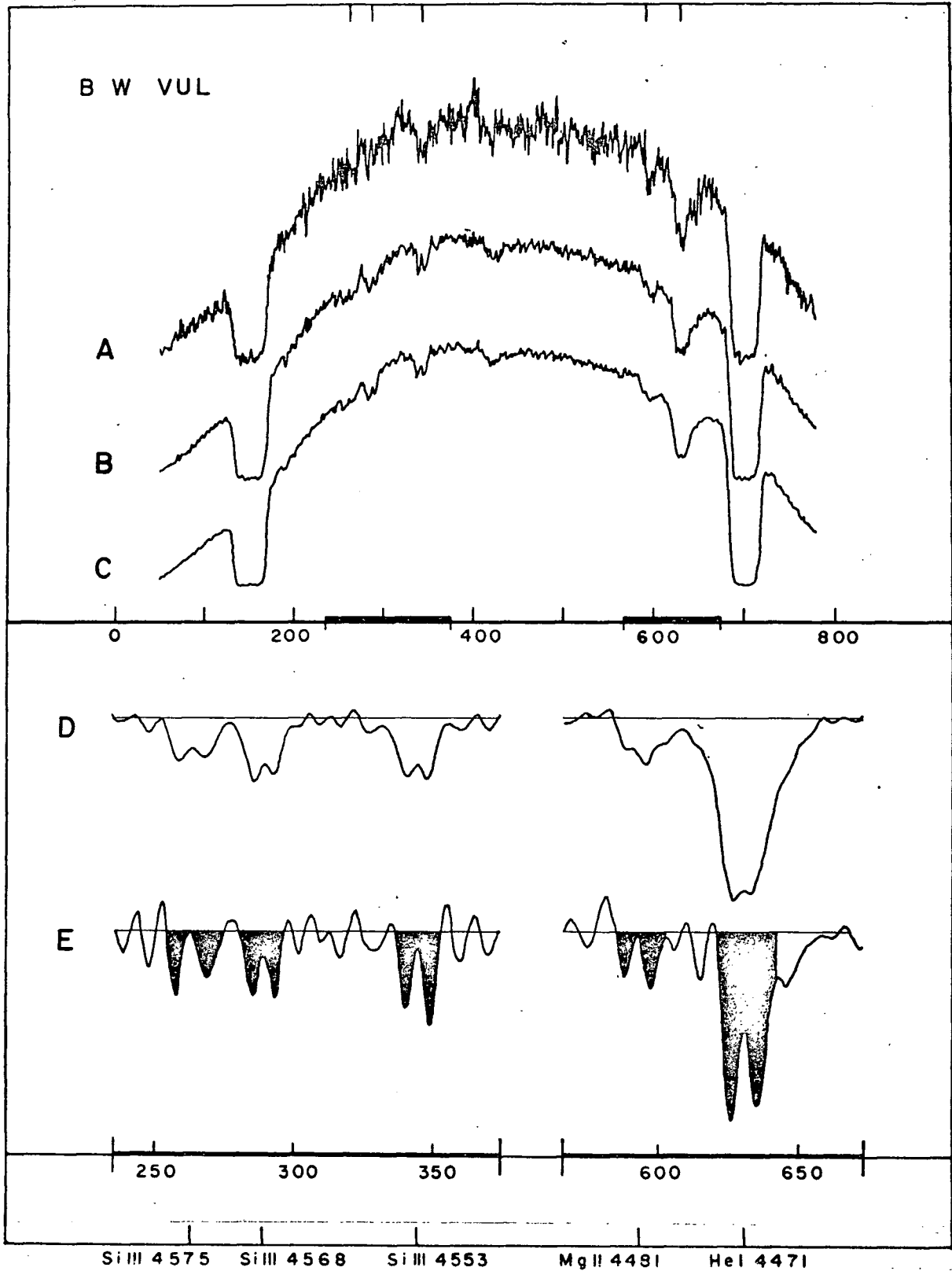


Fig. 4.1 A sample application of the data processing techniques. All spectra shown are centered on the same epoch. They are: (A) a single frame normalized; (B) the mean of 8 frames normalized (a one-minute effective exposure); (C) the mean of 24 frames normalized; (D) the mean of 24 frames rectified and low-pass filtered; (E) the mean of 24 frames rectified, low-pass filtered, and deconvolved. The horizontal scale has also been expanded in the case of (D) and (E).

CHAPTER 5. RESULTS AND DISCUSSION: THE INDIVIDUAL STARS

## BW VULPECULAE

## 5.1 INTRODUCTION

The star BW Vulpeculae is perhaps one of the most interesting periodic variables known (its characteristics are given in Table 4.I). It displays the largest radial velocity, light, and line profile variations of the known  $\beta$  Cephei stars, and has undergone what appear to be significant changes in its period and its radial velocity amplitude during the past several decades.

The star's variable velocity was discovered by Hill (1930), its short period by Petrie (1937), and its light variation by Huffer (1938). The spectroscopic observations were begun in 1924.

Extensive spectroscopic studies have been made by Petrie (1954), Struve (1955a), McNamara and Williams (1955), McNamara et al. (1955), and Odgers (1956). Photometric investigations have been carried out by Huffer (1938), Eggen (1948), Nikonov and Nikonova (1952), Kraft (1953), Walker (1954), Lynds (1954), and Percy (1971). A joint spectroscopic and photometric study has recently been completed by Kubiak (1972).

In contrast to this extensive observational assault, there have been few serious attempts at explaining the observed phenomena. The primary difficulties have been the complexity of the variation, the lack of understanding of the basic instability mechanism, and the inability of traditional observational techniques to resolve the spectral variations during the phases of the rapid change.

## 5.2 THE OBSERVATIONS

The general features of the observations are given in Table 4.II and the details in Table 5.I.

## 5.3 THE RADIAL VELOCITY VARIATION

### *The Velocity Curve*

The radial velocities obtained with the Isocon in 1971 and 1972 from the lines of HeI  $\lambda 4471$ , MgII  $\lambda 4481$ , and SiIII  $\lambda \lambda 4553, 4568, 4575$  are presented here. They are not listed in the customary tabular form for two reasons: (i) because the discrete values obtained are dependent on the method of analysis (in particular on the time increments chosen\* and the treatment of multiple-component profiles) and (ii) because they are presently differential\*\*.

The velocity curve obtained by Method I on 9 August 1972 UT is given in Figure 5.1. Approximately 1.1 cycle was covered. The data were reduced to produce three-minute means at three-minute intervals with a resulting signal-to-noise ratio of  $\sim 25:1$ .

The outstanding features of the velocity curve are its extreme amplitude, the 'discontinuity' at phase  $\sim 0.4$ , the stillstand from phases  $\sim 0.4$  to  $0.55$ , and the extreme blue-shift immediately following stillstand. Also notable are the small red-shift near the end of stillstand, the 'hump' in the curve at phase  $\sim 0.65$ , the increase in the velocity gradient at phase  $\sim 0.2$ , and the scatter in velocities at phase  $\sim 0.25$ . The reality of these features has been verified by a comparison of the present results with pre-

---

\*The effective exposure time and the overlap between the effective exposures.

\*\*The stillstand velocity was taken as the zero level on the basis of previous photographic results. Difficulty is encountered in determining the radial velocity of the center of mass.

Table 5.I. Observations of BW Vulpeculae

UT Date	Heliocentric Julian Date 2441000 +	H.A. @ Start	Frame Time (Minutes)	Effective Exposure Time* (Minutes)	Mean Effective Dispersion** (points/Å)	Phases Covered	Quality Factor <sup>∇</sup>
8 Aug. 71	171.776-.981	1:32E	0.375	4	3.8	0.97-1.0-0.60	2-3
9 Aug. 71	172.838-.917	0:01E	0.333	3.5	3.8	0.23-0.55	2-3
9 Aug. 72	538.751-.985	2:00E	0.125	2	3.5	0.37-1.0-0.50	1

\*The 'best' compromise between time resolution and the signal-to-noise ratio (the average over the time interval).

\*\*The average over the region of interest.

∇An estimate of the quality of the data (1 = excellent to 4 = poor).

Notes:

- (1) Only the data discussed in this paper is listed here. The remainder are either of lower quality or require further analysis (as in the case of the data obtained in the region of H $\alpha$ ).
- (2) The primary lines observed were those of He I  $\lambda$ 4471, Mg II  $\lambda$ 4481, and Si III  $\lambda$ 4553, 4568, 4575.
- (3) The 1971 data was obtained before the addition of new high reflectance coatings to the coude spectrograph of the D.A.O. 48-inch telescope.

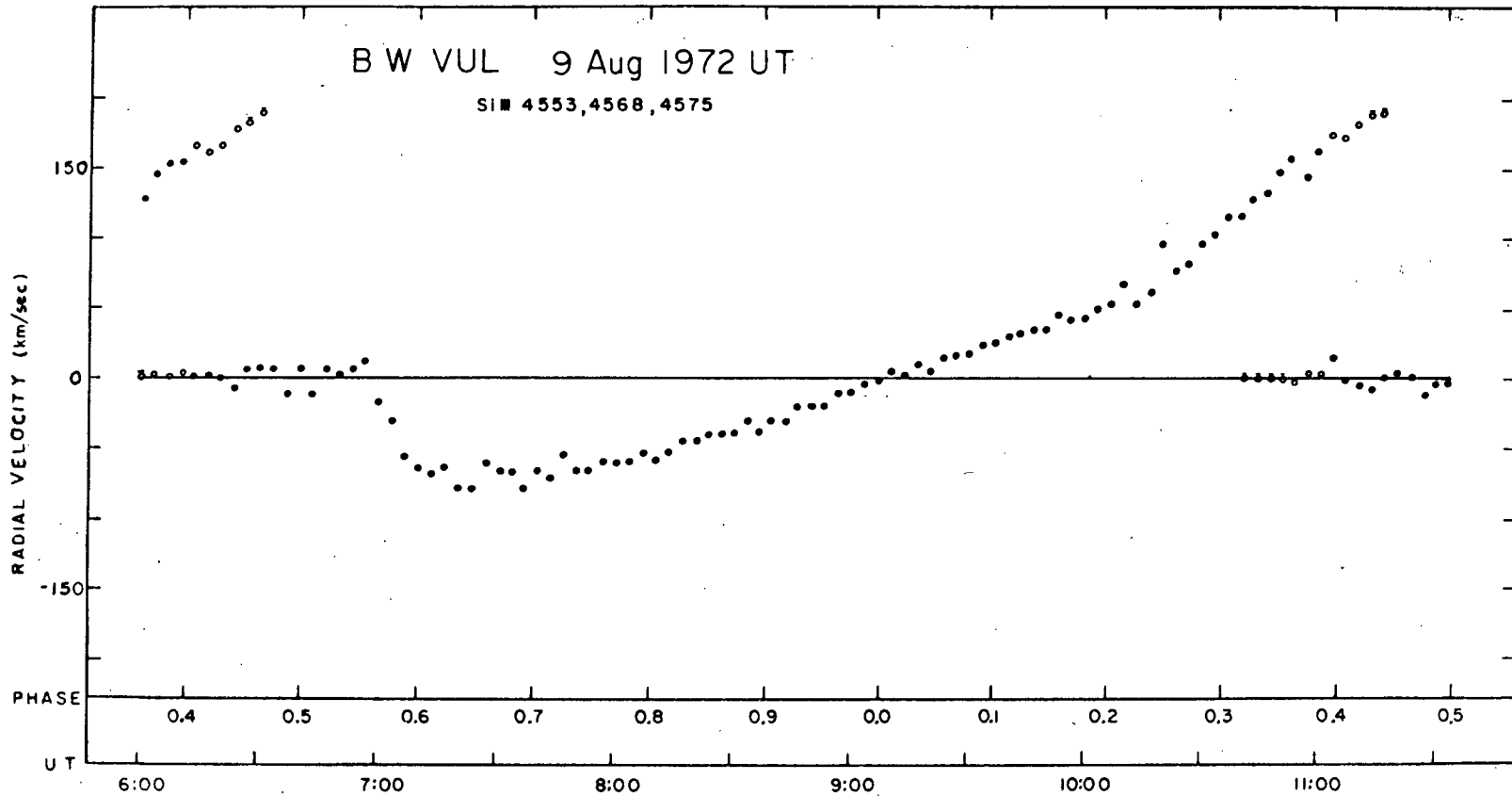


Fig. 5.1 Radial velocities for BW Vul on 9 August 1972 UT: 1.1 cycle of the pulsation. A hollow circle indicates the velocity of the weaker component of a spectral line where two components are present. A bar over the circle indicates that the result is uncertain.

vious photographic data - particularly that of Kubiak (1972) and Odgers (1956).

### *The Accuracy of the Velocities*

The *relative* accuracy of the individual velocities can be inferred from the scatter, which is about 10 km/sec. Where the velocity gradient is small (phases  $\sim 0.8$  to 0.2), the quantization effect discussed in Section 4.3 is more apparent. The scatter may be reduced by increasing the effective exposure time and thus the signal-to-noise ratio. Corrections for instrumental drift (see Section 4.3) have been applied.

### *The 'Van Hoof Effect'*

Evidence of the 'Van Hoof Effect' (van Hoof and Struve, 1953); a systematic time lag in the radial velocities derived from the hydrogen lines relative to the other stellar lines, has been found for a number of  $\beta$  Cephei stars (Laskarides, 1971). An effect that may be interpreted in this vein has been seen in BW Vul. McNamara et al. (1955) found a large positive residual in the difference ( $V_{\text{hydrogen}} - V_{\text{all}}$ ) during the phases immediately preceding and immediately following the stillstand, and Odgers (1956) noted a difference in the strength of the redward component of H $\gamma$  relative to the redward components of the SiIII lines during the phases of doubling.\*

....When the lines are double the redward component of H $\gamma$  remains more intense than the component at the stationary position for about seven minutes after the redward components of SiIII,  $\lambda 4552$ ,  $\lambda 4568$  have become less intense than the components at the stationary position.

No significant difference in either phase or amplitude was ob-

---

\*With reference to a set of observations obtained by A.J. Deutsch at Mount Palomar on 15 October 1954 covering the phase of 'discontinuity' preceding stillstand.

served for the He, Mg, and Si lines. A precise correlation in phase of the H $\alpha$  data obtained with the Isocon and the observations just discussed was not possible.

### *The Repeatability of Successive Cycles*

A comparison of the cycle-to-cycle change in the character of the 'discontinuity' preceding stillstand was used as one test of the repeatability of successive cycles.\* The relevant portions of the velocity curve shown in Figure 5.1 are displayed with much greater time resolution in Figure 5.2. Three-minute means computed at one-minute intervals by Method II are given. The curves thus show the shift in the 'center-of-gravity' of the entire line profiles.

No significant cycle-to-cycle differences are apparent in this case. There have been previous indications, however, that they may occur. Odgers (1956) noted a lack of repeatability between successive cycles in one instance, but attached no great significance to it because of inaccuracies in the data. The data obtained with the Isocon in September 1971 also gave some evidence of a difference (Goldberg et al., 1972), but the result was clouded by instrumental problems.

### *The 1971 Data*

Some of the velocities obtained with the Isocon in 1971 are shown in Figures 5.3 and 5.4. Only portions of cycles, with emphasis on the phase of the 'discontinuity' preceding stillstand, were recorded. The 1971 data are of lower quality than those obtained in 1972 for several reasons: (i) the television system was not functioning as well; (ii) the observations

---

\*Further comparisons are made in Section 5.4 on the basis of the line profiles.

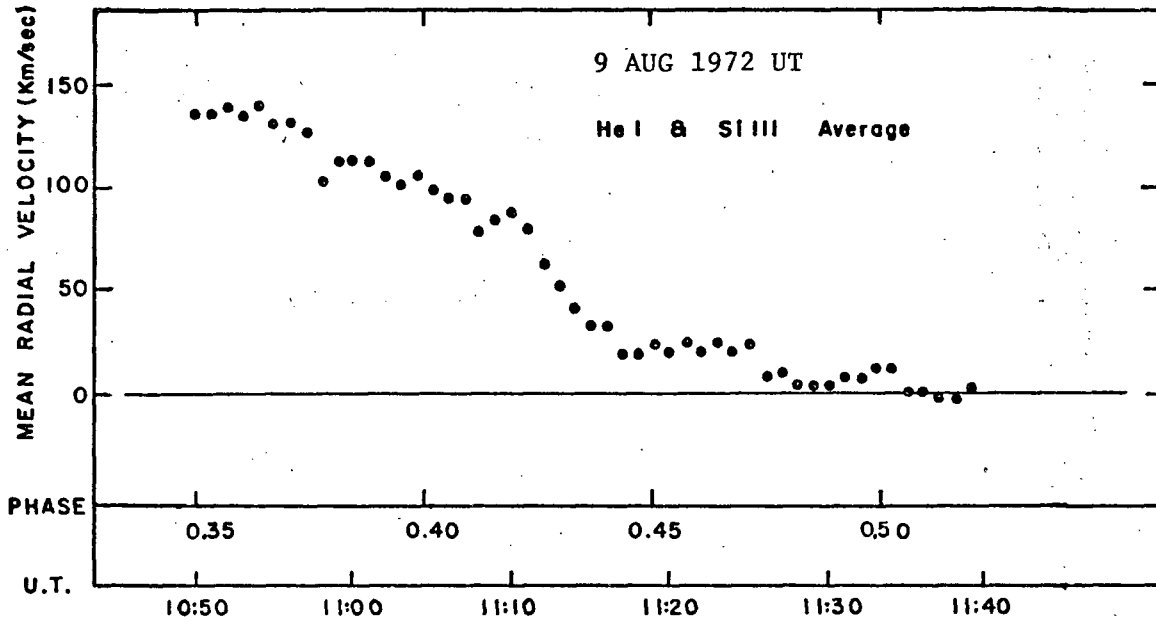
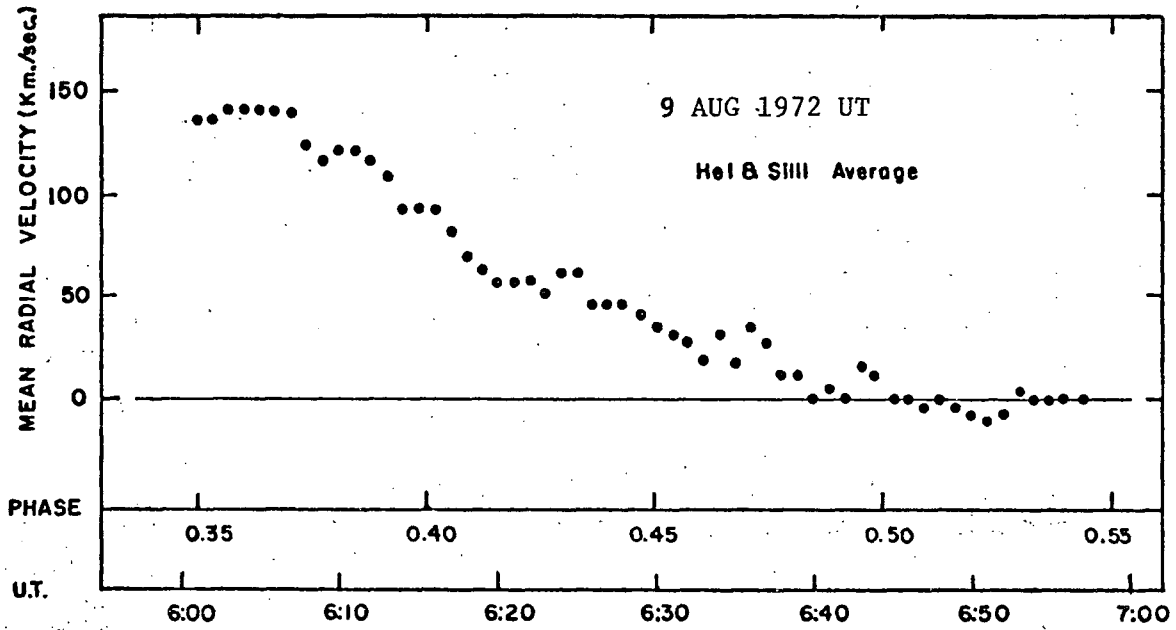


Fig. 5.2 Radial velocities for BW Vul on 9 August 1972 UT: the phases of rapid variation preceding stillstand. Successive cycles are shown.

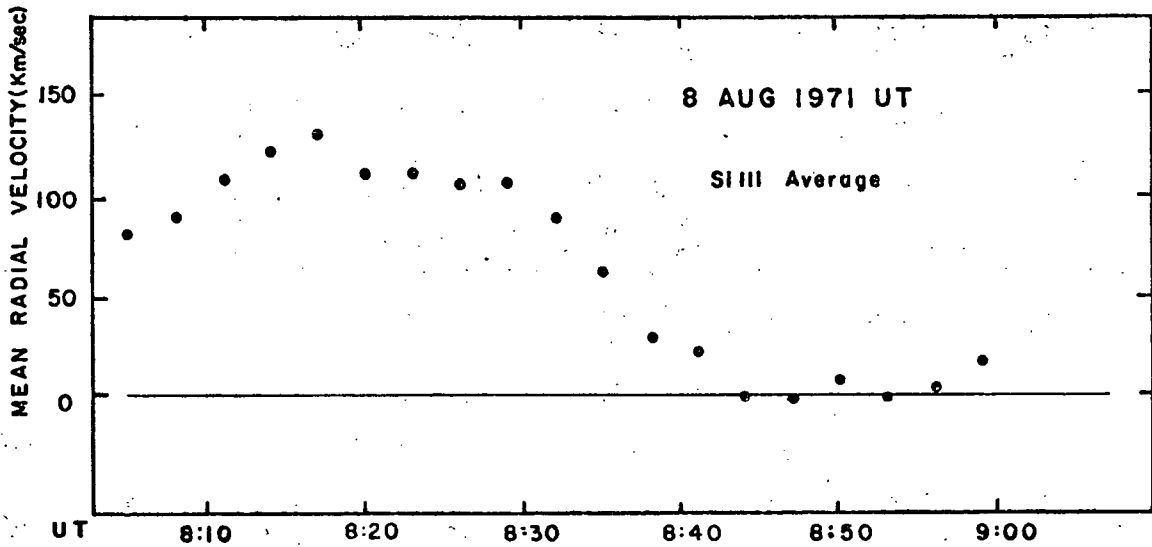


Fig. 5.3 Radial velocities for BW Vul on 8 August 1971 UT: the phases of rapid variation preceding stillstand.

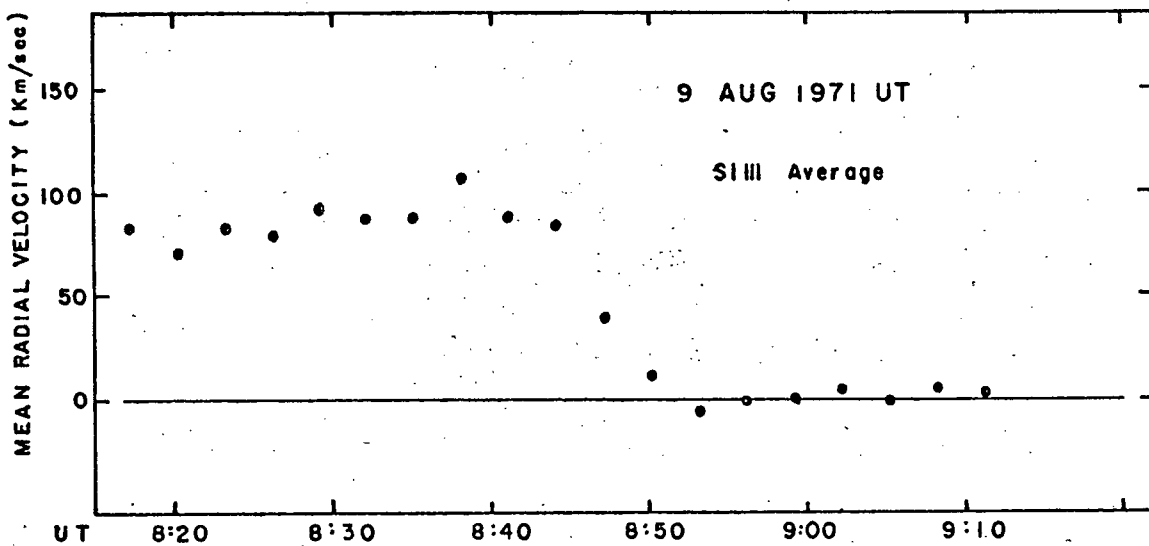


Fig. 5.4 Radial velocities for BW Vul on 9 August 1971 UT: the phases of rapid variation preceding stillstand.

preceded the adoption of more efficient coatings on the coudé optics; and (iii) observing conditions were generally not as good. The magnitude of these differences may be inferred from Table 5.I. The *character* of the 'discontinuity' preceding stillstand is virtually unchanged from 1971 to 1972. The amplitude of the velocity curve has decreased slightly, but not by enough to indicate a meaningful trend. The changes in the amplitude of the velocity curve are discussed further in Section 5.8.

#### 5.4 THE LINE PROFILE VARIATION

The character of the spectral lines changes significantly throughout the pulsation cycle. The changes in line profile are directly correlated with the changes in radial velocity and have the same period of variation. The pattern of the profile variation is indicated in Figures 5.5 and 5.6. The variation in line depth is plotted in Figure 5.7.

Certain deficiencies in the present data,\* which at times affected the accuracy of the continuum level, made precise determinations of equivalent widths difficult. For this reason, the equivalent widths and some of the other line parameters given by Kubiak (1972) are used as an aid in interpreting the present data.

The pattern of variation for the lines of He, Mg, and Si that were observed is as follows. At the  $V_0$ -crossing on the ascending branch of the velocity curve the lines are sharpest and deepest and essentially

---

\*Probably due to an intermittent light leak.

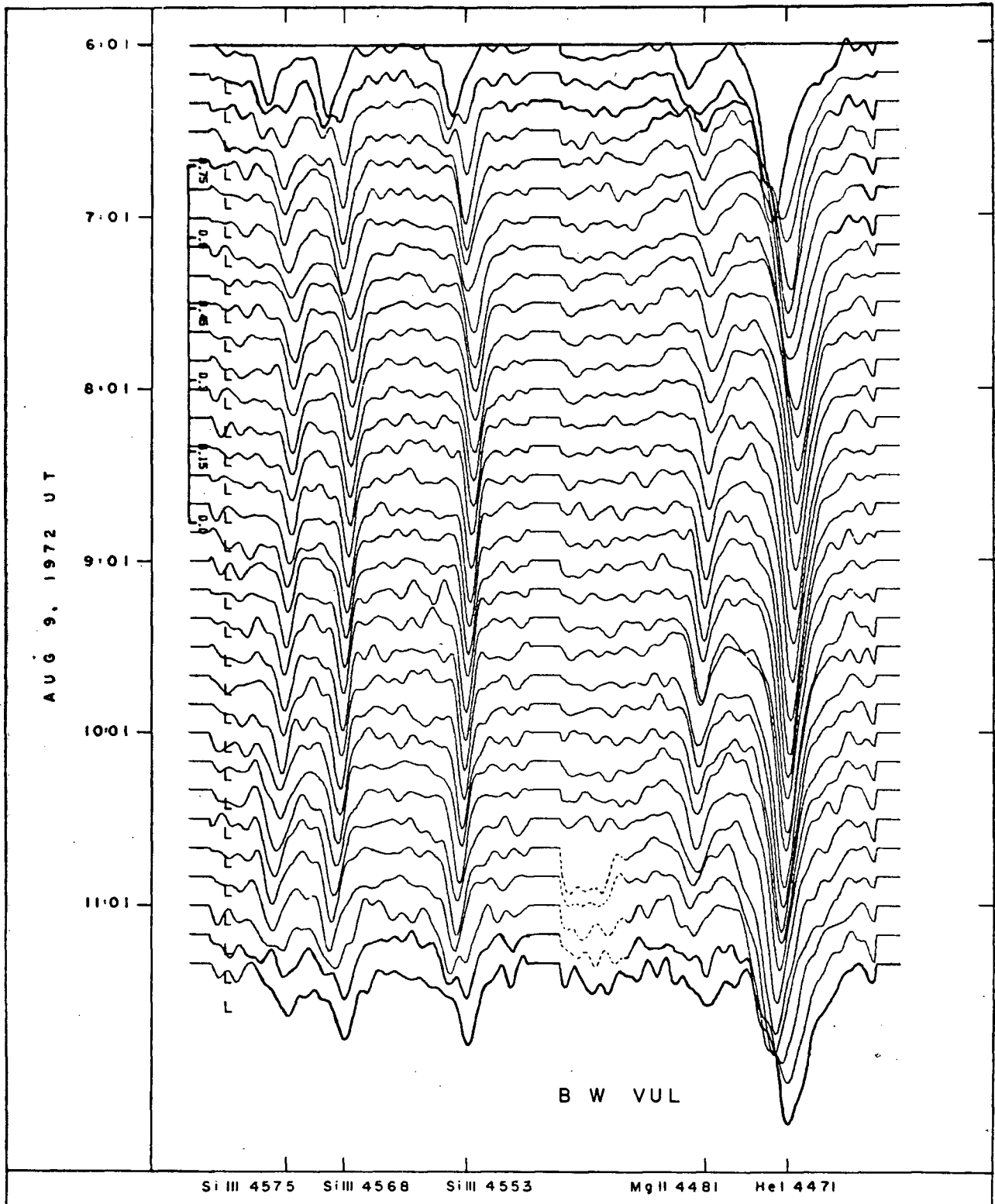
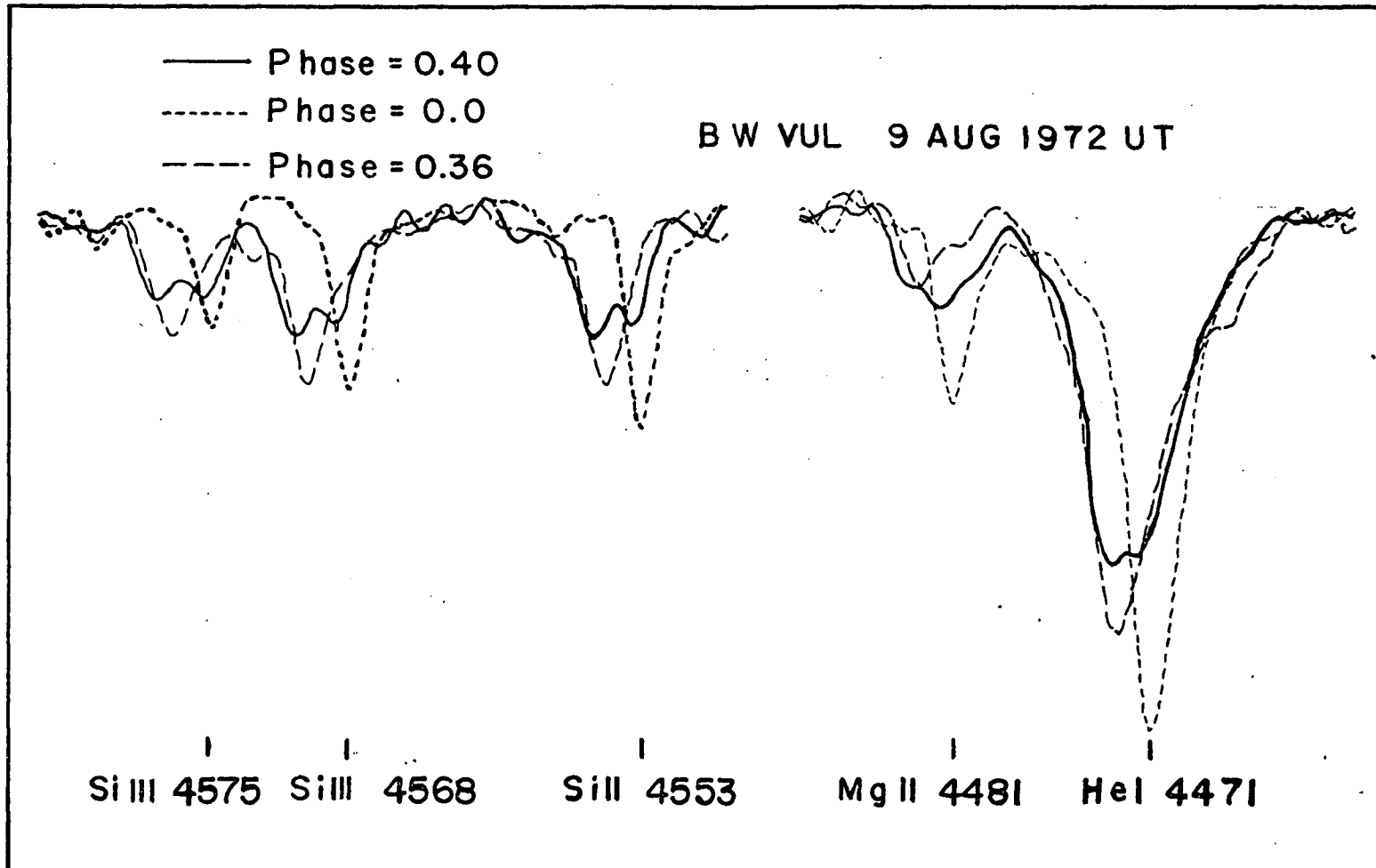


Fig. 5.5 Line profiles for BW Vul on 9 August 1972 UT: the variation over approximately one cycle.



44

Fig. 5.6 Line profiles for BW Vul on 9 August 1972 UT: a demonstration of the extremes in variability over one cycle.

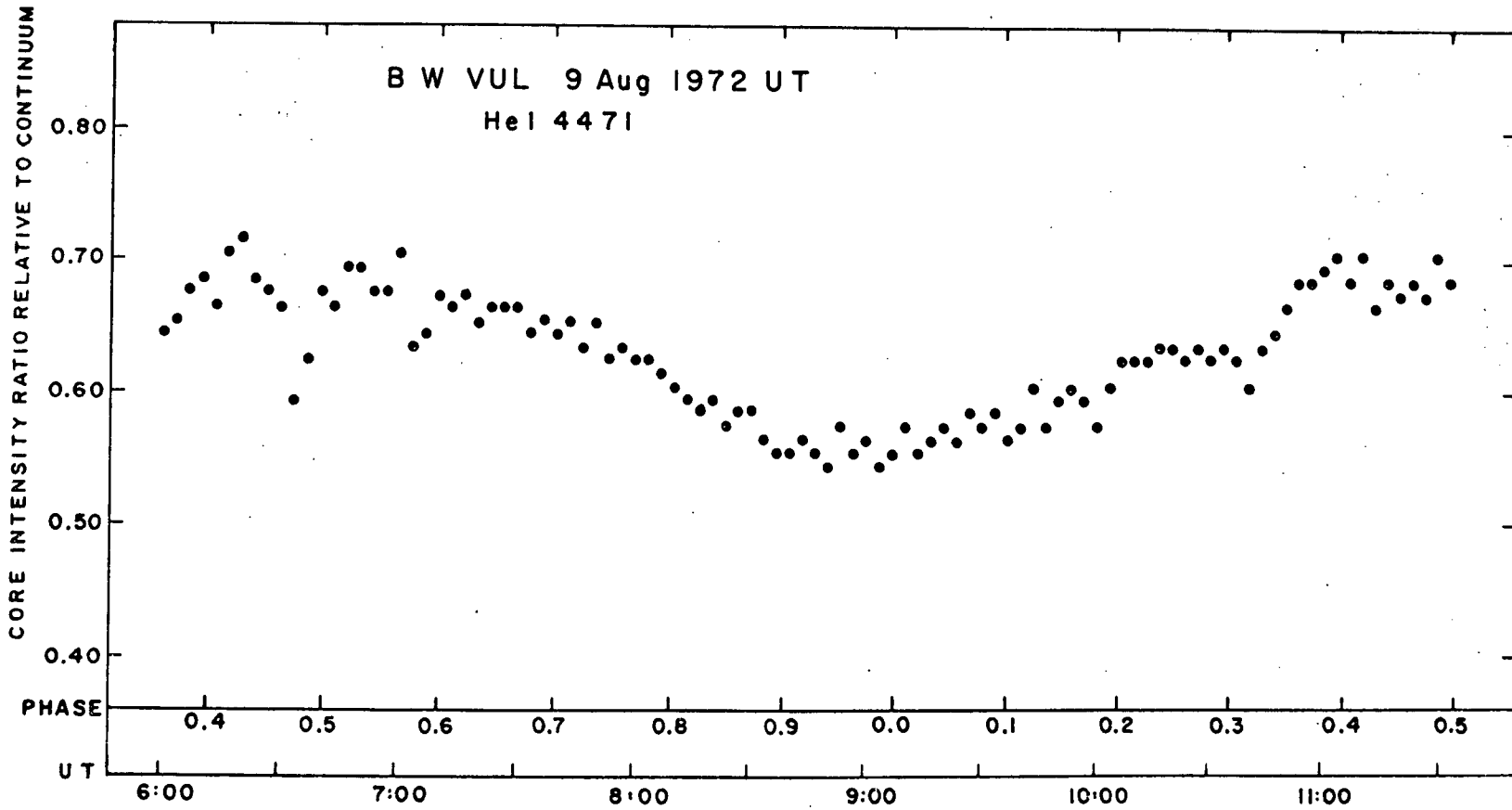


Fig. 5.7 The variation in line depth over 1.1 cycle for BW Vul on 9 August 1972 UT.

symmetric. As the cycle progresses, the lines became shallower, broader, and somewhat asymmetric. The change in the asymmetry appears to be correlated with the change in the slope of the velocity curve (i.e., with the acceleration). At phase  $\approx 0.35$  the lines begin to double as a component develops at approximately the  $V_0$  velocity. This component strengthens while the original red-shifted component weakens and eventually fades away (while its red-shift continues to increase). During stillstand the lines become sharper and deeper again, but less so than during the  $V_0$ -crossing at phase 0.0. During the blue-shift following stillstand, the lines became highly asymmetric, and there is some evidence to suggest that two components may exist for a short time (Odgers, 1956). As the magnitude of the velocity decreases, the lines become sharper, deeper, and more symmetric. The cycle then begins anew.

A more extensive analysis has been made of the profile variations during the phases of line doubling preceding stillstand. Profiles obtained on 9 August 1972 for these phases are given in Figures 5.8, 5.9, and 5.10; and those obtained on 9 August 1971 in Figure 5.11.

The profiles indicate the close repetition of successive cycles, as did the velocity curves discussed in Section 5.3. In comparing the two sets of profiles, differences in the signal-to-noise ratio should be noted. Accurate comparisons of the 1971 and 1972 profiles are difficult because of the substantial differences in the quality of the data. The gross variations are clearly similar for the two years.

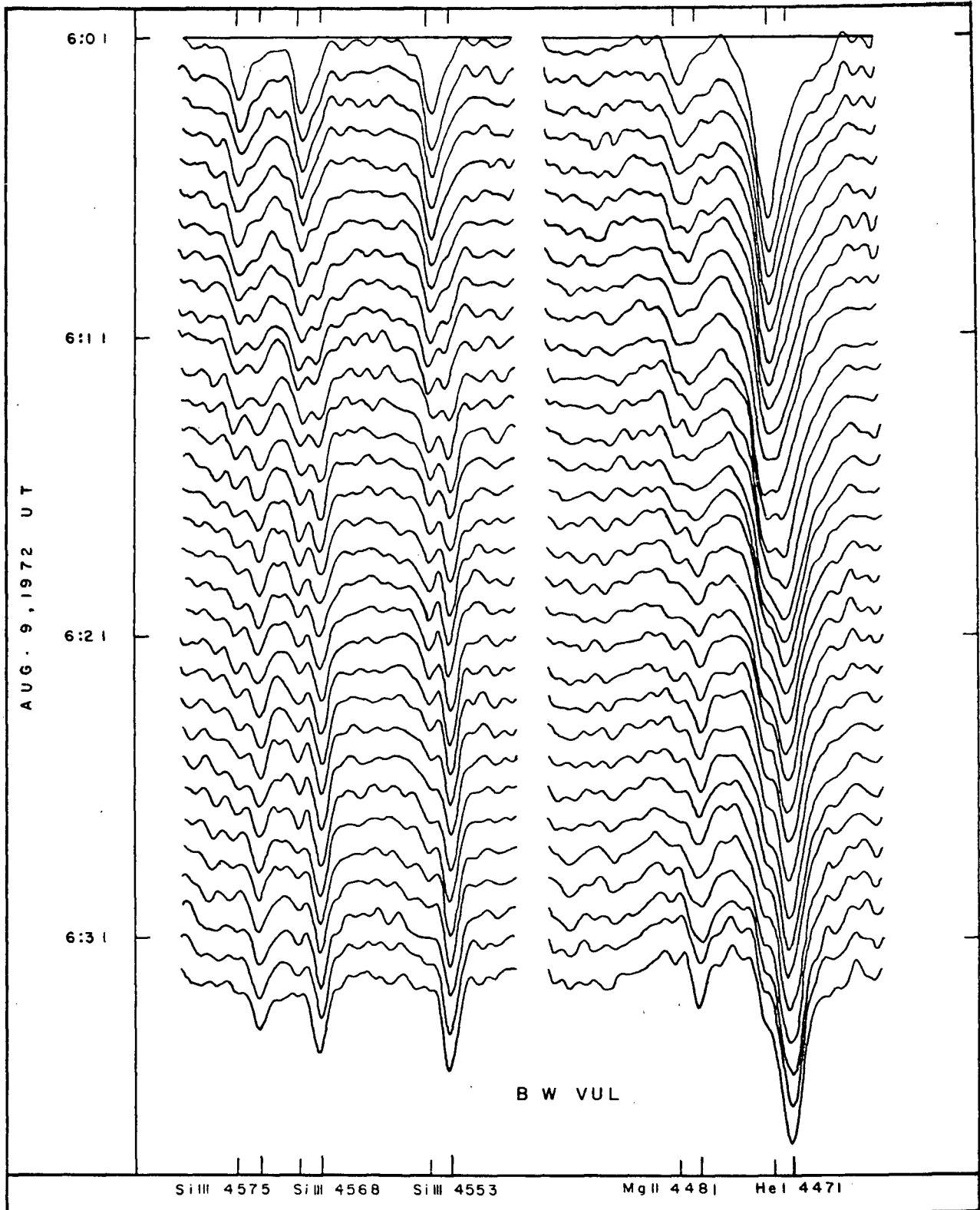


Fig. 5.8 Line profiles for BW Vul on 9 August 1972 UT: the phases of rapid variation preceding stillstand for the first cycle.

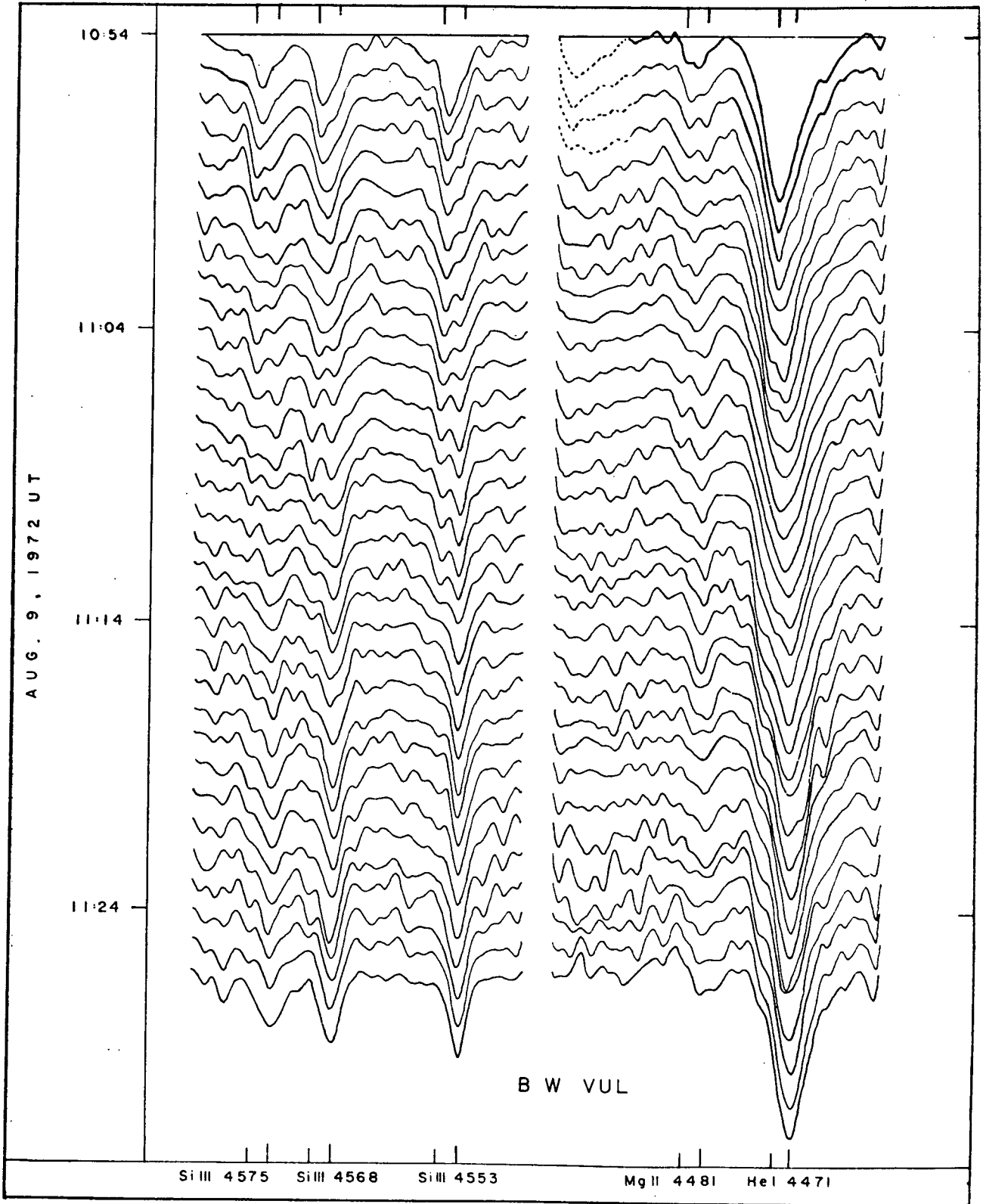


Fig. 5.9 Line profiles for BW Vul on 9 August 1972 UT: the phases of rapid variation preceding stillstand for the second cycle.

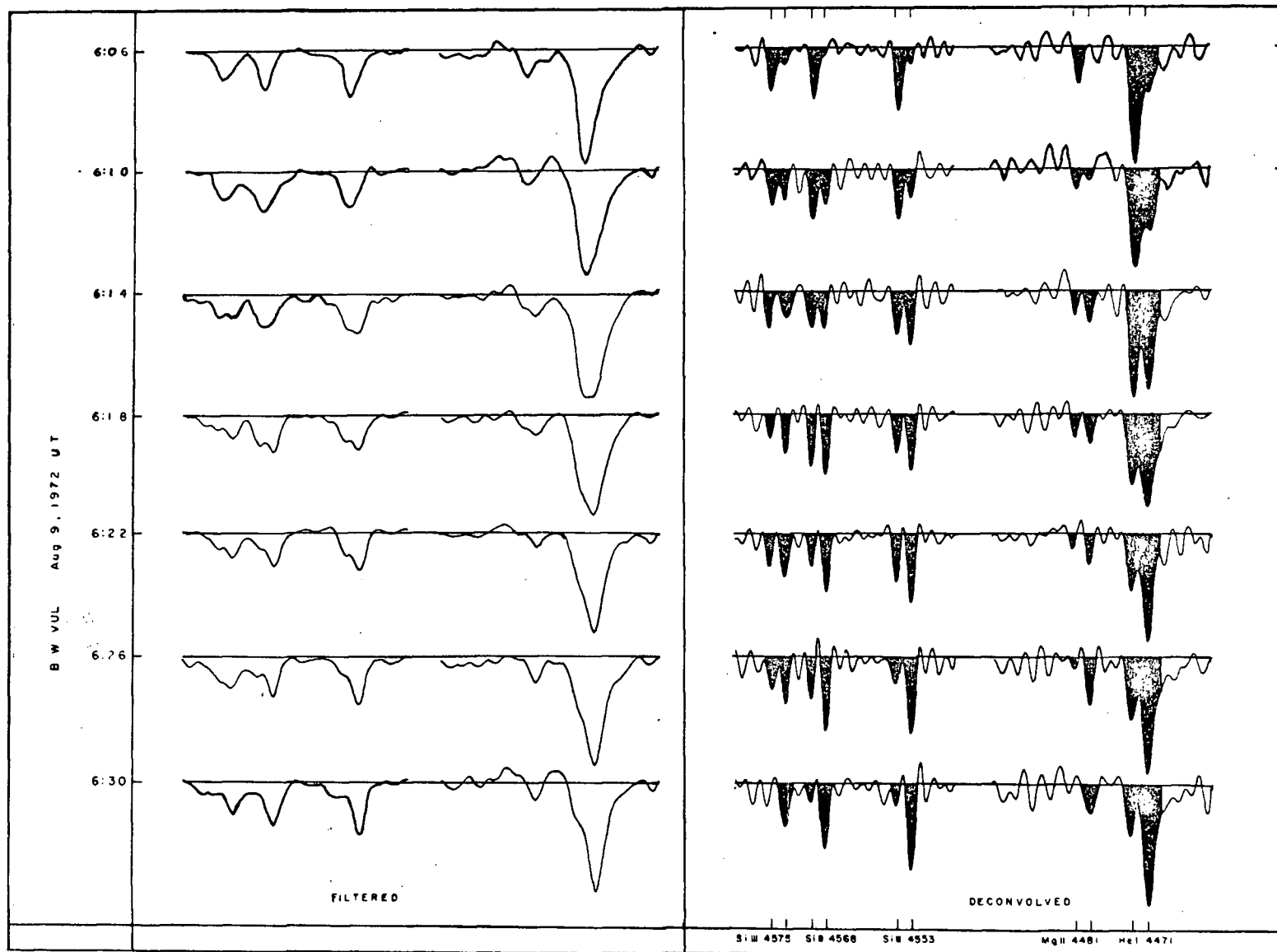


Fig. 5.10 Deconvolved line profiles for BW Vul on 9 August 1972 UT: the phases of rapid variation preceding stillstand for the first cycle.

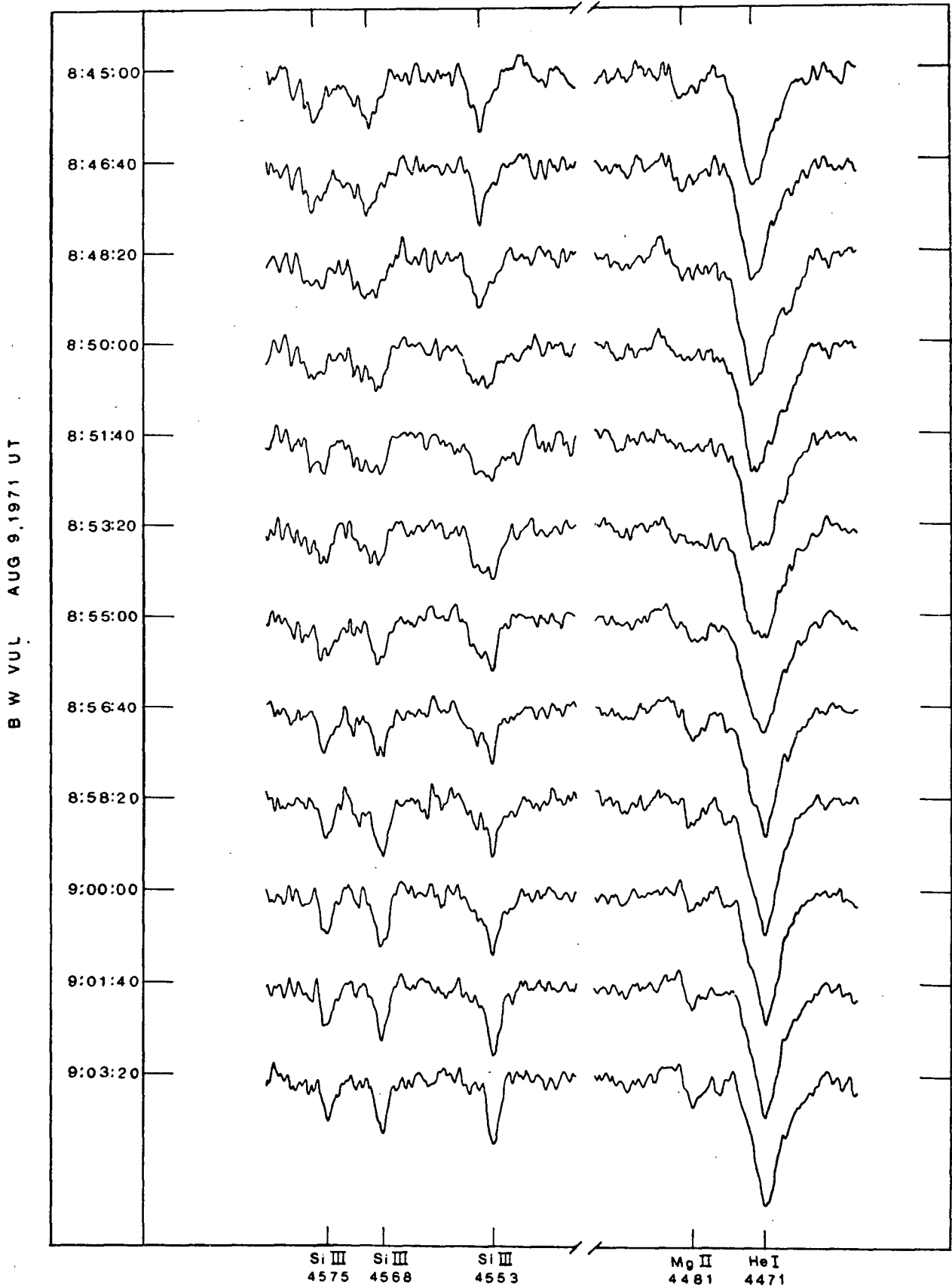


Fig. 5.11 Line profiles for BW Vul on 9 August 1971 UT: the phases of rapid variation preceding stillstand.

Intensity ratios and equivalent widths have been computed from the profiles of the first 'discontinuity' of 9 August 1972 (the latter from planimeter measures). These are given in Figures 5.12 and 5.13 respectively. The total equivalent width remains essentially unchanged during the doubling process, and both the development and weakening of components appear to occur in a smooth and regular fashion.

### 5.5 THE LIGHT VARIATION

Although further observations of the light variation have not been a part of the present investigation, measurements of this type are considered here because of their fundamental importance. Kubiak (1972) presents a set of observations made in a system closely matching the Stromgren  $u, v, b, y$  system\*. These data are given in Figure 5.14. As noted by Walker (1954), there is a variation in the amplitude as a function of wavelength, which agrees fairly well with the variation expected for a black body at the appropriate temperature. There is no detectable shift with wavelength of the times of maximum and minimum light. The star is bluest at maximum light (temperature class B 1.5) and coolest at minimum light (temperature class B 2.5). The amplitude can *generally* be accounted for by changes in the radius obtained by integration of the velocity curve, but attempts at applying semi-empirical tests of pulsation (such as Wesselink's method of points of equal color) to simultaneous observations of light and velocity have not been successful (Walker, 1954).

Kubiak obtains a relation between the Stromgren  $[C_1]$  index,

$$[C_1] = (u-v) - (v-b) - 0.2 (b-y) ,$$

---

\*Stromgren (1963).

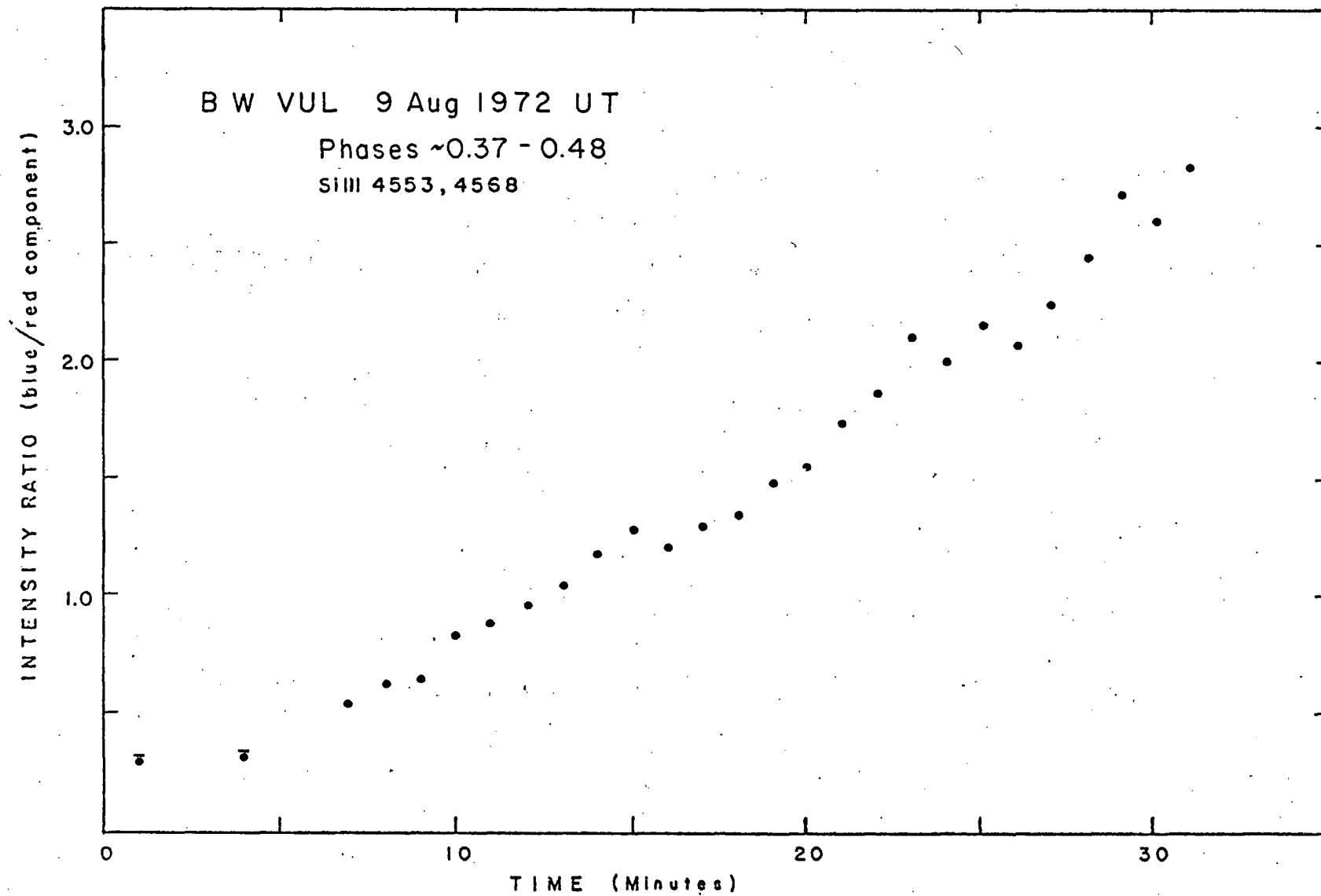


Fig. 5.12 Intensity ratios of the line components for the phases of rapid variation preceding stillstand for BW Vul on 9 August 1972 UT.

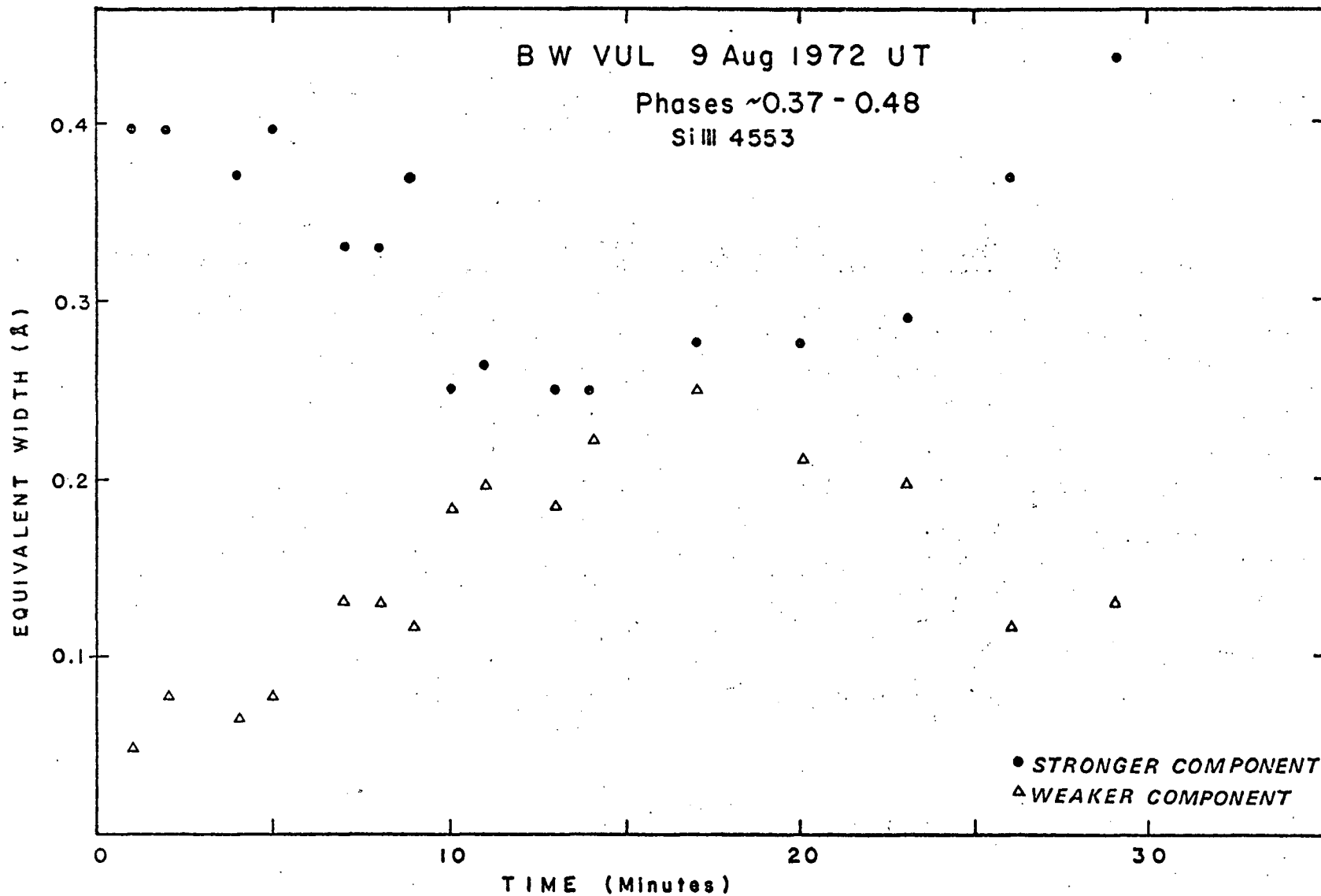


Fig. 5.13 Equivalent widths for the phases of rapid variation preceding stillstand for BW Vul on 9 August 1972 UT.

and the effective temperature:

$$\theta_e = 0.305 [C_1] + 0.188, \quad \theta_e = 5040/Te .$$

He justifies its applicability to BW Vul on the assumption of quasi-static equilibrium. A plot of the  $[C_1]$  index is given in Figure 5.15.

The interesting (and difficult to explain) features of the light curve are the stillstand on the ascending branch at phases  $\sim 0.3$  to  $0.4$  and the rise during velocity stillstand (during which there appears to be no significant change in radius).

#### 5.6 THE VARIATIONS IN RADIUS AND ACCELERATION

The displacement and acceleration of the atmosphere of BW Vul have been derived from the velocity curve of Figure 5.1 by graphical integration and differentiation respectively. The correction for center-to-limb effects (Parsons, 1972) has been applied to obtain the actual pulsational amplitudes. The displacement curve is given in Figure 5.16; the accelerations in Figure 5.17.

The radius of BW Vul is  $\sim 6.8 R_\odot$  or about  $5.0 \times 10^6$  km (Watson, 1972). The maximum displacement of the stellar atmosphere thus corresponds to a change in radius of about 10 percent. The general slope of the displacement curve resembles the trajectory of a projectile. The configuration of the curve for the phase of line doubling preceding stillstand is, to some degree, 'model-dependent'; since the  $V_o$  component appears in a discontinuous fashion, making a determination of its location (i.e., of the material from which it originates) impossible by simple integration techniques. Since the errors in the displacement curve are cumulative, the

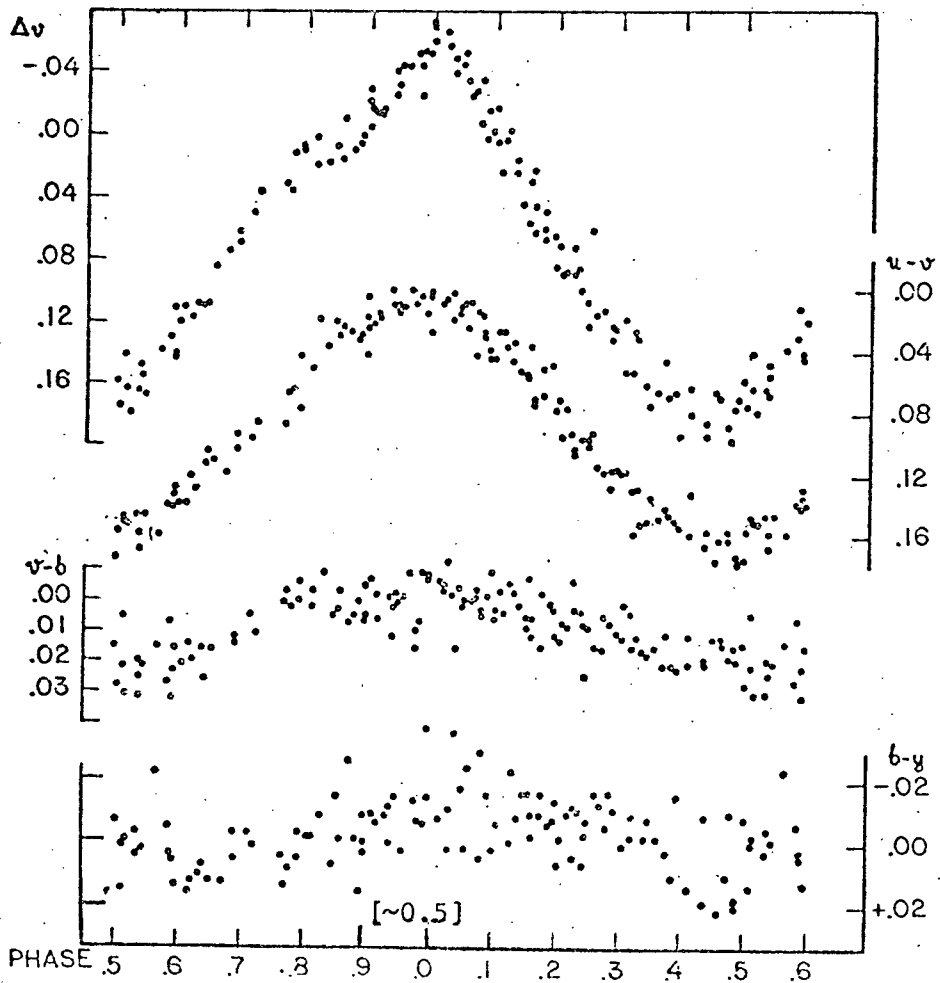


Fig. 5.14 Individual observations of the brightness  $v$ ; and of the Stromgren indices  $(u-v)$ ,  $(v-b)$ , and  $(b-y)$  for BW Vul. Taken from Kubiak (1972, p. 23).

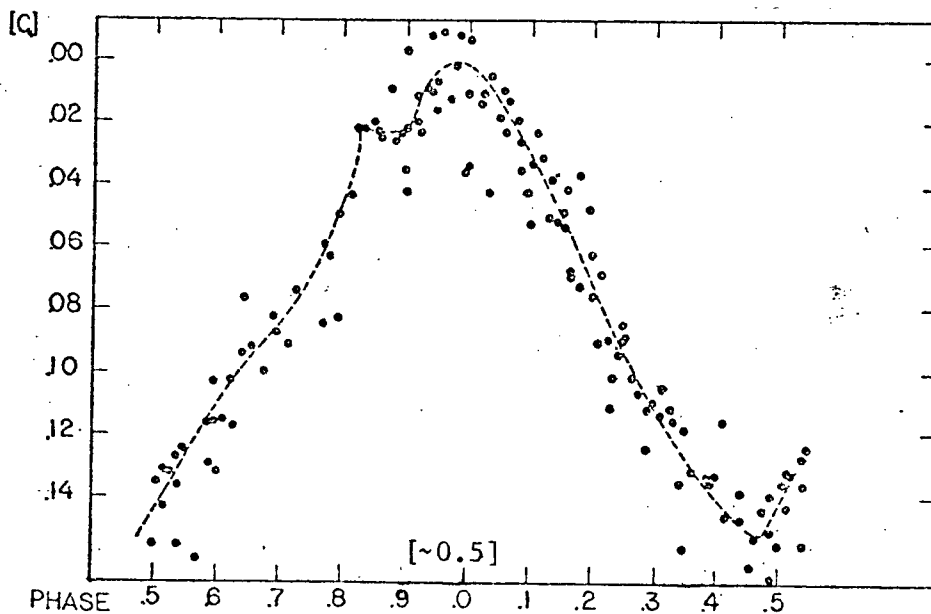


Fig. 5.15 Individual observations of the Stromgren  $[C_1]$  index. The broken curve is the adopted mean. Taken from Kubiak (1972, p. 27).

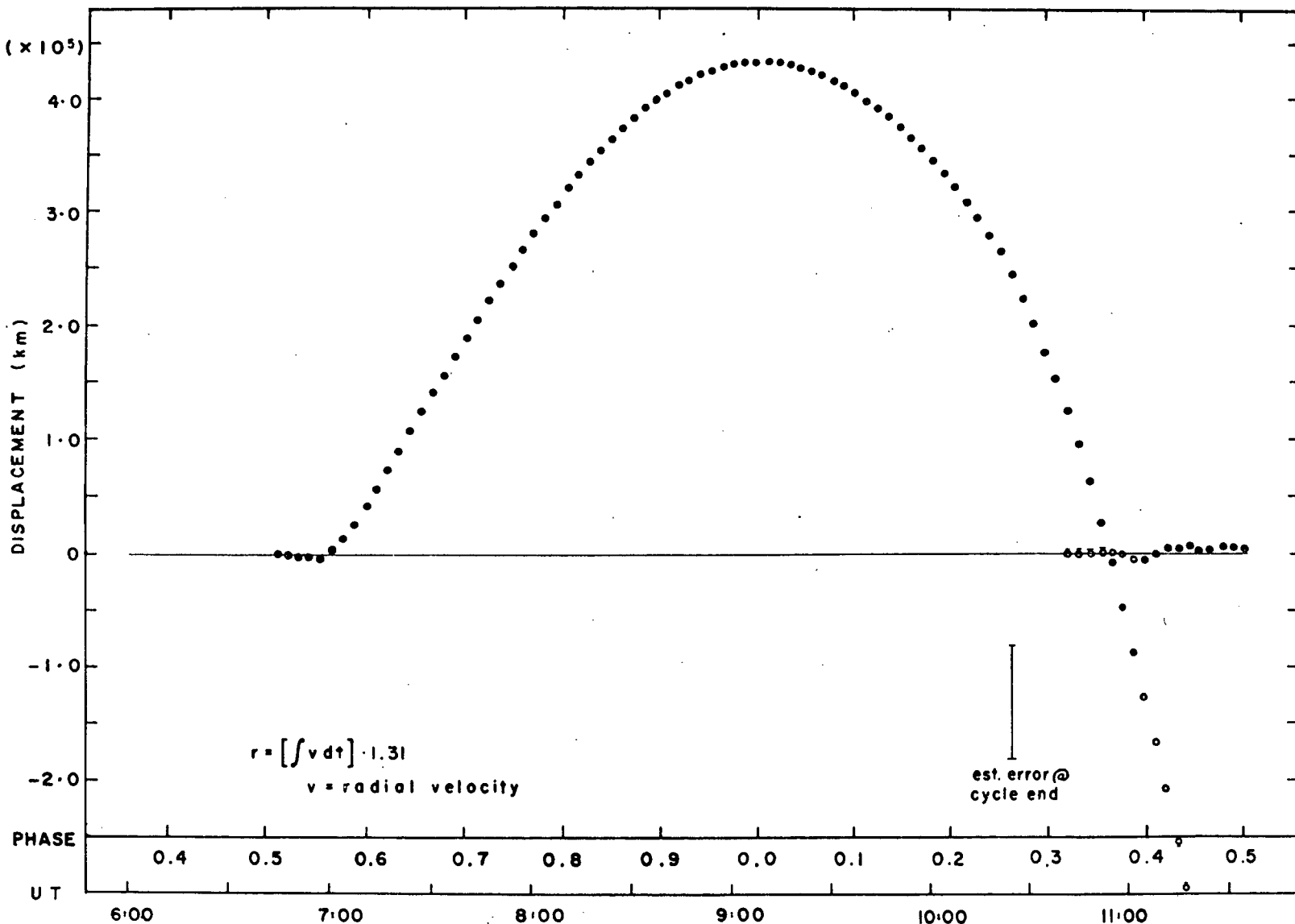


Fig. 5.16 The displacement curve for BW Vul on 9 August 1972 UT: 1.1 cycle of the pulsation. A hollow circle indicates the displacement obtained from the weaker component of a spectral line when two components are present. A bar over the circle indicates that the result is uncertain.

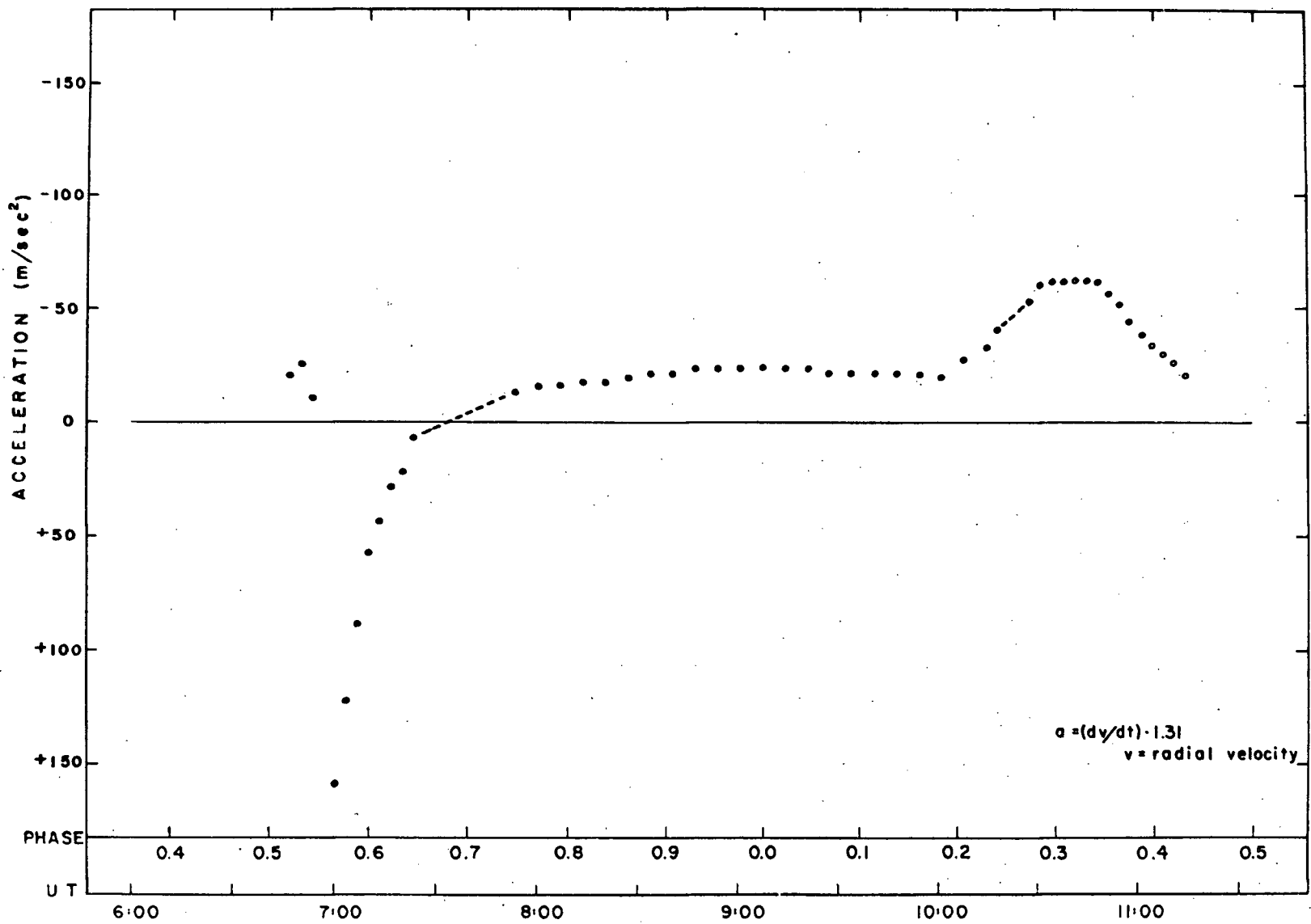


Fig. 5.17 The acceleration curve for BW Vul on 9 August 1972 UT: 1.1 cycle of the pulsation. A hollow circle indicates the acceleration obtained from the weaker component of a spectral line when two components are present.

results at successively later phases are less accurate. An estimate of the probable error near the end of the cycle is given in Figure 5.16.

The acceleration curve emphasizes the subtle changes in the velocity variation that are both real and error-induced, and thus *should be viewed with caution*. The improved time resolution and the internal consistency of the new data are particularly valuable in its determination.

Noteworthy features are the extreme accelerations following stillstand, the interval of nearly constant deceleration from phases  $\sim 0.7$  to  $0.2$ , and the rapid increase in deceleration at phase  $\sim 0.2$ . During the line-doubling phase preceding stillstand, the deceleration is, in a sense, indeterminate.

Odgers (1956) noted that the deceleration computed from the slope at the  $V_o$ -crossing on the ascending branch of the velocity curve was considerably less than the gravitational value calculated from the star's mass and radius. A value of  $\log g = 3.81$  or  $-65 \text{ m/sec}^2$  (corresponding to  $11 M_\odot$  and  $6.76 R_\odot$  for the mass and radius in the relation  $G = GM/R^2$ ) is given by Watson (1972). For the values of  $12 M_\odot$  and  $7.7 R_\odot$  (min.) given by Kubiak (1972), the result is  $g_{\text{sfc}} = -55 \text{ m/sec}^2$ . In comparison, the values obtained from the acceleration curve are  $\sim 24 \text{ m/sec}^2$  at the  $V_o$ -crossing,  $\sim 63 \text{ m/sec}^2$  at phase  $\sim 0.3$  just preceding the onset of line doubling (the maximum deceleration), and  $\sim +160 \text{ m/sec}^2$  following stillstand (the maximum acceleration). The maximum inward acceleration is the same order as  $g_{\text{sfc}}$ . During the phases of nearly constant deceleration the resultant of forces on the gas must be primarily composed of the gravitational force partly balanced by the gas and radiation pressure forces.

## 5.7 DISCUSSION

### *Introduction*

The problem of understanding the variation of BW Vul can be approached on several levels. A first-order analysis will yield some knowledge of the general character of the variation and the most important physical processes involved. Further, a full envelope calculation (i.e., a quantitative modeling of the entire atmosphere) is required to obtain a clear and detailed picture of the relation between the envelope pulsation and radiative and hydrodynamic phenomena. Such atmospheric models can incidentally be of benefit in a determination of the structure of the star as a whole since the parameters describing the atmosphere serve as the outer boundary conditions in certain stellar model computations. Finally, the interrelation between *all* relevant analyses; whether they concern the individual  $\beta$  Cephei stars, the class as a whole, or other types of stars, must be considered.

The *direct* analysis of BW Vul has so far proceeded only at the first level. There has been no detailed quantitative model capable of explaining the atmospheric variation over the entire cycle. Progress has primarily been made by (i) obtaining improved observational data; (ii) making detailed studies of certain critical aspects of the variation; and (iii) formulating general semi-quantitative 'models'. Odgers (1956) and Osaki (1971) have made contributions under one or more of these categories. Their work will be discussed in this section. In addition, several papers have attempted to interpret one aspect of the velocity variation in terms of detailed quantitative shock wave models. These will also be considered in this section in context with more general (but relevant) hydrodynamic

analyses.

The final part of the discussion will deal with a refined picture of the overall variation, incorporating results obtained from the new observational data.

#### *Previous Interpretations*

Odgers (1956) has developed a semi-quantitative model to explain the principal features of the variation. His interpretation is based on the following picture.

... It is supposed that an atmosphere is ejected with high velocity which after travelling outwards for a time then falls back into the general stellar photosphere at high speed. For a time at the stillstand phase the stellar surface proper is visible and then another atmosphere is ejected.

Material is ejected at phase  $\approx 0.55$  by a relatively high Mach number shock wave to form an 'atmosphere' or envelope (essentially a density maximum) separated from the original photospheric layers. The recession of this envelope through the relatively stationary photosphere is assumed to be the cause of the line doubling preceding stillstand. The developing  $V_o$  component arises from the photospheric layers, the fading red-shifted component from the envelope. The rise in light during stillstand is attributed to heating from interaction of the layers. It is implied that the oscillation is purely radial and spherically symmetric in nature.

Osaki (1971) gives a detailed discussion of a particular type of pulsation model and concludes that the existence of non-radial oscillations by themselves can explain most of the fundamental properties of the  $\beta$  Canis Majoris stars. He attempts to show that the line profiles and the velocity curve resulting from a wave travelling in the same direction as the rotation, which is symmetric with respect to the equator; i.e., Ledoux's (1951)

$P_2^2$ -mode also considered by Christy (1966), are similar to those seen in BW Vul. A typical result for the line profiles and the corresponding velocity curve is given in Figures 5.18 and 5.19. The line profiles and velocity curve determined by Osaki bear general resemblance to those of BW Vul, but the time of line doubling is much longer. Furthermore, the model does not demonstrate some of the major structural features of BW Vul's velocity curve. For example, the model curve displays none of the relatively sudden changes in slope nor does it show the non-symmetry with respect to  $V_0$ . The lack of agreement may be due in part (as noted by Osaki) to certain simplifying assumptions made in deriving the model. Therefore a careful assessment of these simplifying assumptions is in order. The method by which the velocity curve is obtained (particularly when more than one component is present) must also be considered carefully while making comparisons.

Nevertheless the agreement between Osaki's model and the variation seen in some of the other  $\beta$  Cephei stars (such as 12 Lac) is quite remarkable. However, in the case of BW Vul it would certainly be more convincing if the time scale of line doubling in the model were more compatible with that observed. Based on the present state of knowledge of BW Vul, Odgers' picture of the variation appears more plausible. The propagation of shock waves in BW Vul's atmosphere, an important part of this picture, is discussed below.

### *The Role of Shock Waves*

Theories concerned with the propagation of shock waves have been applied to explain a number of astrophysical phenomena. As a result, there have been numerous discussions of the topic, some relevant to the case in point. A good general background is provided by Shapiro (1954), Zel'dovich

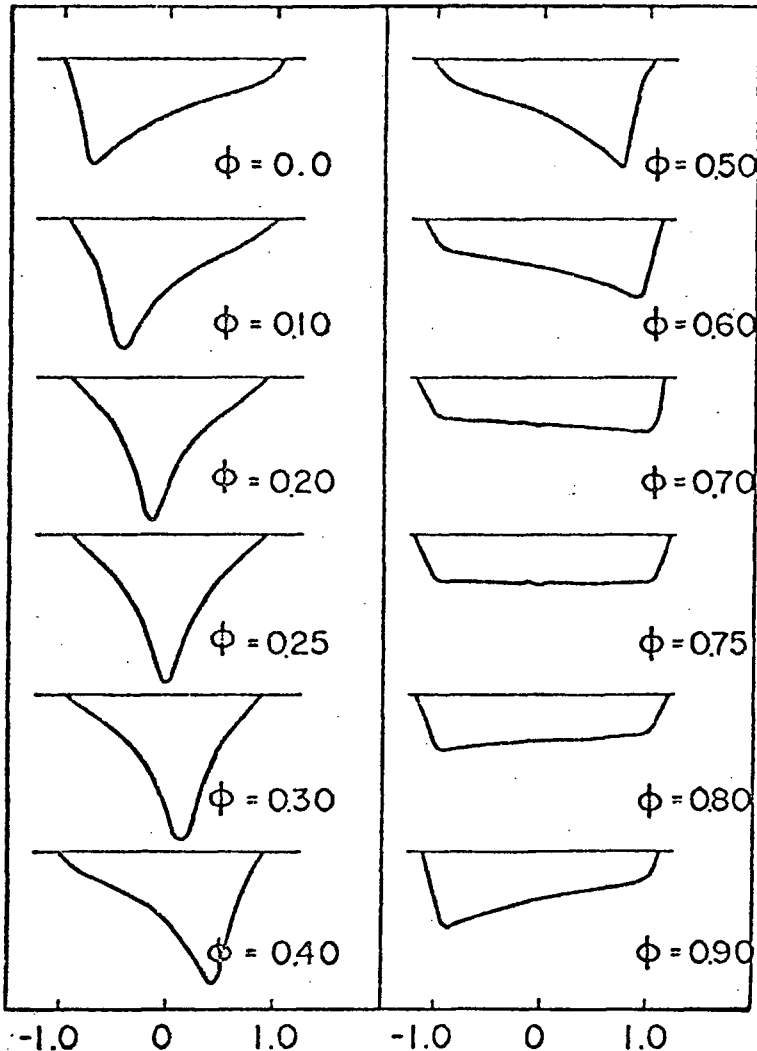


Fig. 5.18 Theoretical profiles for a star undergoing non-radial oscillations in Ledoux's (1951)  $P_2^2$  mode. The abscissa is  $\Delta\lambda/\Delta\lambda_R$  (or  $V/V_e \sin i$ ), where  $\Delta\lambda_R$  is the rotational width defined as  $\Delta\lambda_R = \lambda (V_e \sin i/c)$ ;  $V_e$  denotes the equatorial rotational velocity,  $i$  the inclination of its equator to the celestial plane ( $90^\circ$  for this case), and  $c$  the velocity of light. The ordinate uses an arbitrary scale and  $\Phi$  is the phase. A 'typical' result from Osaki (1971, p. 488).

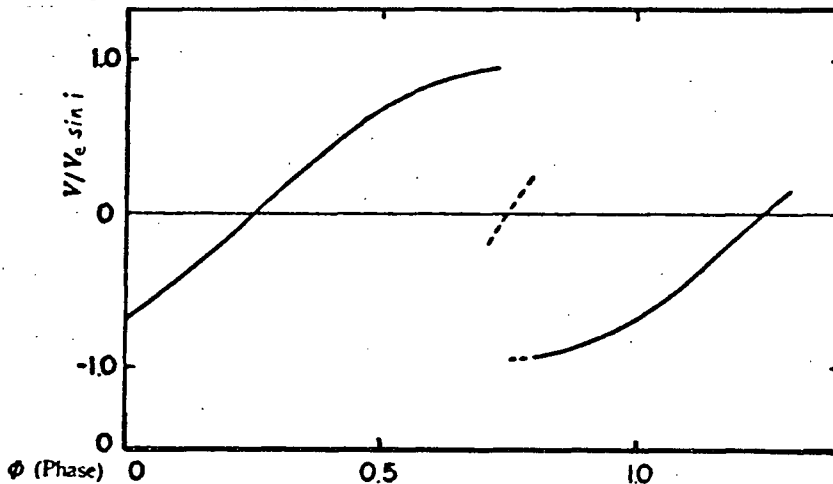


Fig. 5.19 The radial velocity curve corresponding to the line profiles given in Fig. 5.18. Taken from Osaki (1971, p. 489).

and Raizer (1966, 1967), and Thompson (1972), and a comprehensive discussion of the related astrophysical problems by Thomas (1967).

Evidence of shock waves has been found in several types of stars. Perhaps the most convincing is the emission in the Balmer lines and doubling of the metal lines in Population II variables (e.g., Castor, 1972). In BW Vul, the large accelerations and velocities (in context with the general pattern of variation) provide the primary evidence. There is also *direct* evidence for the existence of shock waves in the sun. The situation is highly complex even for such a 'normal' stable star (e.g., Wentzel and Tidman, 1969).

A few of the analyses have been reasonably thorough in attempting to define the relationship between the atmospheric oscillation and the associated shock wave structures [e.g., Hill (1972) and Keeley (1970) for R.R. Lyrae and long-period variables respectively and Hillendahl (1969, 1970a, b) for classical Cepheids]. Hillendahl constructed a series of radiative-hydrodynamic models which included an extensive atmosphere. A mechanism was identified whereby material was accelerated outward by a series of outward-moving shock waves, each followed by an inward-moving rarefaction wave. This *shock wave-rarefaction process* (hereafter termed the *Hillendahl Mechanism*) may have importance in the BW Vul variation.

Most studies of shock wave phenomena in stars have been based on a similar set of restrictive assumptions. The pattern has been to consider planar, hydrodynamic, isothermal shocks of a self-similar character propagating through an atmosphere which obeys a certain density law (see, e.g., Carrus et al., 1951; Laumbach and Probststein, 1971; Sachdev and Ashraf, 1971). In general, the 'strong shock' approximation is adopted and the

gas assumed to be collision-dominated. Turbulent, magnetic, and viscous stresses are ignored, as well as precursor effects; the ratio of specific heats is assumed to remain constant (although comparisons are made for different adopted values); the flow behind the shock is taken as isothermal (justified on the basis of the high rate of radiative transfer in the optically thin gas); and the physical conditions for the undisturbed gas are generally obtained from *static* stellar atmospheres when such models are required. Despite these many assumptions and restrictions, useful results are sometimes obtained.

A few shock wave studies have been aimed directly at BW Vul (Odgers and Kushwaha, 1959; Bhatnagar and Kushwaha, 1961a, b, 1963; Bhatnagar et al., 1971). All stem from Odgers' (1956) attempt to explain the velocities seen *after* the rapid blue-shift following stillstand, from phases  $\sim 0.6$  to  $0.9$ , by the *decay* of a shock wave of relatively high Mach number (about 6). All are similar in their approach, but each in succession offers refinements by incorporating the effects of radiation and magnetic fields. The problem as treated here is essentially that of blast wave propagation in a star (see, e.g., Sakurai, 1965; Korobeinikov et al., 1961; Kochina and Mel'nikova, 1958, 1960).

The existence of the shock is assumed *a priori* and the highest observed gas velocity taken as an initial condition - essentially the velocity of the gas seen *through* the transparent shock front when it first becomes visible. From that time, it is postulated that the shock front decays, with its energy ultimately being transferred to the gas.\* A rela-

---

\*The radiative flux *leaving* the star as a result of the process is not considered.

tion between the relaxation time of the shock and the velocity of the gas is derived and good agreement with the observed velocities obtained. The best agreement between the theoretical and the observed velocity curves is achieved by considering the decay of an isothermal shock in the presence of a weak magnetic field (about 2.1 Gauss) with a ratio of radiation to gas-pressure of  $\sim 0.2$  (Bhatnagar et al., 1971). The results are shown in Figures 5.20 and 5.21. On this basis, it is concluded that (i) the observed humps in the velocity curve at these phases can best be accounted for by the decay of a shock in the presence of a weak magnetic field; and (ii) that magnetic fields are important in the interpretation of the radial velocity variation in  $\beta$  Cephei stars. These conclusions are interesting, but probably not particularly significant in light of the scatter in the observational data, the substantial variation in the appearance of the fitted features between cycles, and the fact that similar features are seen in the velocity curves of other  $\beta$  Cephei stars (e.g.,  $\beta$  Cep and  $\nu$  Ari) where the pulsation amplitude is such that shock waves may be unimportant. It should also be noted that there is no observational evidence for the existence of magnetic fields in any of the  $\beta$  Cephei stars.\* An additional explanation of the humped appearance of the velocity curve is given by Bhatnagar and Kushwaha (1963) in terms of the interaction of incoming and outflowing material, and by the present paper. The general results of these analyses are important in that they lend strength to the shock wave hypothesis. The velocity changes and time scales are of the correct order of magnitude.

An alternative way of looking at the problem is to consider the effects that a shock wave would have on the characteristics of the gas (particularly its velocity) when passing with undiminished strength through

---

\* The effects of such a small field, however, would be virtually impossible to detect by present observational methods.

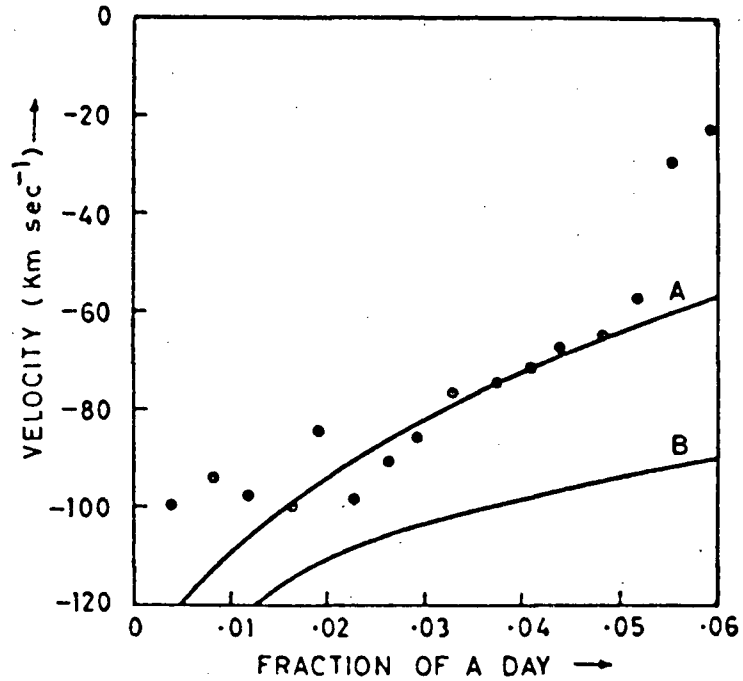


Fig. 5.20 Theoretical radial velocity curves; A and B respectively represent the cases for  $\alpha = 0$  and  $\alpha = 0.2$ , where  $\alpha$  is the ratio of radiation pressure to the gas pressure. The observations of Odgers (1956) during the cycle beginning J.D. 2435009.760 are represented by solid dots. Taken from Bhatnagar et al. (1971, p. 136).

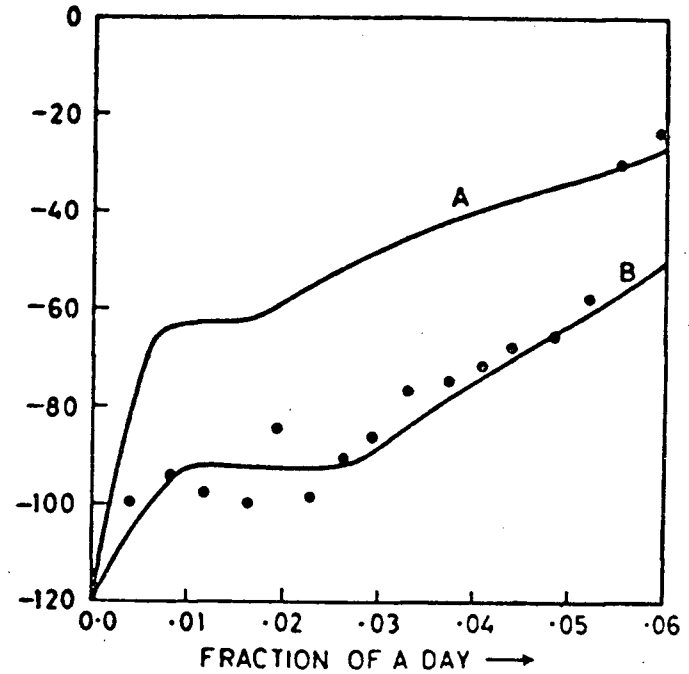


Fig. 5.21 The same as Fig. 5.20 but with the effects of a 2.1 Gauss magnetic field included. Taken from Bhatnagar et al. (1971, p. 136).

the region of the stellar atmosphere in which the spectral lines are produced. An approximate calculation of the shock conditions in this circumstance have been made using the model atmosphere grids of Gingerich (1969) and Van Citters and Morton (1970) and adopting the analytical procedures outlined by Sachdev and Ashraf (1971). The computations are given in Appendix E. Results obtained in this fashion are also compatible with the shock wave hypothesis. The analyses are too coarse to recommend a definite model.

The important problem of determining the behavior of a shock wave at the surface of a star where the density goes to zero has been considered by Zel'dovich and Raizer (1966), Gandel'man and Frank-Kamenetskii (1956), and Sakurai (1960).

#### *A Refined Interpretation*

A refined picture, which *attempts* to go somewhat further in explaining the more detailed aspects of the variation over the entire cycle and is compatible with most of the available observational data, is presented here in qualitative terms. It essentially stems from the basic idea proposed by Odgers (1956) and is based on the following assumptions:

- (1) The discontinuous nature of BW Vul's velocity variation is essentially an amplitude effect - the amplitude of the basic variation sufficient in this circumstance to promote the development of shock waves, which in turn are responsible for the ejection of an "envelope"\* and the extreme accelerations observed.
- (2) The velocity variation can thus be explained on the basis of two 'mechanisms':
  - a. Shock-induced mass motions

---

\*Essentially a density maximum separated from the general photospheric layers.

- b. Motion of the envelope and interaction between it and the underlying layers.
- (3) Beneath the optically thick (only in the line) envelope, the star is undergoing an essentially sinusoidal oscillation, similar to that displayed by stars such as  $\beta$  Cephei.
- (4) The oscillation of the general photosphere (and not that of the ejected envelope) is *most* decisive in the light variation.

A summary of the observed variation [from Kubiak (1972) and the present program] and a description of the proposed underlying oscillation is presented in Figures 5.1, 5.16 and 5.22 for general comparisons only. One cycle will be considered on the basis of this information. At phase 0.55, the approximate epoch of maximum light and minimum radius, and therefore the time of maximum compression of the gases, a compression wave is formed in the stellar atmosphere in the vicinity of the photosphere. The wave propagates outward with increasing amplitude and becomes a shock wave.

The effects of this shock (plus the rarefaction wave that *may* succeed it after its arrival at the stellar 'surface' as per the Hillendahl Mechanism) are observed as the extreme acceleration of the gas from phases 0.55 to 0.6. The velocity of the accelerated material increases rapidly and an envelope is formed above the original photospheric layers. Concurrently, the underlying layers begin their outward expansion, but are left behind by the rapidly accelerating envelope. The drop in temperature during this process takes place smoothly and is associated primarily with the underlying oscillation.

From phases 0.6 to 0.75, the velocity curve has the peculiar humped appearance described in Section 5.3. This effect is associated with the formation of a rarefied region behind the envelope as it separates further from the general photosphere. As this occurs, the gas pressure

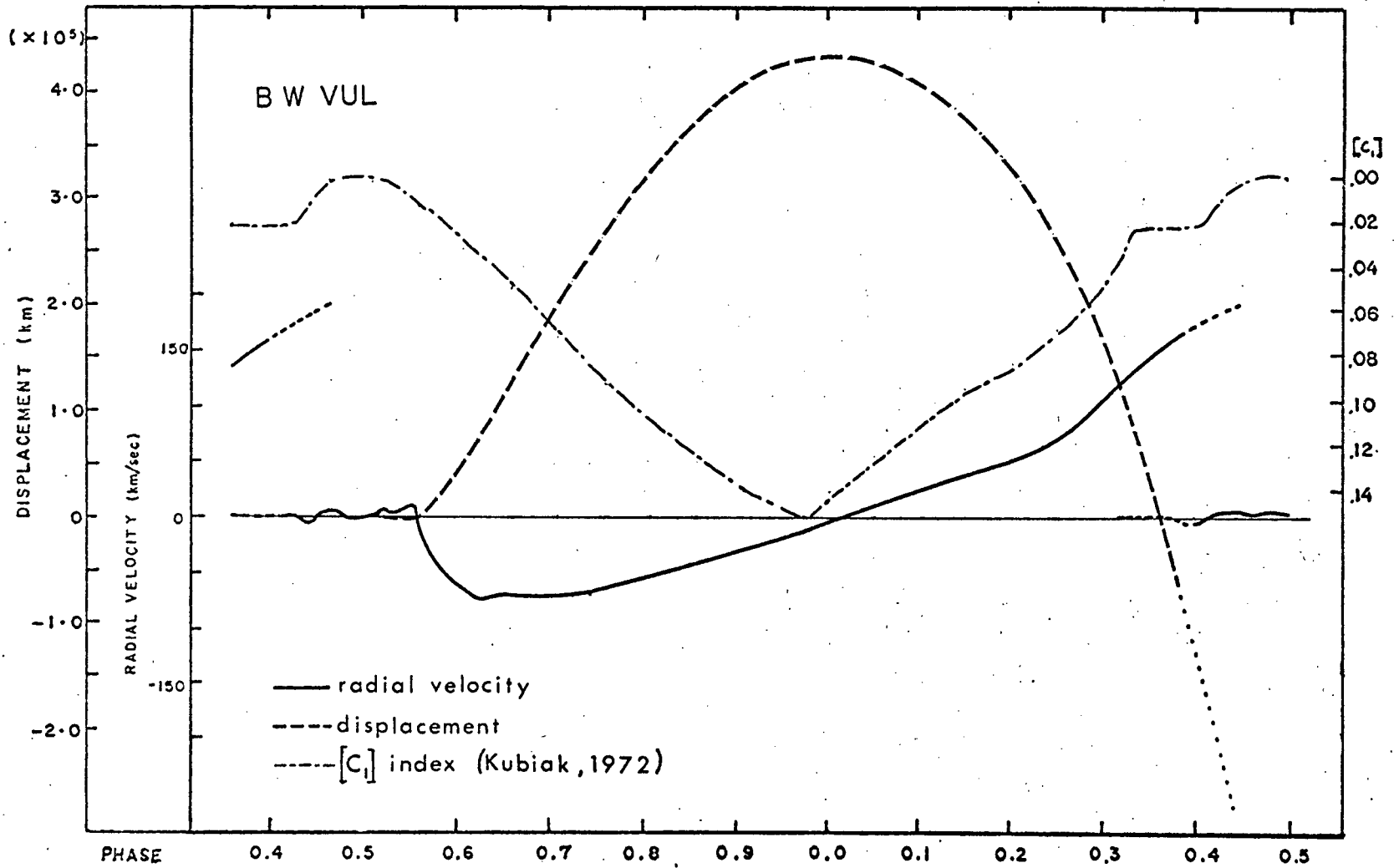


Fig. 5.22 A summary of the observed features of the variation of BW Vul.

from the underlying layers decreases. The pressure forces increase significantly again at phase 0.74, when the underlying layers 'catch up'. A slight increase in the outward velocity at this time is indicated by some of the previous data.

The motions of the envelope and its underlying layers are essentially parallel until phase 0.2. Throughout this interval, the deceleration of the envelope is nearly constant, but substantially less than the gravitational value; due to the modifying effects of gas and radiation pressure. The envelope reaches its maximum altitude in this interval and the variation in temperature continues in a smooth fashion.

Near phase 0.2, the underlying layers begin to recede from the envelope, again producing a rarefied zone with an associated reduction in the force of gas pressure on the envelope. The deceleration of the envelope increases until it approaches the free-fall value ( $g_{sfc}$ ) at phase 0.3 at which it remains for about 0.05 cycle.

At nearly the same time as the free-fall acceleration is attained, the lines become double, with the appearance of a weak component at the  $V_0$  velocity. The outward features of this process have been discussed in Sections 5.3 and 5.4. An explanation of its physical significance will be deferred to the following section. The line doubling terminates at phase 0.45 with the disappearance of the original component, now highly red-shifted.

During the phases of line doubling, the envelope rejoins the general photospheric layers. A stillstand in temperature is observed over much of this interval.

During the latter part of stillstand (phases 0.45 to 0.55) con-

traction of the star continues until minimum radius and maximum temperatures are again reached. A part of the temperature rise that takes place during this interval is probably due to factors other than the simple contraction of the photosphere.

*The Line Doubling Phase Preceding Stillstand*

The line doubling preceding stillstand appears to be a complex process with no simple explanation. The displacement curve indicates that it may begin due to the onset of transparency in the envelope and may end with the passage of the envelope into the general photospheric layers, the highly red-shifted component originating from increasing optical depths. Precisely how the transparency in the envelope may occur, why the new components develop at the  $V_0$  velocity and remain there, why the components remain so sharp and distinct, why the total equivalent width remains nearly constant, why there is a lag in the hydrogen line velocities, and why the stillstand in light occurs, are some of the questions that may be answered by a detailed quantitative analysis. Some of the possible 'mechanisms' are:

- (1) Onset of transparency in the falling envelope (the red-shifted component arising from the envelope, the  $V_0$  component from the photospheric layers below it).
- (2) Physical interaction between the falling envelope and the photosphere (the red-shifted component arising from the envelope, the  $V_0$  component from the photospheric layers above it).
- (3) Shock wave (or shock wave-rarefaction) ejection of material to a location above the envelope (the red-shifted component arising from the envelope, the  $V_0$  component from the ejected material above it).
- (4) Non-radial pulsations.
- (5) The movement of 'spots' (localized regions having particular characteristics) along the stellar equator, as suggested by Struve (1950) as a possible explanation for the spectral changes in 12 Lac,

Considered individually, all of these suffer from certain fundamental deficiencies. Perhaps several in combination may provide the basis for a satisfactory explanation. On the other hand, perhaps none of them holds a clue.

### 5.8 THE LONG-TERM\* VARIATIONS

#### *Introduction*

The long-term variations in the period, and in the light and radial velocity amplitudes, are of particular importance from considerations of stellar evolution and stability. Studies of some of these parameters over time intervals of tens of years have been made for a few of the well-known  $\beta$  Cephei stars (e.g.,  $\beta$  Cep and BW Vul). Interpretation of the results has generally been difficult because of the small magnitude of the changes and the problems of instrumental and observational nonuniformities.

#### *Variation in the Period*

Petrie (1954) noted that an increasing period was required to explain the advancing phase with time of any part of the radial velocity curve. He found that the phase of  $V_0$ -crossing, on the ascending branch of the velocity curve, could be represented by the relation

$$\phi = +0.24 - 1.56 \times 10^{-5}(t-2,425,405) + 0.30 \times 10^{-8}(t-2,425,405)^2$$

between 1924 and 1952. The mean rate of change in the period over this interval was +3.7 seconds per century. The study was continued by Odgers (1956), and by Percy (1971). Approximate phases were computed from the

---

\*Relative to the pulsation period.

data obtained with the Isocon in 1971 and 1972. The results were compatible with those obtained previously. The character of the variation is shown in Figure 5.23.

The observed period changes appear to be significant. It is not clear whether they are continuous, or are the result of a number of essentially discontinuous changes. Furthermore, an ambiguity exists because of the possibility of a 'missing' cycle between successive measures. The *mean* rate of change is greater than that predicted by stellar evolution (Percy, 1971). If the observed changes represent a true secular variation, Lesh's hypothesis (Section 3.2) is strengthened.

There appears to be a pseudo-sinusoidal oscillation superimposed on the mean rate of increase. The physical significance of this oscillation is not clear. It is reminiscent of the changes seen in the periods of close binary systems, which are also a mystery. The effect may be statistical in origin, or it may be connected with the basic variation of the star.

#### *Amplitude Variations in the Light and Radial Velocity Curves*

Petrie (1954) found that BW Vul's radial velocity amplitude varied in an irregular fashion over short intervals and also appeared to be increasing with time. The increase in *semi-amplitude* amounted to  $\sim 16$  km/sec over the period extending from 1928 to 1952, the rate of increase being 0.7 km/sec/yr. If both the period and the velocity amplitude are increasing, the amplitude of the *pulsation* must be increasing as well.

Further increases in the velocity amplitude have been demonstrated by Odgers (1956), by Kubiak (1972), and by the present investigation. The data are shown in Figure 5.24. Part of this increase must be attributed to

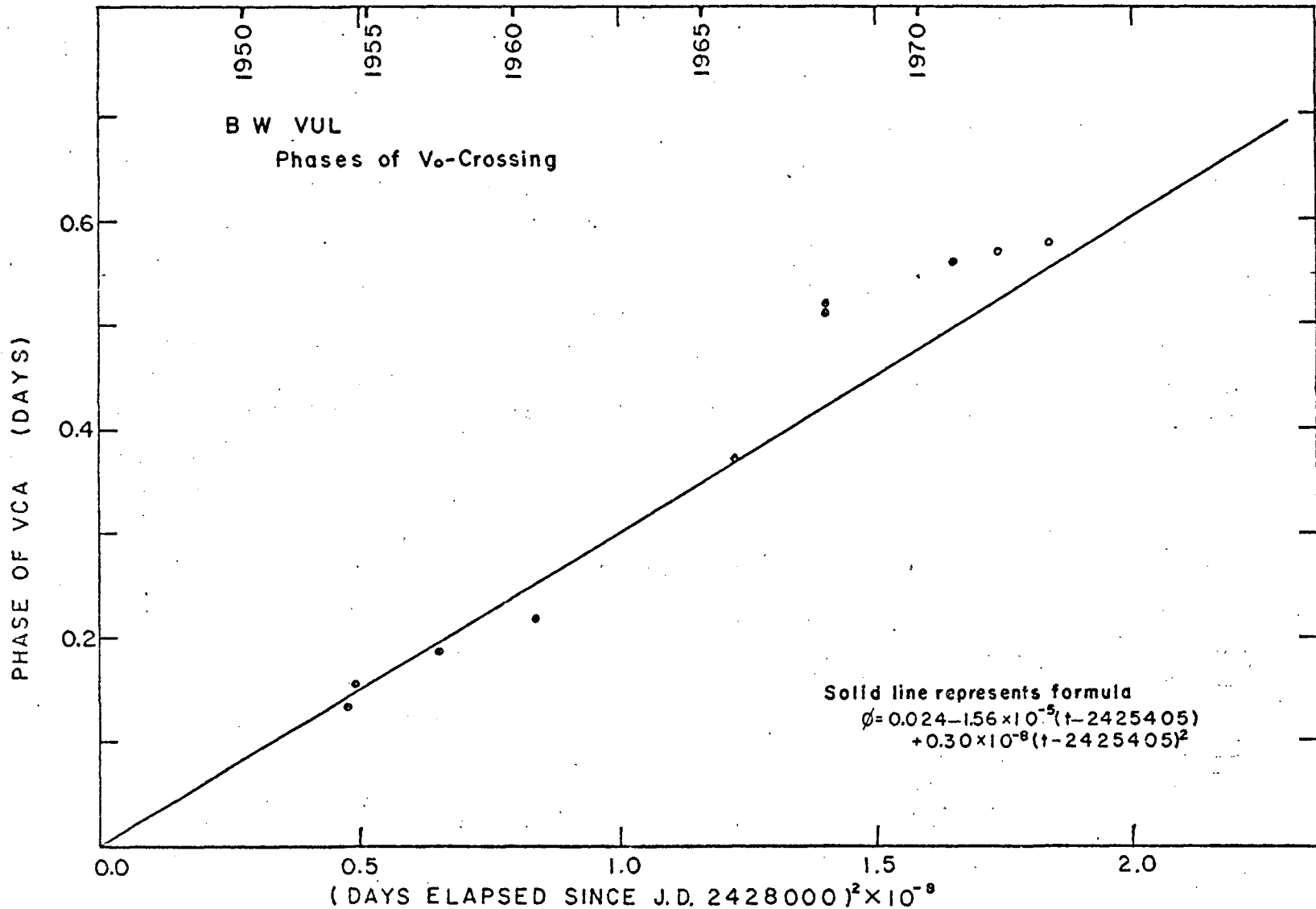


Fig. 5.23 The variation in the period of BW Vul as indicated by the phase of V<sub>0</sub>-crossing, plotted against the square of the time elapsed since J.D. 2428000. The line represents the relation found by Petrie (1954) to fit the observations of 1924-1952; the data are based on observations made since 1952 (the hollow circles from the present program). The Figure is taken from Percy (1971).

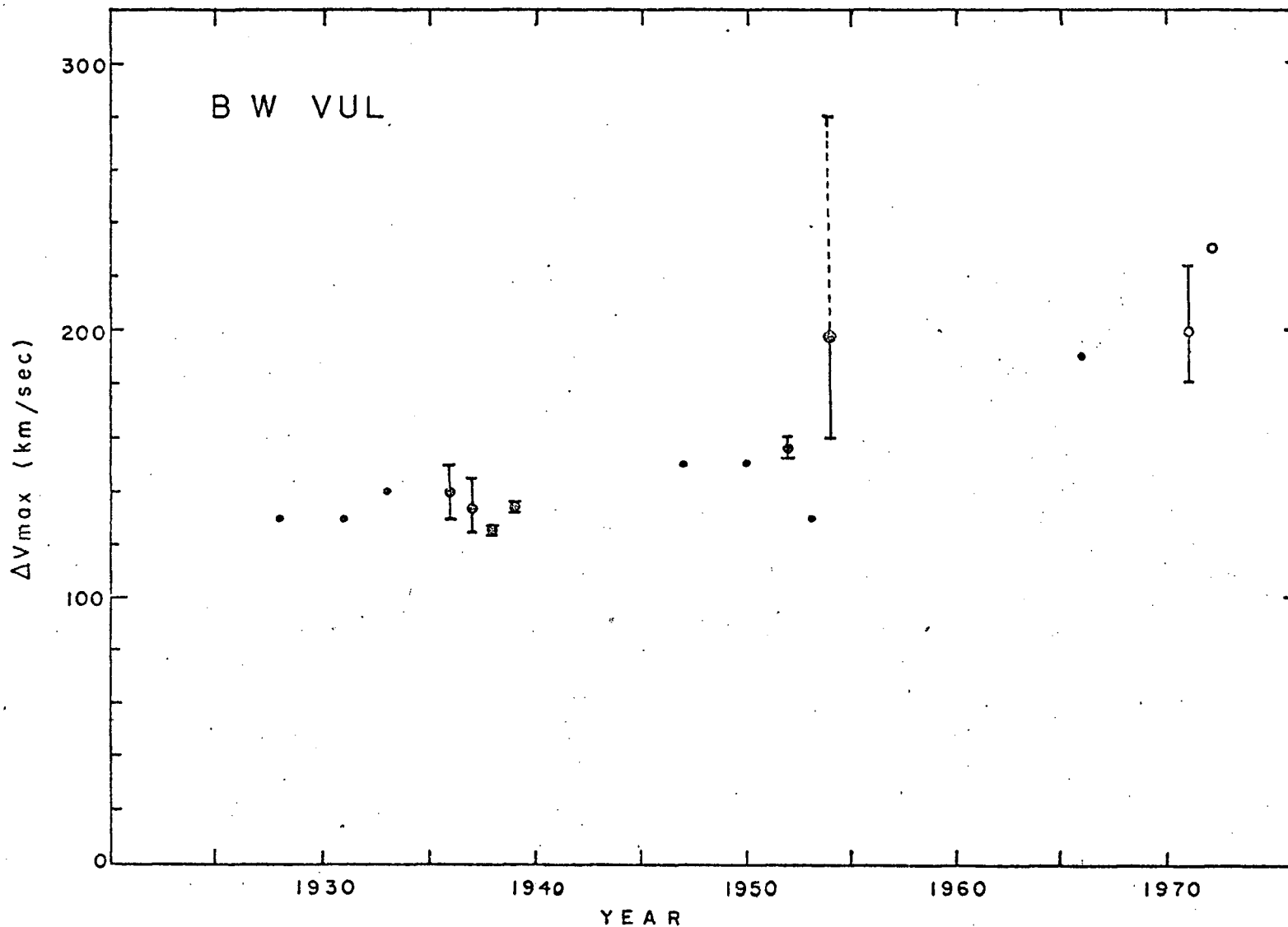


Fig. 5.24 The variation in the radial velocity amplitude ( $2K$ ) for BW Vul. The vertical bars indicate the range in the observed amplitude in a single year if there were more than one observation; the dots are the mean. Observations through 1952 are from Petrie (1954); from 1953 to 1954 from Odgers (1956), from 1966 from Kubiak (1972), and from 1971 to 1972 from the present program.

continuing improvements in the instrumentation, particularly since the recorded velocity amplitude is critically dependent on the time and spectral resolution realized during the phases of rapid variation. The sudden increase in amplitude observed in 1954 may have been due in part to improvements in the data. If the true variation is to be determined, all data must be compared on a uniform basis.

If the radial velocity amplitude has actually increased, an increase in the amplitude of the light variation might also be expected. Unfortunately, the photometric data are far less extensive than the spectroscopic and are quite nonuniform. There are some tenuous indications of an increase in the amplitude since 1938. There is also a considerable amount of scatter in the data. Huffer (1938) obtained a value of  $\sim 0.18$  mag. Kraft (1953) found that the amplitude increased from 0.19 to 0.23 mag. in the 'blue' during the period August 22-26, 1952. Eggen (1948) recorded a flaring of the star of an unknown amplitude. The most recent observations (Kubiak, 1972) provide amplitudes nearly the same as those obtained in the 1950's.

### *Summary*

The trend of an increasing amplitude in the pulsation of BW Vul as indicated by the increasing period and radial velocity amplitude seems to be real. However, the extent of this increase is not clear.

### 5.9 FUTURE WORK

The most immediate need is for an extension of the theoretical analysis, which has obviously lagged behind the observational study. Analysis of the present set of observations continues, with emphasis on obtaining better radial velocities through improved analysis techniques, and deriving useful information from the rather limited set of observations made at H $\alpha$  with the Isocon.

A continuing program of surveillance of the long-term changes in the period and radial velocity amplitude would be of considerable interest and value.

$\beta$  CEPHEI

## 5.10 INTRODUCTION

The star  $\beta$  Cephei has been labelled as the prototype of its class, having a 4.6-hour period of variation in light and radial velocity (its characteristics are given in Table 4.I). Its variable velocity was discovered by Frost (1902) and it has since been the subject of numerous spectroscopic studies, many of which have been summarized by Struve et al. (1953). The photometric observations have been relatively sparse, beginning with those of Guthnick and Prager (1914) and extending to those of Gray (1970) at widely-spaced intervals. Observations of  $\beta$  Cep in the UV have recently been made with OAO-2 (Fischel and Sparks, 1972).

The radial velocity variation of  $\beta$  Cep is *approximately* sinusoidal. The recorded range in amplitude is 18-46 km/sec, with small changes (of at most a few km/sec) between successive cycles.

The  $\gamma$ -velocity also varies from cycle to cycle. Fitch (1969) carried out a periodogram analysis using the velocity data obtained by Struve et al. (1953), and found a systematic variation in the  $\gamma$ -velocity which he interpreted as an orbital period of  $10.893^d$ . He also found a correlation between the pulsational velocity amplitude and the phase of the adopted orbital period. On this basis, minimum pulsation amplitude would occur at (or near) maximum tidal compression and maximum amplitude at minimum compression. Osaki (1971) noted, however, that the variation in the  $\gamma$ -velocity claimed as 'orbital' by Fitch could well be 'physical', resulting from a long-period modulation due to a superposition of two oscillations.

The light variation also appears to be sinusoidal, but has a minimum about 25% wider than the maximum (Gray, 1970). It is somewhat irregular and significant changes in amplitude between successive cycles have been noted. Stebbins and Kron (1954) have made six-color observations of  $\beta$  Cep in the UVBGRI system. A typical range in amplitude for one cycle was 0.057 mag. in U, decreasing to 0.011 mag. in I. The differences could essentially be explained in terms of a black-body radiation curve. The radiation curves were found to agree in phase. The color change was small, amounting to 0.007 mag. for V-G. The star was bluest at (or very near) maximum light in the usual pattern of the  $\beta$  Cephei stars. However, it was smallest at  $0.^P.04$  before radiation maximum, compared with  $0.^P.08 - 0.^P.12$  for this difference in several classical Cepheids.

Stebbins and Kron also tried to derive a radius for  $\beta$  Cep on the basis of the available light and radial velocity measures. On the condition that the ratio of amplitudes in short and long wavelengths agree with the computed ratio for small variations in the temperature of a B1 star at  $23000^\circ\text{K}$ , a value of  $9.0 R_\odot$  (with a large probable error) was obtained. It was obvious that simultaneous light and radial velocity measures were required if a reasonable accuracy was to be realized - primarily because of the significant cycle to cycle variation. Popov (1971) obtained a radius of  $8.0 R_\odot$  using Wesselink's method (Wesselink, 1946).

Conclusive evidence for a systematic line profile variation in  $\beta$  Cep has been long in coming. Observations of  $\text{H}\alpha$  by Greaves et al. (1955), which were briefly discussed by Wilson (1956), indicated a substantial variation in the  $\text{H}\alpha$  profile relative to  $\text{HeI } \lambda 6678$  as a result of incipient emission. It was thought that this variation was of a long-term nature and

thus probably not correlated with the pulsation cycle. Struve (1955b) did not share this view. He found that the emission feature was strongest half-way on the ascending branch of the velocity curve (in agreement with similar effects seen in other  $\beta$  Cephei stars) and noted further that some of the other hydrogen lines might also have been influenced by emission - as suggested by Karpov (1933).

Further evidence for a systematic line profile variation has come from the observations of OAO-2 (Fischel and Sparks, 1972). A total of 64 scans over 76 days covering 400 cycles of the pulsation were obtained of the region centered on the SiIV  $\lambda 1400$  and CIV  $\lambda 1550$  resonance lines. It was found that the strength of the CIV line (as determined from measurements of the flux at its central wavelength) followed the pulsation cycle, and that it also varied with a period of about 6 days - a variation shared neither by the continuum nor the SiIV line! The possibility that tidal effects related to Fitch's orbital motion were responsible for this variation was termed most probable. It should be noted that the CIV line is very luminosity sensitive while SiIV is not.

#### 5.11 THE NEW DATA

Observations covering  $\sim 0.8$  cycle of the pulsation period were made on October 16, 1972 UT. The Isocon plus the 5X transfer lens developed by E.H. Richardson of the D.A.O. was used to observe the SiIII  $\lambda\lambda 4553$  and  $4568$  lines. Observations were also made of the region centered on H $\alpha$  on September 2, 1972 UT with the silicon vidicon. Approximately one cycle was covered. The general features of these observations are given in Table 4.II

and the details in Table 5.II.

The data obtained with the Isocon provided *the first definitive record of a variation in line profile correlated with the variations in light and radial velocity*. The profiles are given in Figure 5.25 and measures of the radial velocity, line depth, and line-profile asymmetry in Figure 5.26. The *basic* pattern of variation in the line profiles is as follows. When the radial velocities are positive, the lines have a more pronounced absorption wing on the blueward side; when the velocity is zero, the lines are symmetric; and when the velocity is negative, the lines have a more pronounced absorption wing on the redward side.

This result represents a significant step toward defining the variation of  $\beta$  Cep. The change in the asymmetries of the profiles indicates that differential motion takes place in the atmosphere as a result of the pulsation. A comparison of theoretical and observed profiles *should* provide a critical test of the nature of this pulsation (which appears to be radial and spherically symmetric) as well as an indication of the limb darkening and the magnitude of the turbulent velocities (van Hoof and Deurink, 1952).

In more general terms, further weight is given to the notion that line profile variations are fundamental to the  $\beta$  Cephei phenomenon. Thus some degree of variation in the spectral lines, and the atmospheric motions that produce them, should be present in all of the  $\beta$  Cephei stars.

#### 5.12 THE LONG-TERM VARIATION

Struve et al. (1953) found a secular change in the pulsation period which he expressed as

$$P = 0.1904844 + 5.8880 \times 10^{-11} n + 9.8013 \times 10^{-17} n^2 ,$$

Table 5.II. Observations of  $\beta$  Cephei

Detector	UT Date	Julian Date 2441000+	H.A. @ Start	Frame Time (Minutes)	Effective Exposure Time* (Minutes)	Mean Effective Dispersion** (points/Å)	Quality Factor $\nabla$
Vidicon	2 Sept. 72	562.674-.689	2:50E	8.5	17	6	3
Isocon	16 Oct. 72	606.926-.965	6:08W	0.129	6	20	1
		606.968-.999		0.098	6	20	1
		607.000-.083		0.129	10	20	2-3

\*The 'best' compromise between time resolution and the signal-to-noise ratio (the average over the time interval).

\*\*The average over the region of interest.

$\nabla$ An estimate of the quality of the data (1 = excellent to 4 = poor).

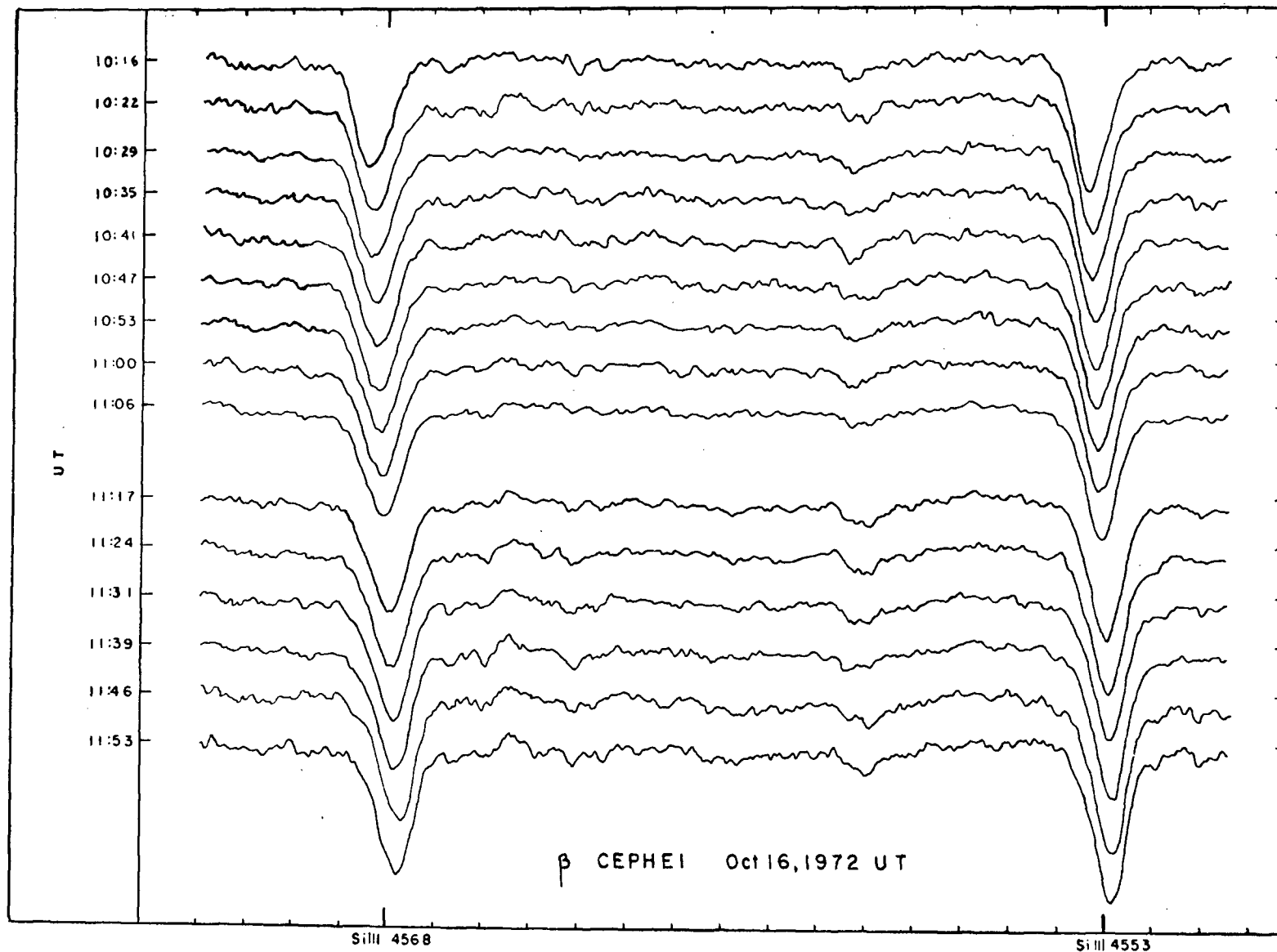


Fig. 5.25 Line profiles for  $\beta$  Cep on 16 October 1972 UT. Only a portion of the observations are shown.

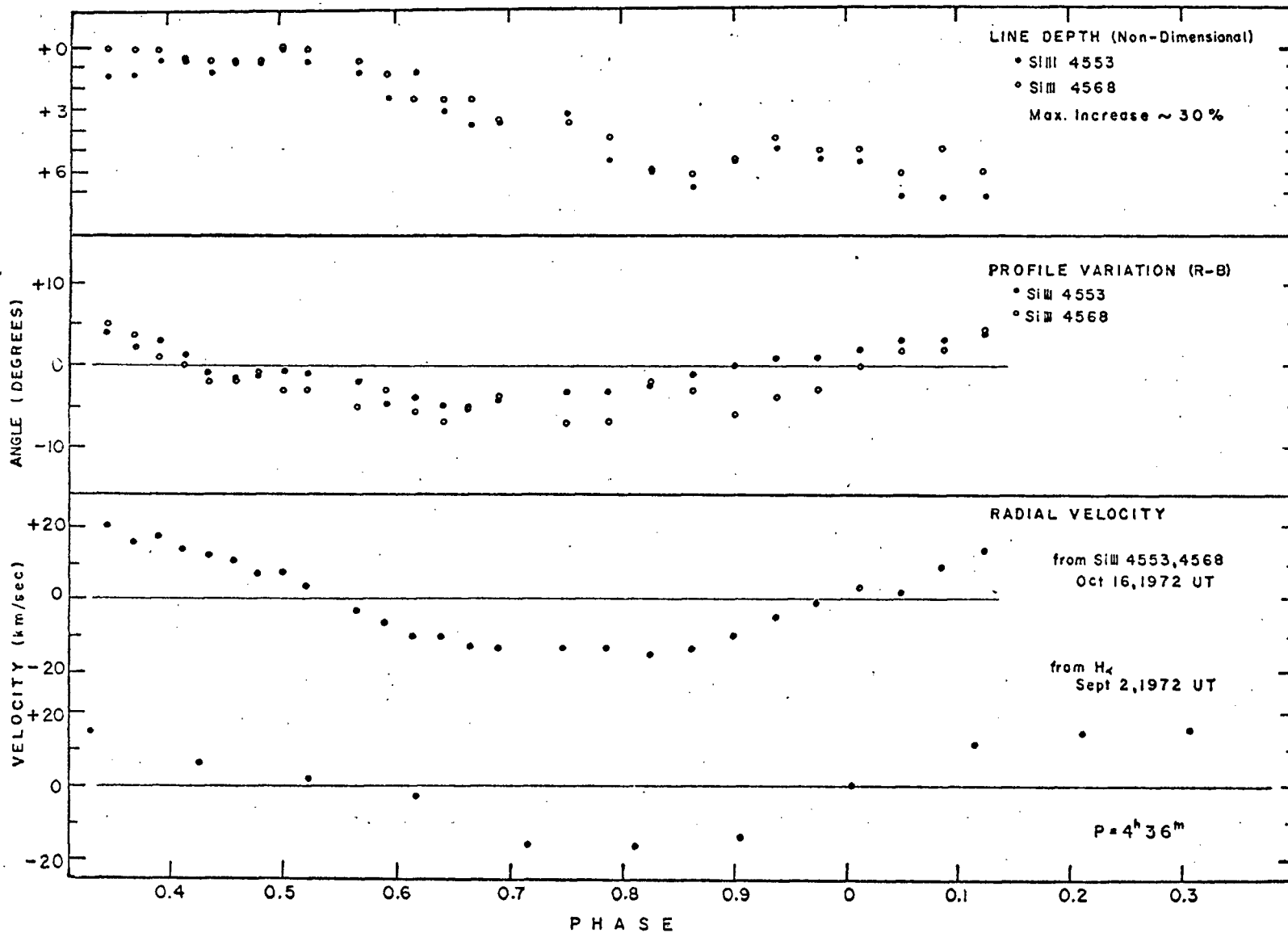


Fig. 5.26 Measures of the radial velocity, line asymmetry, and line depth for  $\beta$  Cephei. The asymmetries of the lines are indicated by the difference between the angle of a straight line fitted through the red side of the profile and one through the blue.

where  $n$  is the number of cycles since J.D. 2422203.790. He noted that an erratic jump in the period had occurred between 1914 and 1919. On the other hand, Gray (1970) concludes (on the basis of both the velocity and light measures) that there are no secular changes in the period of  $\beta$  Cep but instead one or more essentially discontinuous changes exemplified by the earlier change.

### 5.13 FUTURE WORK

The star  $\beta$  Cep is an excellent subject for a detailed pulsational analysis (i) because of the relatively large amplitude and relatively simple pattern of its variation; (ii) because of the substantial light and velocity data already available; and (iii) because of the relative ease with which new observations can be obtained. Computation of theoretical profiles and additional observations aimed at resolving the profile variation should be given high priority.

The new detection system has proved to be well-suited to the study of the spectral variations in the  $\beta$  Cephei ( $\beta$ CMa) stars and other relatively bright objects. Continuing use of the Image Isocon for these types of programs is certainly warranted. The more recently developed detectors (such as the silicon vidicon and *Reticon*\*) hold promise of even further gains, but perhaps of a different nature.

The portion of the instrumentation developed as part of the present project - the cooling system for the Image Isocon - has been an important and reliable part of this detection system. It represents an unusual and versatile approach to the cooling of astronomical detectors and provides a practical solution to one of the most important problems in the fabrication of detection systems of this type. The compactness and simplicity of the hardware associated directly with the detector, the inherent system stability, and the ease of system control are some of the more noteworthy features.

The software package developed for handling the substantial data output from the detection system has also proved satisfactory. The processing can be carried out rapidly and efficiently, the instrumental effects reduced to negligible levels, and the required quantitative analysis easily completed. Refinements are continually being incorporated into this package.

---

\* A self-scanned array of silicon diodes (see, e.g., Tull, R.G. and Nather, R.E. 1973, *Astronomical Observations with Television-Type Sensors*, (Symposium held at the University of British Columbia 15-17 May 1973).

Data have been obtained with the detection system of the  $\beta$  Cephei stars BW Vul and  $\beta$  Cep which have contributed significantly to an understanding of their pulsational characteristics and have provided further insights into the  $\beta$  Cephei phenomenon.

An extensive amount of data has been obtained of BW Vul over the past 50 years; providing a fairly detailed picture of its short-term light, radial velocity, and line profile variations as well as an indication of the long-term changes in its period and radial velocity amplitude. The new observations represent the best effort so far at reducing the degrading effects of limited time and spectral resolution. As a result, the line profile changes occurring during certain critical phases of the pulsation have been resolved for the first time, and a more accurate determination of the atmospheric motions throughout the pulsation cycle (e.g., the displacement and acceleration) has been made possible. In addition, certain features appearing in the photographic data which were previously ascribed to chance effects or to noise are now seen to represent real astrophysical occurrences. This data can now provide further useful information if subject to additional analysis.

The data gives the following picture of the star's variation. At the approximate epoch of minimum radius a violent ejection of the stellar atmosphere takes place with a maximum acceleration in excess of  $150 \text{ m/sec}^2$  and a maximum outward velocity (in the frame of the star) of more than  $100 \text{ km/sec}$ . The time scale for the process is about 15 minutes. The material then appears to undergo projectile motion for about one-half of the pulsation cycle. The deceleration during this interval is nearly constant at  $\sim 25 \text{ m/sec}^2$  (less than one-half the value of  $g_{\text{sfc}}$ ) and the maximum displacement  $\sim 5 \times 10^5 \text{ km}$  (or about 10% of the stellar radius). A short time before the return of the ejected material to the general

stellar surface the deceleration increases rapidly and approaches the value of  $g_{\text{sfc}}$ . At roughly this time the spectral lines become double as a new component develops and strengthens at the  $V_0$  position. The original component (originating from the ejected material) disappears in a time scale of about 30 minutes leaving only the  $V_0$  component. For approximately the next 30 minutes the stellar surface appears to remain nearly stationary. The process then begins anew.

The data were examined for phase effects in the radial velocities and in the profile variations of the spectral lines, for differences between cycles (particularly successive ones), and for evidence of binary effects and multiple periodicities.

Phase differences in the variations of different spectral lines (or in the radial velocities derived from them) are indicative of dynamic stratifications in the atmosphere. The 'Van Hoof Effect', discussed in Section 5.3, is one of the most obvious manifestations of such a stratification. Evidence of this effect has previously been found for BW Vul but simultaneous observation of the hydrogen lines and those other elements were not carried out in the present program. The principal lines that *were* observed simultaneously (those of He I, Mg II, and Si III in the region  $\sim 4450$  to  $4590 \text{ \AA}$ ) appeared to vary in a synchronous fashion throughout the entire cycle, indicating that the motion of the atmosphere in the zone of their formation was essentially uniform. It should be noted that these lines are all formed under similar conditions.

The reproducibility of successive cycles serves as one criterion for determining the coupling between the observed atmospheric motion and the basic oscillation of the star, and for obtaining some idea of the nature of the basic instability. Some evidence of a cycle-to-cycle varia-

tion in the pulsation amplitude was given both by the previous photographic data and by the observations obtained in 1971 with the Isocon. The results are uncertain because of the low quality of this data. Higher quality observations obtained with the Isocon in 1972 covering  $\sim 1.1$  cycle of the pulsation demonstrated no such variation.

Binary effects and multiple periodicities (with their associated beat effects) can strongly influence the observational characteristics of the  $\beta$  Cephei stars. They are also of importance from stability considerations. There is little evidence to suggest that BW Vul is a binary or that it displays more than one period.

The complexity of the variation of this star has discouraged theoretical analysis. The existing studies are discussed in this paper and the avenues for extending them indicated.

It appears that the extreme changes in the radial velocities are an atmospheric effect, to a certain degree unrelated to the basic oscillation of the star. The effects of large scale shock wave propagation in the atmosphere are probably responsible for much of the variation in the radial velocities and line profiles. The light variation, which occurs in a relatively smooth fashion, is more closely tied to the basic oscillation.

A refined picture is presented which attempts to explain many features of the variation in terms of the interaction between two relatively distinct layers - an envelope ejected by a high Mach number shock wave and the general photospheric layer. The assumption of a radial, spherically symmetric oscillation is implicit in this approach. The line doubling preceding stillstand is perhaps due to two mechanisms: (i) the onset

of transparency in the receding envelope and (ii) the interaction of this envelope with the general photospheric layer.

The present program has also provided further information concerning the long-term changes in the period and the radial velocity amplitude. Both appear to be increasing, providing evidence for an increase in the *pulsation* amplitude as well. The star may be in a phase of rapid evolution.

For  $\beta$  Cep, the first definitive record of a variation in line profile correlated with the variations in light and radial velocity was obtained. The change in the asymmetries of the line profiles indicates that differential motion takes place in its atmosphere as a result of the pulsation. The implications are discussed in Section 5.11.

The new data represents an important observational gain relative to the previous spectroscopic studies of these stars. The result has been a significantly clearer picture of their individual variations.

The total value of these results to the understanding of the  $\beta$  Cephei phenomenon is at present unclear. A continuing record of the changes in period, radial velocity, and other fundamental features of the variation are important from evolutionary considerations. Detailed pictures of the atmospheric behavior should provide some insight into the cause and nature of the instability and serve as critical tests of theoretical *models*. The full value of these observations and others like them can only be realized when realistic quantitative models are developed and the internal structural changes due to evolutionary processes in the appropriate regions of the H-R diagram are understood. At present,

the quality of the observations has outdistanced that of the theory. The present data should serve as a *stimulus* for a more realistic theoretical analysis of these extremely interesting stars and for further observations with the detection system.

## BIBLIOGRAPHY

- Ahlborn, B. 1966, *Phys. Fluids* 9, 1873.
- Barbon, R., Bernacca, P.L., Tarengi, M. 1972, *Nature* 240, 182.
- Bhatnagar, M.S., Kushwaha, R.S. 1961a, *Ann. Astrophys.* 24, 211.
- Bhatnagar, M.S., Kushwaha, R.S. 1961b, *Proc. Nat. Inst. Sci. India A*, 27a, 441.
- Bhatnagar, M.S., Kushwaha, R.S. 1963, *Proc. Nat. Inst. Sci. India A*, 29a, No. 2, 143.
- Bhatnagar, M.S., Kulshrestha, K.P., Tandon, J.N. 1971, *Astrophys. Letters* 9, 135.
- Biraud, Y. 1969, *Astron. Astrophys.* 1, 124.
- Bonsack, W.K. 1971, *Astron. Astrophys.* 15, 374.
- Brault, J.W., White, O.R. 1971, *Astron. Astrophys.* 13, 169.
- Buchholz, V.L. 1972, unpublished Masters thesis, University of British Columbia.
- Butler, H.E., Seddon, H. 1958, *Publ. Royal Obs. Edinburgh* 2, No. 4.
- Carrus, P.A., Fox, P.A., Haas, F., Kopal, Z. 1951, *Ap.J.* 113, 496.
- Carruthers, G.R. 1971, *Astrophys. Space Sci.* 14, 332.
- Castor, J.I. 1972, "The Evolution of Population II Stars", *Dudley Obs. Reports*, No. 4, A.G.D. Philip, ed., p.147.
- Chandrasekhar, S., Lebovitz, N.R. 1962, *Ap.J.* 136, 1105.
- Christy, R.F. 1966, *A.J.* 72, 293.
- Clement, M.J. 1965, *Ap.J.* 141, 1443.
- Clement, M.J. 1966, *Ap.J.* 144, 841.
- Clement, M.J. 1967, *Ap.J.* 150, 589.
- Davey, W.R. 1973, *Ap.J.* 179, 235.
- Dukes, J. 1973, personal communication, University of Arizona.
- Eggen, O.J. 1948, *A.J.* 53, 197.

- Evans, D.H., Brown, R.H., Davis, F., Allen, L.R. 1971, *M.N.* 151, 161.
- Fischel, D., Sparks, W.M. 1972, *The Scientific Results from the Orbiting Astronomical Observatory (OAO-2)*, A.D. Code ed., NASA SP-310, p. 475.
- Fitch, W.S. 1969, *Ap.J.* 158, 269.
- Frost, E.B. 1902, *Ap.J.* 15, 370.
- Gandel'man, G.M., Frank-Kametski, D.A. 1956, *Dokl. Akad. Nauk SSSR* 107, 811.
- Gingerich, O., ed. 1969, *Theory and Observation of Normal Stellar Atmospheres* (Cambridge, Mass.: The M.I.T. Press).
- Goldberg, B.A., Walker, G.A.H., Auman, J.R., Odgers, G.J. 1972, *B.A.A.S.* 4, 218.
- Goldberg, B.A., Walker, G.A.H., Glaspey, J., Odgers, G.J. 1973a, *B.A.A.S.* 5, 5.
- Goldberg, B.A., Walker, G.A.H., Rotem, Z. 1973b, *Can. Congress of Appl. Mech. (CANCAM)*, 1973 Proceedings.
- Goldstein, S., ed. 1965, *Modern Developments in Fluid Dynamics* (New York: Dover Publ., Inc.) p.84.
- Gray, D.F. 1970, *A.J.* 75, 958.
- Greaves, W.M.H., Baker, E.A., Wilson, R. 1955, *Publ. Royal Obs. Edinburgh* 1, No. 6.
- Guthnick, P., Prager, R. 1914, *Ver. Königlichem Stern. Berlin - Babelsberg* 1, 23.
- Hill, G. 1966, Ph.D. thesis, University of Texas, Austin.
- Hill, G. 1967, *Ap.J. Suppl.* 14, 263.
- Hill, S.J. 1972, *Ap.J.* 178, 793.
- Hill, S.N. 1930, *Publ. D.A.O.* 5, 10.
- Hillendahl, R.W. 1969, *Astrophys. Letters* 4, 179.
- Hillendahl, R.W. 1970a, *National Bureau of Standards Special Publication No. 322*, H.G. Groth and P. Wellmann, eds.
- Hillendahl, R.W. 1970b, *Publ. A.S.P.* 82, 1231.
- Hoof, A. van, Deurinck, R. 1952, *Ap.J.* 115, 166.

- Hoof, A. van, Struve, O. 1953, *Publ. A.S.P.* 65, 158.
- Hoof, A. van. 1970, in *Spectroscopic Astrophysics*, ed., G.H. Herbig (Berkeley: Univ. of Calif. Press), p.343.
- Howe, D.A., Craig, J.R., Harris, R.L., Hadidiacos, C.G. 1969, *Jour. Geol. Edu.* 17, No. 2, 35.
- Huffer, C.M. 1938, *Ap.J.* 87, 76.
- Hutchison, R.B. 1971, *A.J.* 76, 711.
- Isherwood, B.C. 1971, unpublished Masters thesis, University of British Columbia.
- Karpov, B.G. 1933, *Lick Obs. Bull.* 16, No. 457, 167.
- Kochina, N.N., Mel'nikova, N.S. 1958, *Dokl. Akad. Nauk SSSR* 122, 192.
- Kochina, N.N., Mel'nikova, N.S. 1960, *Zh. Prikl. Mat. i Mekhan* 24, 213.
- Korobeinikov, V.P., Mel'nikova, N.S., Ryazanov, E.V. 1961, *Theory of Point Explosions* (in Russian). Goz. Izdot. Fiz.-Mat., Moscow.
- Kraft, R.P. 1953, *Publ. A.S.P.* 65, 45.
- Kubiak, M. 1972, *Acta Astronomica* 22, No. 1
- Kutz, M. 1968, *Temperature Control* (New York: John Wiley & Sons, Inc.).
- Laskarides, P.G., Odgers, G.J., Climenhaga, J.L. 1971, *A.J.* 76, 363.
- Laumbach, D.D., Probststein, R.F. 1971, *Phys. Fluids* 13, 1178.
- Le Contel, J.M., Sareyan, J.P., Dantel, M. 1970, *Astron. Astrophys.* 8, 29.
- Ledoux, P. 1951, *Ap.J.* 114, 373.
- Lesh, J.R., Aizenman, M.L. 1973, *Astron. Astrophys.* 22, 229.
- Liller, W. 1968, *Ap.J.* 151, 589.
- Livingston, W.C. 1963, *Jour. S.M.P.T.E.* 72, 771.
- Livingston, W.C. 1973, submitted to *Ann. Rev. Astr. Astrophys.*
- Lorre, J.J. 1973, *A.J.* 78, 67.
- Lynds, C.R. 1954, *Publ. A.S.P.* 66, 197.
- McNamara, D.H., Williams, A.D. 1955, *Ap.J.* 121, 51.
- McNamara, D.H., Struve, O., Bertiau, S.C. 1955, *Ap.J.* 121, 326.
- McNamara, D.H., Hansen, .K. 1961, *Ap.J.* 134,207.

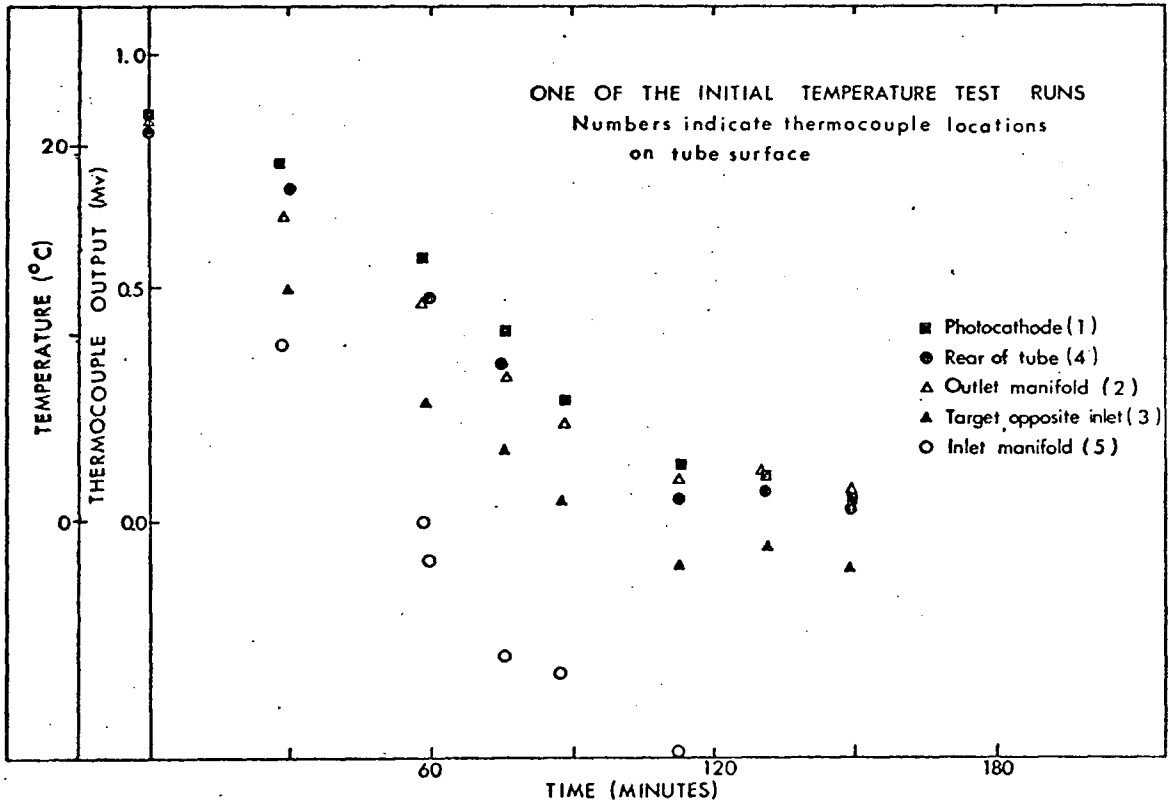
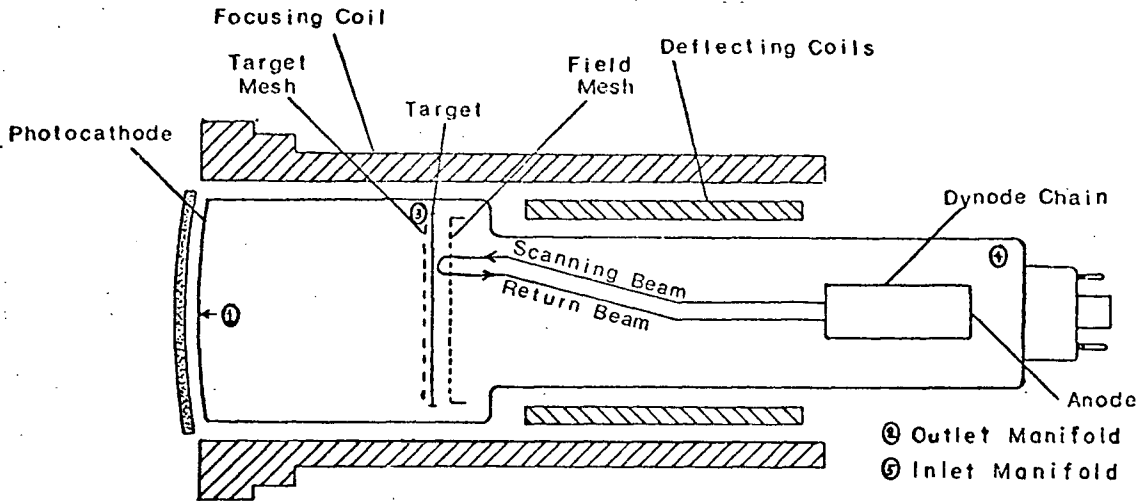
- Nelson, P.D. 1969, *Adv. E.E.P.* 28A, 209.
- Nikonov, W., Nikonova, E. 1952, *Izv. Krim. Astr. Obs.* 9, 135.
- Odgers, G.J. 1956, *Publ. D.A.O.* 10, No. 9, 215.
- Odgers, G.J., Kushwaha, R.S. 1959, *Publ. D.A.O.* 11, No. 6,
- Osaki, Y. 1971, *Publ. Astr. Soc. Japan* 23, 485.
- Parsons, S.B. 1972, *Ap.J.* 174, 57.
- Percy, J.R. 1967, *J.R.A.S. Canada* 61, 117.
- Percy, J.R., 1971, *J.R.A.S. Canada* 65, 217.
- Petrie, R.M. 1937, *Publ. D.A.O.* 9, 53.
- Petrie, R.M. 1954, *Publ. D.A.O.* 10, No. 2, 39.
- Popov, V.S. 1971, *ИЗВЕСТИЯ ГЛАВНОЙ Astr. Obs.*, No. 187, p.34.
- Sachdev, P.L., Ashraf, S. 1971, *Phys. Fluids* 14, 2107.
- Saito, M., Sato, H. 1972, *Publ. Astron. Soc. Japan* 24, 503.
- Saito, M. *et.al.* 1972, *Tokyo Astron. Bull.* No. 219, 2557.
- Sakurai, A. 1960, *Commun. Pure Appl. Math.* 13, 353.
- Sakurai, A. 1965, *Basic Developments in Fluid Dynamics* 1, M.H. Holt, ed. (New York: Academic Press).
- Shapiro, A.H. 1954, *The Dynamics and Thermodynamics of Compressible Fluid Flow* 1 and 2 (New York: The Ronald Press Co.)
- Shobbrook, R.R., Evans, D.H., Johnston, I.D., Lomb, N.R. 1969, *M.N.R.A.S.* 145, 131.
- Shobbrook, R.R., Lomb, N.R., Evans, D.H. 1972, *M.N.R.A.S.* 156, 165.
- Stebbins, J. 1914, *Ap.J.* 39, 459.
- Stebbins, J., Kron, G.E. 1954, *Ap.J.* 120, 189.
- Stothers, R., Simon, N.R. 1969, *Ap.J.* 157, 673.
- Stothers, R., Simon, N.R. 1971, "Criteria for the Discovery of Beta Cephei Stars According to the Mu-Mechanism Theory", Preprint (New York: Goddard Institute for Space Studies, NASA).
- Stromgren, B. 1963, *Basic Astronomical Data*, K.Aa. Strand, ed. (Chicago: The University of Chicago Press) Chapter 9.
- Struve, O. 1948, *Ap.J.* 108, 154.

- Struve, O., McNamara, D.H., Kung, S.M., Beymer, C. 1953, *Ap. J.* 118, 39.
- Struve, O. 1955a, *Publ. A.S.P.* 67, 135.
- Struve, O. 1955b, *The Observatory* 75, 179.
- Struve, O., Sahade, J., Huang, S.S., Zebergs, V. 1958, *Ap.J.* 128, 310.
- Thomas, R.N., ed. 1967, *Aerodynamic Phenomena in Stellar Atmospheres*, IAU Symposium No. 28 (New York: Academic Press).
- Thompson, P.A. 1972, *Compressible-Fluid Dynamics* (McGraw-Hill Book Co.).
- Ulrych, T.J., Auman, J.R., Eilek, J.A., Walker, G.A.H. 1972, *Astron. Astrophys.* 21, 125.
- Underhill, A.P. 1966, *The Early Type Stars* (Dordrecht, Holland: D. Reidel Co.).
- Van Citters, G.W., Morton, D.C. 1970, *Ap.J.* 161, 695.
- Vogel, H.C. 1890, *Astr. Nachr.* 125, 305.
- Walker, G.A.H., Auman, J.R., Buchholz, V., Goldberg, B., Isherwood, B. 1971, *Publ. Royal Obs. Edinburgh* 8, 86.
- Walker, G.A.H., Auman, J.R., Buchholz, V.L., Goldberg, B.A., Gower, A.C., Isherwood, B.C., Knight, R., Wright, D. 1972, *Adv. E.E.P.* 33B, (London: Academic Press).
- Walker, M.F. 1954, *Ap.J.* 119, 631.
- Watson, R.D. 1971, *Ap.J.* 169, 343.
- Watson, R.D. 1972, *Ap.J. Supple.* 24, 167.
- Wellmann, P. 1957, *Ap.J.* 126, 30.
- Wentzel, D.G., Tidman, D.A. 1969, *Plasma Instabilities in Astrophysics* (Gordon and Breach).
- Wesselink, A.J. 1946, *B.A.N.* 10, 91.
- Wilson, R. 1956, *Publ. Royal Obs. Edinburgh* 2, No. 1
- Wright, K.O. 1952, *Publ. D.A.O.* 9, No. 5, 189.
- Wright, K.O. 1964, *Publ. D.A.O.* 12, No. 7, 173.
- Zel'dovich, Y.B., Raizer, Y.B. 1966, *Physics of Shock Waves and High-Temperature Hydrodynamic Phenomena* 1 (New York and London: Academic Press).
- Zel'dovich, Y.B., Raizer, Y.B. 1967, *Physics of Shock Waves and High-Temperature Hydrodynamic Phenomena* 2 (New York and London: Academic Press).

APPENDIX A. EXPERIMENTAL ANALYSIS OF THE COOLING SYSTEM

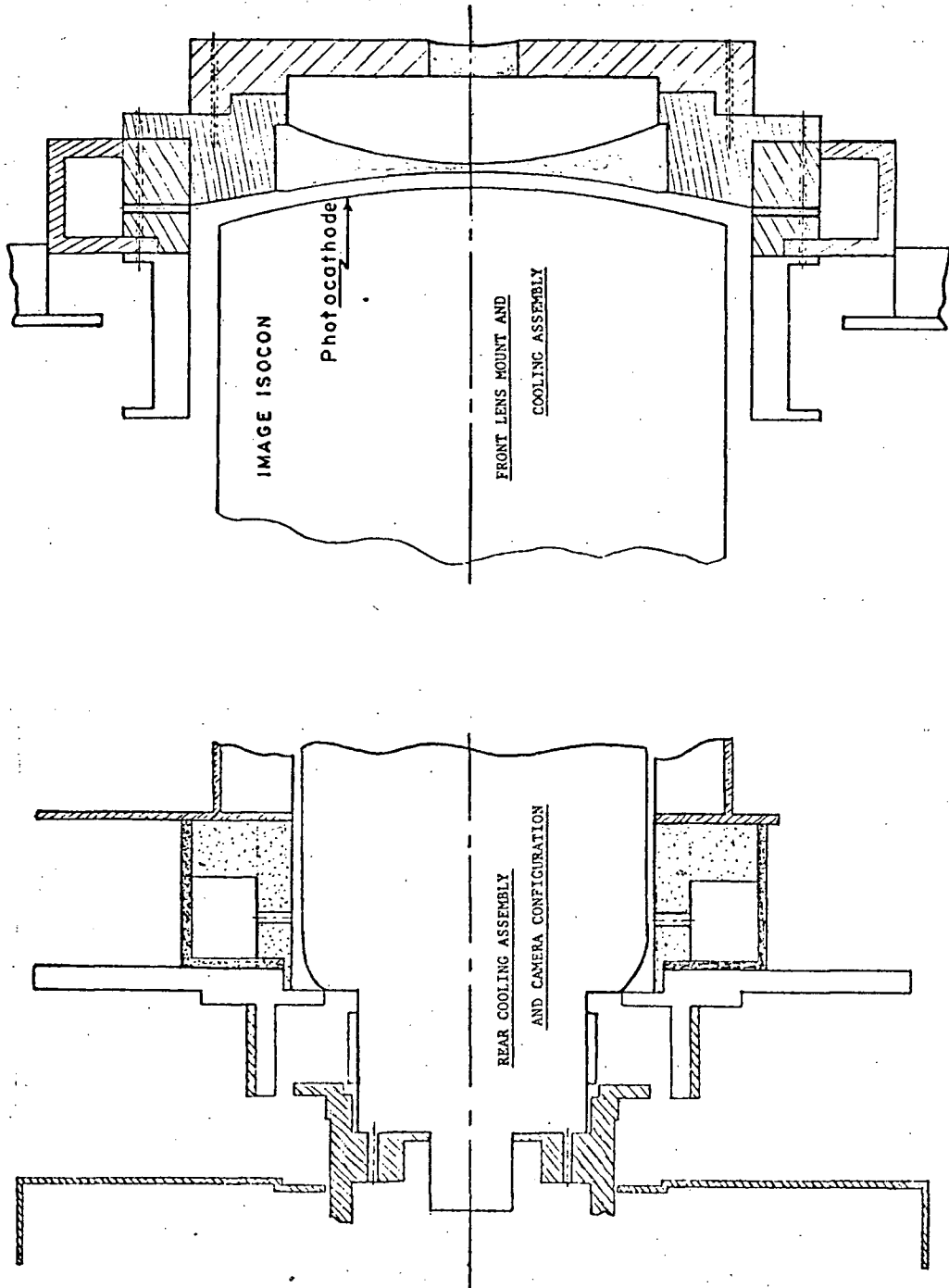
Carrying out temperature measurements of the Isocon was one of the most important parts of the feasibility analysis. Temperature and temperature differentials were measured by using copper-constantan thermocouples located at strategic points on the tube surface.

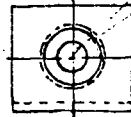
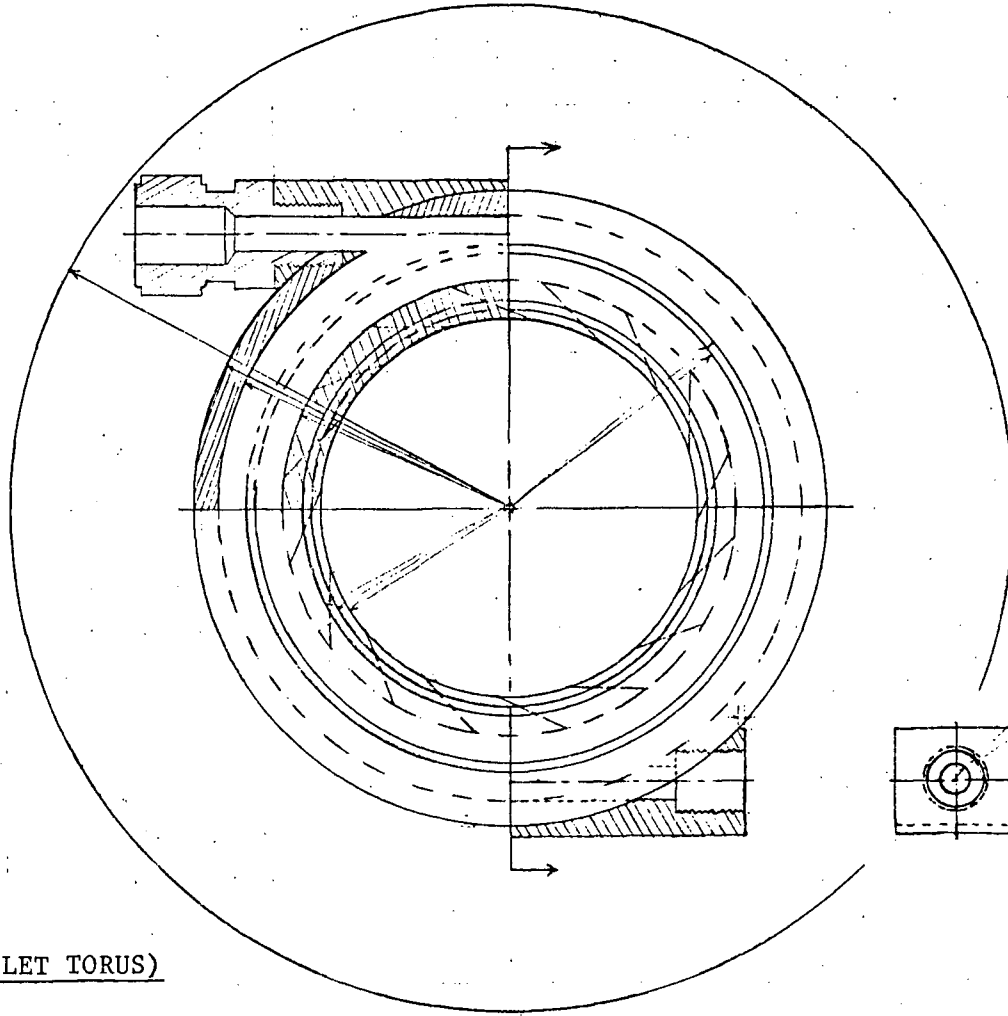
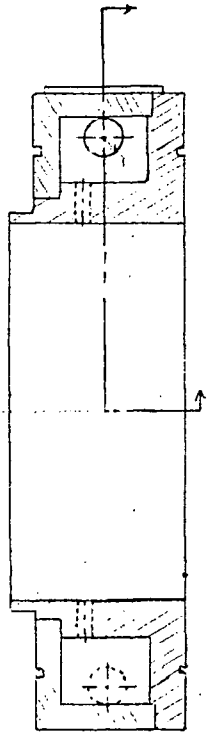
One test setup is shown here as well as the result of one test run. The performance of the 'final' system is considerably better than indicated by these results.



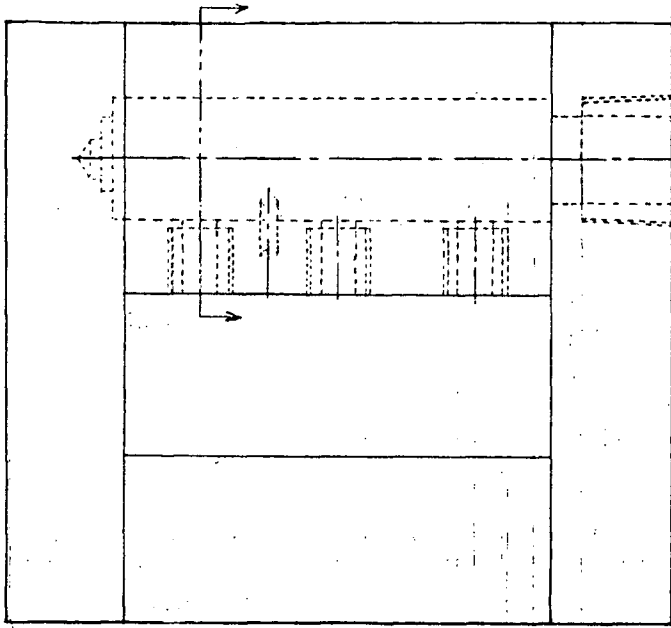
APPENDIX B. DESCRIPTION OF THE COOLING SYSTEM HARDWARE

Drawings of some of the more important components are given.



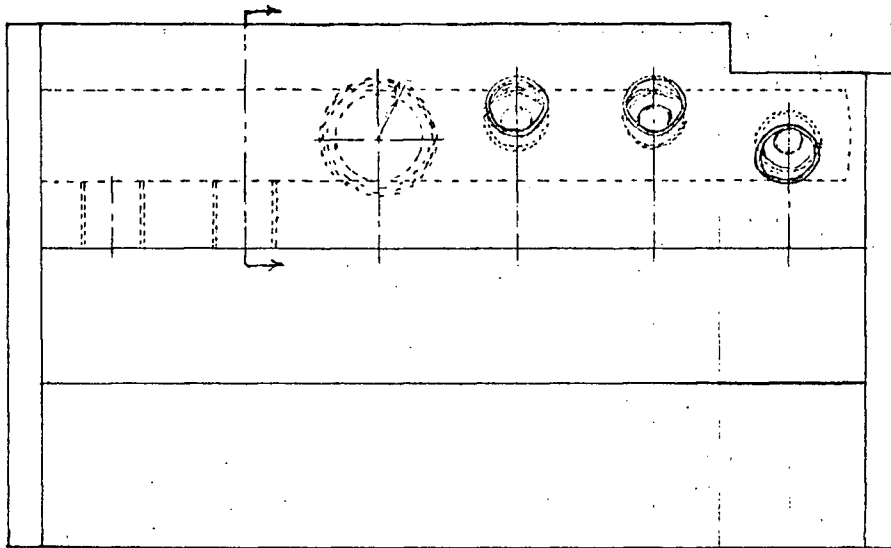
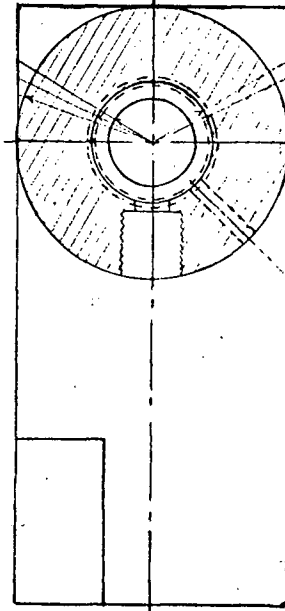


REAR COOLING ASSEMBLY (OUTLET TORUS)



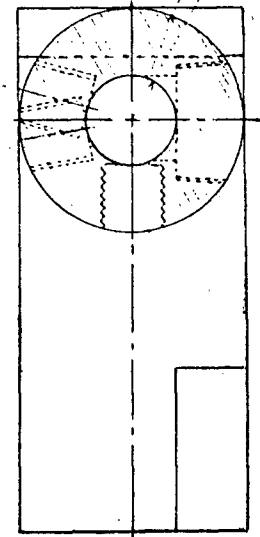
FLOW MANIFOLD

(ENTRANCE)



FLOW MANIFOLD

(EXIT)



## APPENDIX C. THE RECTIFICATION PROGRAM

Rectification of the spectra with the consequent removal of the instrumental response characteristic is of central importance. The spectra must be rectified before most quantitative analyses can be carried out. The rectification portion of the program is presented here.

The primary inputs to this program are:

- (1) The normalized spectra (which may or may not be filtered);
- (2) The regions of continuum (in terms of channel numbers);
- (3) The extents of the spectral lines;
- (4) Various scaling factors.

The continuum regions are subdivided into small segments from which individual values are computed (representing the noise-corrected average or maximum in the segment). These continuum values are then fitted by orthogonal polynomials of a specified order (usually third). The data are scaled to the values that the polynomials take in each channel. The program follows.

```

126.2  C SET STARTING VALUES FOR NEW LARGE INT CALC
-----
126.201      N1=1
126.21      1220 CONTINUE
126.22      NCSS=0
-----
126.23  C
126.3  C SET STARTING VALUES FOR NEW SMALL INT CALC
-----
126.31      1230 NCSS=NCSS+NCS
-----
126.32      IF ((NLA(N1)+NCSS-NCS).GE.NLA(N1+1)) GOTO 1250
126.33      AVE=0.
126.34      DEV=0.
-----
126.35      YMS=0.
126.36      YMSN=0.
126.37      SUM1=0.
-----
126.38      SUMSQU=0.
126.39      LS=NLA(N1)+(NCSS-NCS)
126.4      LF=LS+NCS
-----
126.5  C DETERMINE MAX VALUE IN ONE SMALL INT
126.51      DO 1240 I=LS,LF
126.52      SUM1=SUM1+SIG(I)

```

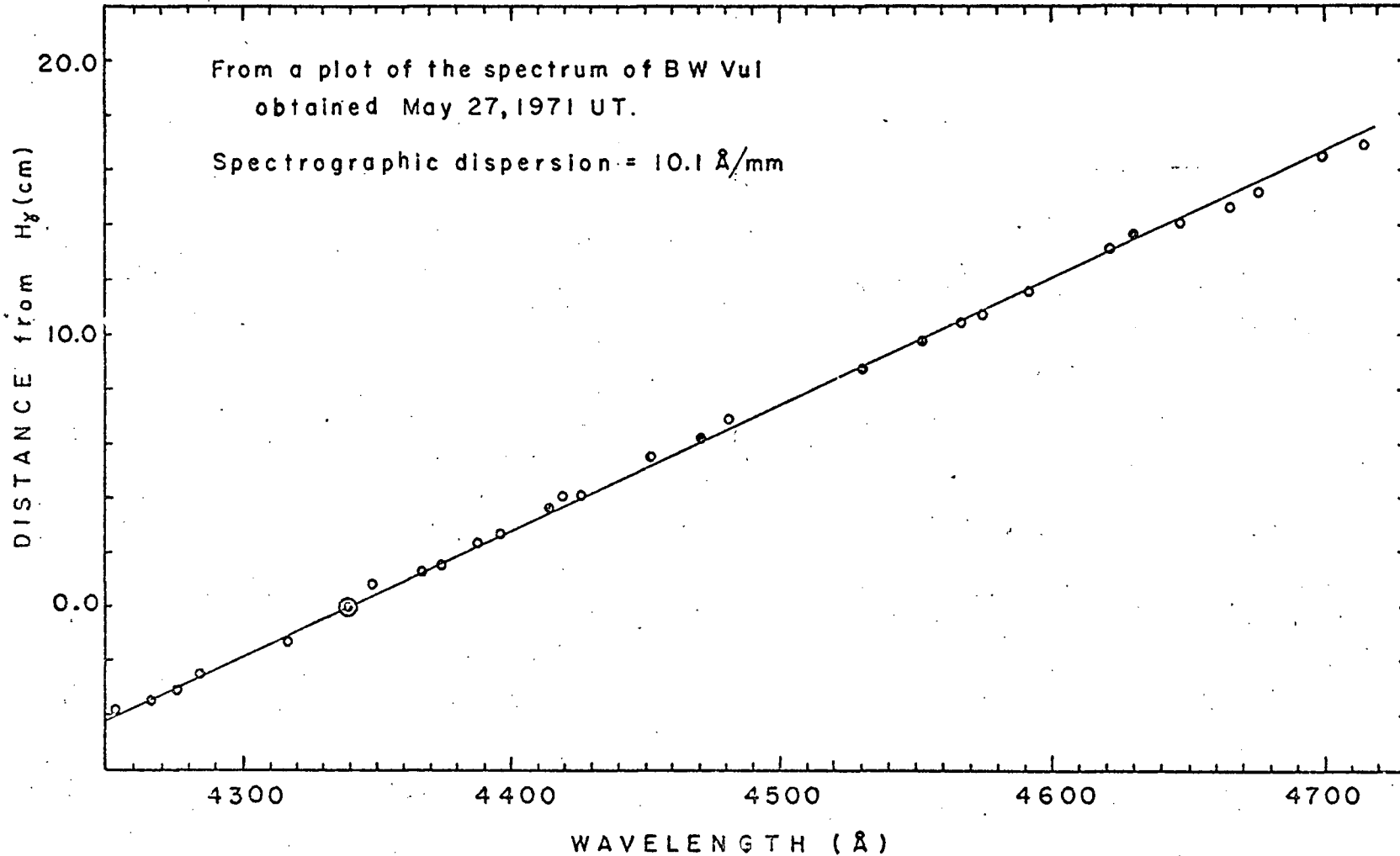
126.53		SUMSQU=SUMSQU+SIG(I)**2
126.54		IF (ABS(YMS).GT.ABS(SIG(I))) GOTO 1239
126.55		YMS=SIG(I)
126.56		NCYMS=I
126.565	1239	CONTINUE
126.57	1240	CONTINUE
126.58		AVE=SUM1/(NCS+1)
126.59		DEV=SQRT((SUMSQU/(NCS+1))-AVE**2)
126.6		YMSN=YMS-DEV
126.601		NCENT=(LS+3)
126.61		Y7(J)=AVE+DEV
126.611		IF(MAXSI.EQ.0) GOTO 7097
126.612		Y7(J)=YMS
126.613	7097	CONTINUE
126.62		X7(J)=FLOAT(NCENT)
126.63		J=J+1
126.64	C	PROCEED TO NEXT SMALL INT
126.65		GOTO 1230
126.66	C	PROCEED TO NEXT LARGE INT
126.67	1250	IF (NLA(NL1+1).GE.NLA(NL2)) GOTO 1300
126.68		NL=NL+2
126.69		GOTO 1220
126.7	1300	CONTINUE
126.701		J=J-1
126.702		WRITE(6,615)
126.71		WRITE(6,613) (X7(K),K=1,J)
126.711		WRITE(6,616)
126.72		WRITE(6,613) (Y7(K),K=1,J)
126.73	613	FORMAT(10E12.5)
126.74	614	FORMAT(10E12.5)
126.75	615	FORMAT(1X,'X CHOSEN VALUES FOR CONTINUUM')
126.76	616	FORMAT(1X,'Y CHOSEN VALUES FOR CONTINUUM')
126.769		JCNT=0
126.771		NLQ2=NLQ1+1
126.772		NLQ3=J
126.776		DO 8021 I=1,NLQ1
126.777		X(I)=X7(I)
126.778		Y(I)=Y7(I)
126.779	8021	CONTINUE
126.78		M=NLQ1
126.781		IF (JCNT.EQ.0) GOTO 8029
126.782	8024	CONTINUE
126.783		DO 8022 I=1,NLQ1
126.784		X(I)=0.
126.785		Y(I)=0.
126.786	8022	CONTINUE
126.787		JST=1
126.788		DO 8023 I=NLQ2,NLQ3
126.789		X(JST)=X7(I)
126.79		Y(JST)=Y7(I)
126.791		JST=JST+1
126.792	8023	CONTINUE
126.793		M=(NLQ3-NLQ1)
126.794	8029	CONTINUE

```

126.8 C SET STARTING VALUES FOR OLQF FOR SINGLE AVE CALC
126.801 K=4
126.802 KSAVE=4
-----
126.82 DO 1301 I=1,M
126.83 YF(I)=0.
126.84 YD(I)=0.
126.85 1301 CONTINUE
126.86 DO 1302 I=1,K
126.87 SIGMA(I)=0.
126.88 A(I)=0.
126.89 B(I)=0.
126.9 1302 CONTINUE
-----
126.909 K1=K+1
126.91 DO 1303 I=1,K1
126.92 S(I)=0.
126.93 P(I)=0.
126.94 1303 CONTINUE
126.95 SS=0.
-----
127 C DETERMINE POLYNOMIAL FIT
127.01 CALL OLQF(K,M,X,Y,YF,YD,WT,NWT,S,SIGMA,A,B,SS,LK,P
127.02 C PRINT ORIG DEG,FINAL DEG,COEFF OF POLY,AND SUM OF SQ.
127.03 WRITE(6,1310) KSAVE,K,(P(L),L=1,K)
127.04 WRITE(6,1311) SS
127.05 1310 FORMAT(1X,I5,10X,I5,(4F15.5))
127.06 1311 FORMAT('SUM OF SQUARES IS',E15.5)
127.07 C CALCULATE CONTINUUM FOR ALL CHANNELS
127.071 IF (JCNT.EQ.1) GOTO 8025
127.08 DO 1361 I=1,NCUT1
127.09 XX1=FLOAT(I)
127.1 CALL FITTER(K,XX1,YY1,A,B,S)
127.11 CONT(I)=YY1
127.12 1361 CONTINUE
127.13 7081 CONTINUE
127.131 7083 CONTINUE
127.132 C WRITE CONTINUUM ON FILE IF FILE=FILENAME
127.133 WRITE(1) CONT
127.134 C READ IN CONTINUUM IF MCONSF=1
127.135 IF (MCONSF.EQ.0) GOTO 7082
127.136 READ(2) CONT
127.137 7082 CONTINUE
127.15 C NORMALIZE TO CONTINUUM AND SCALE
127.16 DO 1370 I=1,NCUT1
127.17 CNORM(I)=(SIG(I)/CONT(I))
127.18 1370 CONTINUE
127.181 IF (MCONSF.EQ.1) GOTO 7084
127.182 IF (IAN.EQ.1) GOTO 7085
127.183 IF (MCONS.EQ.1) GOTO 7086
127.184 7085 CONTINUE
127.19 JCNT=JCNT+1
127.191 IF (NCUT1.EQ.NCH) GOTO 8028
127.192 GOTO 8024
127.2 8025 CONTINUE
127.201 NCUT2=NCUT1+1
127.21 DO 8026 I=NCUT2,NCH

```

```
127.22      XXI=FLOAT(I)
127.23      CALL FITTER(K,XX1,YY1,A,B,S)
127.24      CONT(I)=YY1
-----
127.25      8026 CONTINUE
127.26      C NORMALIZE TO CONTINUUM AND SCALE
127.261     7086 CONTINUE
-----
127.262     7084 CONTINUE
127.263      NCUT2=NCUT1+1
127.27      DO 8027 I=NCUT2,NCH
-----
127.28      CNORM(I)=(SIG(I)/CONT(I))
127.29      8027 CONTINUE
```



The figure indicates that the effective dispersion is fairly constant across the raster for this set of observations. Some of the scatter may be attributed to inaccuracies associated with the measurement of the positions of the spectral features on the computer plot.

APPENDIX E. SHOCK WAVE COMPUTATIONS FOR BW VUL*Introduction*

The following is based on the paper by Sachdev and Ashraf (1971).

The undisturbed density  $\rho_0$  ahead of the shock is *assumed* to be

$$\rho_0 = bX^\delta,$$

where  $b$  and  $\delta$  are constants such that  $\rho_0 = 0$  on the stellar 'surface'.

The time  $t$  is taken to be negative before the shock reaches the surface, and  $t = 0$  is the time of shock emergence at the surface.

The shock position is *assumed* to be

$$X = A(-t)^\alpha,$$

where  $X$  is the distance of the shock from the stellar surface as measured from that surface,  $t$  is the time (which is negative) before the shock reaches the surface, and  $A$  and  $\alpha$  are constants.

It is *assumed* that the heat flux across the optically thin shock front is continuous so that the classical shock conditions hold. The strong shock approximation can be applied.

The boundary conditions at the shock (expressed as dimensionless values) are then

$$U_s = (1-\rho)\dot{X} \quad \rho_s = \rho_0/\beta \quad P_s = (1-\beta)\rho_0\dot{X}^2,$$

where  $U_s$ ,  $\rho_s$ , and  $P_s$  are respectively the velocity, density, and pressure of the fluid immediately behind the shock;  $\beta$  is the density ratio across the shock [ $\beta = (\gamma-1)/(\gamma+1)$ ]; and  $\dot{X}$  is the velocity of the shock.

For the case of a spatially isothermal flow behind the shock, the values of  $\gamma = \frac{5}{3}$  and  $\delta = 3.25$  (noted as being particularly relevant to stellar envelopes in radiative equilibrium) are used. The corresponding value for the exponent  $\alpha$  is 0.3136. Thus  $\beta = \frac{1}{4}$  and

$$U_s = \frac{3}{4}\dot{X} \quad \rho_s = 4\rho_0 \quad P_s = \frac{3}{4}\rho_0\dot{X}^2$$

### *Application to BW Vul*

The non-isentropic sound speed (corresponding to the isothermal derivative) is given by

$$a = \left(\frac{P}{\rho}\right)^{\frac{1}{2}}$$

where  $P$  = pressure and  $\rho$  = density. For comparison, the isentropic sound speed (as noted by Ahlborn, 1966) is

$$v_s = [(\partial P/\partial \rho)]^{\frac{1}{2}} = (\gamma_s P/\rho)^{\frac{1}{2}}$$

where  $\gamma$  is the ratio of specific heats. The isothermal sound speed is applicable to the problem at hand (since a strong shock is non-isentropic).

The approximate value for the sound speed under conditions similar to those found in the atmosphere of BW Vul (as obtained using the grids of model atmospheres of Gingerich (1969) and Van Citters and Morton (1970) is 20 km/sec. It is relatively insensitive to changes in optical depth.

The primary region of spectral line formation is in the range of  $P \approx 10^2$  to  $10^3$  dynes/cm<sup>2</sup>. Interpolating in the atmospheric grids just noted, a value of  $\Delta r \sim 15000$  km is obtained. This contrasts with the displacement of  $\sim 5 \times 10^5$  km obtained by integrating the BW Vul radial velocity data.

### *The shock velocity*

The maximum velocity of the gas is observed to be  $\sim 100$  km/sec (with the correction for projection effects applied). The shock velocity is then  $\dot{X} = (4/3) U_s \approx 140$  km/sec and the Mach number about 7. The time scale for the passage of the shock through the region of line formation is approximately  $\Delta r/\dot{X} = 1.5$  minutes.

### *Formation of the shock*

For the isothermal case, the shock velocity is

$$\dot{X} = BX^{-(1-\alpha)/\alpha},$$

where B is a constant.

Using the value  $\alpha = 0.3136$ , and applying the condition that  $\dot{X} = 140$  at  $x = 10,000$ , the relation

$$\dot{X} \approx BX^{-2}$$

is obtained, where  $B = 1.4 \times 10^{10}$ .

Therefore,

$$X = (B/\dot{X})^{1/2} \approx [1.4 \times 10^{10} / \dot{X}]^{1/2}$$

Taking  $\dot{X} = 20$ , the approximate distance from the stellar surface of the formation of the shock is 26000 km.

### *Summary*

This analysis demonstrates that the *order of magnitude* of the distances, velocities, and time scales is correct in the shock wave interpretation of BW Vul. It should be emphasized that the approximations are rather crude and that it is impossible at this stage to distinguish between

the various shock wave models. The observability of the atmospheric changes associated with the passage of the shock front is one of the most important considerations.

*Further considerations*

If the possibility of the outward acceleration of material in a rarefaction wave (i.e., by Hillendahl Mechanism) is accepted, then the shock velocity may be considerably lower since a part of the gas velocity is derived from the rarefaction wave. The terminal velocity achieved by acceleration in a rarefaction wave may be estimated by equating the original thermal energy of the gas to its terminal kinetic energy.

$$U_t = U_2 + \frac{2v_2}{\gamma_2 - 1} \quad \gamma_2 = 1 + P_2/\rho_2 E_2$$

The parameters ahead of the rarefaction front (i.e., behind the original shock front) are

$U_2$  = velocity

$v_2$  = sound speed

$P_2$  = pressure

$\rho_2$  = density

$E_2$  = internal energy

where  $U_2$  represents the acceleration in the shock front and  $2C_2/\gamma_2 - 1$  the acceleration in the refraction wave.

Taking  $\gamma = \frac{5}{3}$  and  $v_2 \approx 20$  km/sec:

$$\frac{2v_2}{\gamma - 1} \approx 60 \text{ km/sec.}$$

Therefore  $U_2 \approx 40$  km/sec, and  $\dot{X} \approx 90$  km/sec. The Mach number is  $\sim 4.5$ .

*Some problems*

In general, realistic boundary conditions are difficult to obtain (e.g., what is the *surface* of a star?), and some of the more important approximations (such as an isothermal flow) require more rigorous justification.